FLEXIBLE OPTICAL NETWORK COMPONENTS

BASED ON

DENSELY INTEGRATED MICRORING RESONATORS

by Douwe Geuzebroek

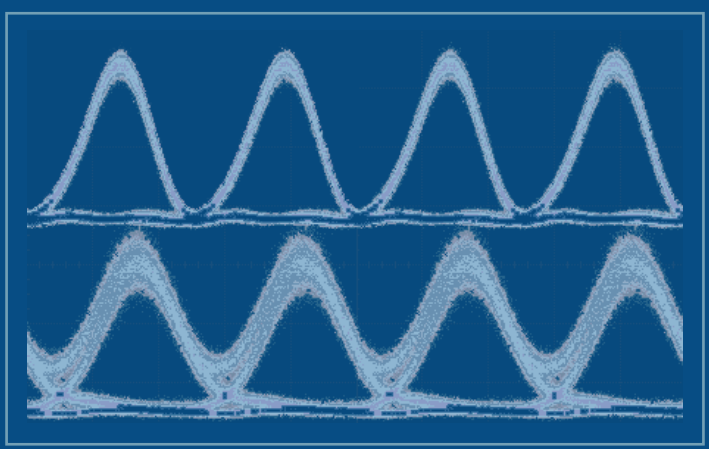

FLEXIBLE OPTICAL NETWORK COMPONENTS BASED ON DENSELY INTEGRATED MICRORING RESONATORS

Promotiecommissie

Promotor:	Prof. Dr. A. Driessen	Universiteit Twente
Leden:	Prof. Dr. M. Pollnau	Universiteit Twente
	Prof. Ir. A. C. van Bochove	Universiteit Twente
	Prof. Dr. Ir. W. C. van Etten	Universiteit Twente
	Prof. Ir. A. M. J. Koonen	Technische Universiteit Eindhoven
	Dr. Ir. R. G. Heideman	LioniX B.V.
	Dr. H. Venghaus	Fraunhofer Institute, Heinrich-Hertz-Institute, Berlin

Integrated Optical Microsystems Group,
University of Twente,
P.O. Box 217, 7500 AE Enschede, the Netherlands

Cover design: Adriaan Meijer

ISBN 90-365-2258-7

FLEXIBLE OPTICAL NETWORK COMPONENTS BASED ON DENSELY INTEGRATED MICRORING RESONATORS

PROEFSCHRIFT

ter verkrijging van
de graad van doctor aan de Universiteit Twente,
op gezag van de rector magnificus,
prof.dr. W.H.M. Zijm,
volgens besluit van het College voor Promoties
in het openbaar te verdedigen
op donderdag 28 oktober 2005 om 16.45 uur

door

Douwe Harmen Geuzebroek
geboren op 9 februari 1977
te Zaandam

Dit proefschrift is goedgekeurd door:
De promotor: Prof.Dr. A. Driessen

It's been a hard day's night,
and I've been working like a dog.
It's been a hard day's night,
I should be sleeping like a log.
But when I get home to you,
I find the things that you do,
will make me feel alright.

. . .

When I'm home everything seems to be alright,
When I'm home feeling you holding me tight, tight, Yeah.

. . .

You know I feel alright.

Lennon & McCartney

Abstract

This thesis addresses the design, realization and characterization of reconfigurable optical network components based on multiple microring resonators. Since thermally tunable microring resonators can be used as wavelength selective space switches, very compact devices with high complexity and flexibility can be created.

In **chapter 1** an introduction to this thesis is given by stating the context in which the work has been done. A brief overview of optical communication networks is given as well as a description of the projects in which the research has been carried out. Finally the basic properties of microring resonator filters are presented, like the Free Spectral Range and Finesse.

In **chapter 2** an application oriented top-down design approach for the microring resonator as wavelength filter is described. A scattering matrix model of a MR is used, that incorporates the coupling constants, radius and the losses. With this model the geometrical design parameters are investigated and chosen such that the network specification can be met. It comes out that for high bandwidth filtering applications the coupling constants need to be relatively large. Furthermore for a MR which drops as much power as possible, the coupling constants need to be equal. Physical layer simulations of the MR in a network environment are done that confirm the high bandwidth filtering application.

In **chapter 3** the thermal properties of a microring resonator are described. These properties allow the filter to be tuned to a specific wavelength. This way switching functions can be realized and fabrication errors and environmental temperature changes can be corrected. The basic properties of thermal tuning are explained, whereafter the design and characterization of a thermally tunable single ring is given. Several SiO_2/Si_3N_4 MRs with chromium Ω-shaped heaters were fabricated. The MRs show good reproducibility and the parameters extracted from measurements show good agreement with the designs. A thermal tunability between 11.3 pm/mW and 20 pm/mW for several different geometries is demonstrated. A method of increasing the switching speed is described, that uses an overshoot and bias of the driving signal. By using this method the rise-time of the MR response was improved by 42%, enabling modulation frequencies of 10 kHZ and switching speeds in the order of 0.1 ms.

Chapter 4 is describing the use of devices built out of more than one single MR to create complex structures with enhanced functionality. Some examples of these complex structures are described, like an optical-cross-connect, a reconfigurable λ-router and an optical network unit. The multiple MR structures are compared to their competing technologies and it is calculated that the used area can be reduced with a factor of 50 by using complex MR functions. Some examples of fabricated and measured structures based on multiple MRs are given. First a wavelength selective switch is demonstrated which has an ON/OFF ratio of 12 dB and a channel separation better than 20 dB. Second, a Vernier switch is shown which has a total Free Spectral Range of 28 nm, by combining the specifications of two rings. Finally a reconfigurable optical add-drop multiplexer is demonstrated which is made out of four MRs and which is pigtailed and packaged. It demonstrates a symmetric add and drop response with 17 dB resonance peaks. Since the tuning range of the rings is larger than the Free Spectral Range of the rings, any wavelength can be addressed. A single channel configuration could be reached by only 20 mW of driving power. A four channel configuration uses 446 mW of driving power.

Chapter 5 gives system level measurements in order to assess the performance of multi MR based structures in optical networks. It describes the system level characterization methods, - setups and the measurements on both single MR as well as multiple MR structures for 10 and 40 Gbit/s datasignals. The results show that 10 Gbit/s non-return-to-zero datasignals can be filtered by the described MR as a clear eye diagram is measured. A measurement of the groupdelay confirms this also since the delay of 7 ps does not contribute significantly at this datarate. The 40 Gbit/s return-to-zero measurement results show that the reconfigurable add-drop multiplexer can filter these signals with clear eye diagrams to all add and drop ports. A power penalty of 1 dB was measured at a bit-error-rate of 10^{-9}. The measurements also demonstrate the principle of multicasting the 40 Gbit/s signals to more than one output port at once.

Finally, in **chapter 6**, a discussion is given of the results presented in this thesis and of the use of MRs in optical telecommunication components. This discussion will lead to the conclusion that it is possible to design and realize multiple MR devices allowing high bitrate optical network components with reconfigurable functions. The chapter also gives an outlook recommending future research for multi MR structures in optical telecommunications components. In this context also some brief comments on recent picosecond pulse measurements are given, where pulses with a length in the order of the round-trip time of the MR are filtered.

Samenvatting

Dit proefschrift beschrijft het ontwerp, de realisatie en karakterisatie van herconfigureerbare optische netwerkcomponenten die gebaseerd zijn op meervoudige microringresonatoren. Omdat thermisch verstembare microringresonatoren kunnen worden gebruikt als gollfengte-selectieve schakelaars, is het mogelijk om zeer compacte componenten te maken met een grote complexiteit en flexibiliteit.

Hoofdstuk 1 is een introductie voor dit proefschrift waarin de context staat beschreven waarbinnen dit werk heeft plaatsgevonden. Een kort overzicht van optische telecommunicatienetwerken wordt gegeven, alsmede een beschrijving van de projecten waarbinnen het onderzoek heeft plaatsgevonden. Ten slotte worden de basiseigenschappen van een microringresonator (MR) behandeld.

In **Hoofdstuk 2** wordt een toepassingsgerichte ontwerpaanpak beschreven voor de MR als gollfengtefilter. Een scattering-matrix-model van de MR wordt gebruikt, dat de respons van de MR in termen van de koppelconstanten, de radius en de verliezen beschrijft. Met dit model worden de geometrische parameters van de MR onderzocht en worden deze parameters zo gekozen dat aan de netwerkspecificaties kan worden voldaan. Het blijkt dat voor breedband filterapplicaties relatief hoge koppelconstanten nodig zijn. Verder dienen de koppelconstanten zo symmetrisch mogelijk te zijn om de MR zoveel mogelijk vermogen te laten schakelen. Simulaties van de MR op the physical-layer binnen netwerkomgevingen bevestigen de

breedband filtercapaciteit van de MR filters.

In **Hoofdstuk 3** worden de thermische eigenschappen van een MR behandeld. Door deze eigenschappen kan een filter worden verstemd naar een specifieke golflengte. Op deze manier zijn schakelfuncties te creëren en kunnen fabricagefouten en omgevingsinvloeden worden gecorrigeerd. Eerst worden de basiseigenschappen van thermisch verstemmen behandeld, waarna het ontwerp en de karkakterisatie van thermisch verstembare enkele microringen wordt beschreven. Meerdere SiO_2/Si_3N_4 MRen met een chromen verwarmingselement zijn gefabriceerd, waarbij een thermische verstembaarheid van 11.3 pm/mW tot 20 pm/mW is gemeten voor verschillende filters. Een methode om de schakelsnelheid te verbeteren wordt beschreven, waarin gebruik wordt gemaakt van een overshoot en een bias om het aandrijvende signaal te optimaliseren. Op deze manier kon een verbetering van 42% worden bereikt in de rise-tijd van de respons, waardoor modulatiefrequenties van 10 kHZ of schakelsnelheden van 0.1 ms konden worden bereikt.

Hoofdstuk 4 beschrijft het gebruik van meerdere microringen om zo complexe structuren te realiseren met een uitgebreide functionaliteit. Voorbeelden van deze complexe structuren zijn onder andere een optical-cross-connect, een herconfigureerbare λ-router en een optische netwerkunit. De multi-microringstructuren worden vergeleken met hun concurrerende technologien en aangetoond wordt dat de gebruikte oppervlakte kan worden verkleind met een factor 50 door gebruik te maken van de multi-MR-structuren. Enkele voorbeelden worden gegeven van gerealiseerde structuren gebaseerd op multi-MR'en en de bijbehorende metingen. Ten eerste wordt een gollfengte-selectieve schakelaar gedemonstreerd die een AAN/UIT ratio heeft van 12 dB en een kanaalscheiding die beter is dan 20 dB. Vervolgens wordt een Vernier-schakelaar gepresenteerd die, door het combineren van de eigenschappen van twee ringen, een totale Free Spectral Range heeft van 28 nm. Tenslotte wordt een herconfigureerbare add/drop multiplexer gedemonstreerd die bestaat uit vier ringen en volledig is gepigtailed en behuisd. Het component laat symmetrisch add- en dropgedrag zien met een resonantiepiek van 17 dB. Omdat het verstembereik van de ringen groter is dan hun Free Spectral Range, kan iedere golflengte worden geadresseerd. De multiplexer kan in een enkel-kanaal-configuratie

worden gesteld met een aandrijfvermogen van 20 mW en in een vier-kanaal configuratie met een vermogen van 446 mW.

Hoofdstuk 5 geeft de systeemniveau-metingen weer die zijn gedaan om het gedrag van multi MR-structuren in optische netwerken te bepalen. De resultaten laten zien dat een 10 Gbit/s non-return-to-zero datasignaal kan worden gefilterd, omdat een duidelijk open oog-patroon is gemeten. Een meting aan de groupdelay van de MR bevestigt dit, omdat een vertraging van 7 ps geen significante bijdrage levert aan deze snelheid. De resultaten met een 40 Gbit/s return-to-zero datasignaal tonen aan dat de herconfigureerbare add/drop multiplexer deze signalen kan filteren met open oog-patronen voor alle in- en uitgangspoorten. Een power-penalty van 1 dB is gemeten bij een Bit-Error-Rate van 10^{-9}. De metingen tonen tevens dat deze structuren de mogelijkheid bieden om de 40 Gbit/s datasignalen te multicasten naar meer dan n uitgang tegelijk.

Tenslotte worden in **Hoofdstuk 6** de resultaten uiteengezet die worden gepresenteerd in dit proefschrift. De discussie van deze resultaten leidt tot de conclusie dat het mogelijk is om om multi MR-structuren te ontwerpen en te realiseren, die datasignalen met grote bandbreedte kunnen filteren. Zo kunnen deze MR structuren leiden tot optische netwerkcomponenten met herconfigureerbare complexe functies. De aanbevelingen in dit hoofdstuk kunnen leiden tot toekomstig onderzoek op het gebied van multi MR-structuren voor optische telecommunicatienetwerken. Binnen deze context wordt tevens een korte beschrijving geven van recente picosecondemetingen, waarbij de duur van de puls ongeveer even groot is als de rondgangtijd van de microring.

Contents

CHAPTER 1

Introduction

This chapter gives an introduction to this thesis by stating the context in which the work has been done. A brief overview of optical communication networks will be given as well as a description of the projects in which the research has been carried out. Finally the basic properties of microring resonator filters are presented.

Parts of this chapter were extracted from:

Geuzebroek, D.H. and A. Driessen "Ring Resonator Based Wavelength Filters", in *Wavelength Filters For Fiber Optics*, Venghaus, H (edt.), to be published 2006

1.1 Preface

This thesis deals with a topic that is covered by the term *telecommunication*. All the activities, both academic as well as commercial, within this particular branch is driven by the ever increasing demand for data-transport facilities. Since the Internet has dramatically changed the way we work, communicate, relax or in general how we live, the demand for data bandwidth will keep on rising. Every forecast of any subject related to the demand and transport of data, shows rising graphs. Maybe the only exception to this is the profitability of the commercial activities, especially in optical telecommunications, in the past few years. Currently however, positive sounds are appearing showing prudence effort with commercial investments in optical telecommunications.

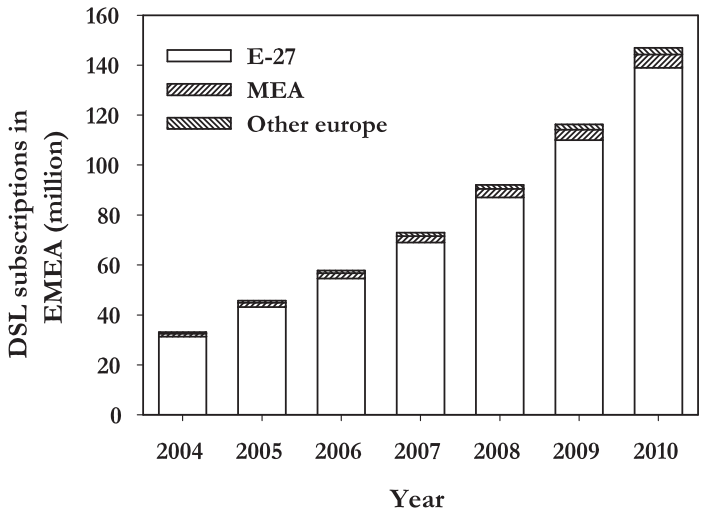

FIGURE 1.1: Expected number of DSL subscriptions in EMEA with compound annual growth rate of 26% [1]

A positive side of the telecommunication downturn, was in the increase in academic interest in this area. Topics, like how to decrease operating cost and manageability of telecommunication networks, are now thoroughly investigated. All these activities are driven by the potential demand of a broadband data connection for every household. Which needs low cost components, since the costs

can not be shared, and manageable network components since large numbers of customers with changing demands need to be handled.

Meanwhile the demand for bandwidth keeps on growing. For example the amount of broadband Digital-Subscriber-Lines (DSL) subscriptions in 2004 in Europe, Middle East and Afrika (EMEA) was 33.1 million of which 95% in the 27 largest European countries [1]. Figure 1.1 shows a market prediction [1] that shows that in 2010 this will be increased to 146.9 million in 2010, with a compound annual growth rate of 26%. The question remains what is regarded as a broadband connection. Sometimes anything with a higher bandwidth as an analog modem was regarded as broadband. Weldon [2] states that currently a broadband connection is one that exceeds 24 Mbit/s. Furthermore, in the near future real broadband connections should have a bitrate of 50 to 100 Mbit/s and in 5 to 10 years this will exceed 1 Gbit/s . These numbers are driven by the applications which consume

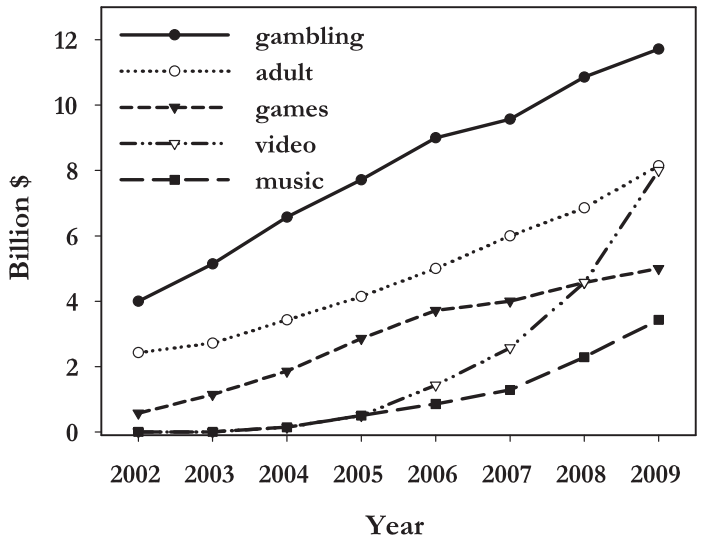

FIGURE 1.2: Predicted broadband online entertainment market for various drivers [1]

more and more bandwidth like Video-on-demand, were high quality video stream are streamed towards the customer. As is shown in Figure 1.2 the applications concerning video will have a strong increase in application, driven on one side by

the demand for video services and on the other hand by the bandwidth available. But this will not be the big cash-cow everybody was searching for. The increase for bandwidth will most likely come from a process now known as "triple-play", were telephone, television and (internet) data-services are combined. Extending this towards more services, like e.g. remote computing, together with lots of users per household (all machines will have an IP number, even the refrigerator), "multiple-play" service will demand more bandwidth. Furthermore a change in data traffic direction can be noticed, since more and more users are also uploading data for peer-to-peer networks or distributed computation. This changes the network from being asymmetric (more toward customer) into a symmetric one.

According to [2,3] the only way to be able to meet these demands is the optical implementation.

1.2 Optical Telecommunication Networks

Since more than 30 years optical telecommunication networks have been in the spotlight, of both academic as well as industrial research, as the most promising method of transporting large amounts of data over large distances. In [4] a system capacity, incorporating both the practical amplification window (80 nm) and non-linear system impairments, is in the order of 150 Tb/s . This kind of capacities are possible since the introduction of low loss fibers together with amplification in the optical domain. By the introduction of wavelength division multiplexing (WDM) very high speed point to point connections became possible which made as much as possible use of the available bandwidth (high spectral efficiency).

(Optical) networks can be divided into three categories according to the average span between the network nodes and the bandwidth used. Wide Area Networks (WAN) span typically several hundreds to thousands of kilometers with total bitrates of Tbit/s. A Metropolitan Area Network (MAN) spans normally the area of a large city up to several hundreds of kilometers. The Access Network (AN) connects the end-user to the higher level networks and can span up to a few tens of kilometers.

The transport of data between the network nodes in WAN and MAN network are already nearly all optical, since there is no good competing technology which can span large distances with low loss and high bitrates. The network nodes, switching and routing the data through the network, are still electrical since all-optical techniques have not yet matured. The transport of data in the AN is still done by the electrical counterparts, like Digital Subscriber Lines (xDSL) and cable access. Though optical techniques are customary for use in the Internet backbone, fiber connections to the home (FTTH) or office building (FTTB) so far only are implemented in densely populated areas were no fibers have to be put into the ground. In these areas, like the urban regions in Japan, point-to-point FTTH is employed successfully. However in less dense populated areas FTTH still proved to be too expensive. Several developments are aimed at reducing the costs of optical access methods.

1.3 Fiber to the Home

A lot of effort has been done in investigation of bringing the fiber into the customers homes. When fiber to the home (FTTH) is discussed the following statement from Mattew Peach sets the right context: "*FTTH is a bit like politics. Almost everybody has an opinion about it but not many people know what's really happening, pretty much until after it has happened. And as with politics, there is a range of views as diverse as society itself*". [5]

1.3.1 Passive Optical Networks

First of all, the type of optical network is a factor of major influence. When opting for an optical access network, there are several possible layouts [3] of which the three mainly used are schematically given in Figure 1.3. The first is a point-to-point dedicated fiber connection for each subscriber. This option requires significant amounts of fiber to be deployed, and would therefore be a very costly architecture as subscribers are mostly located at rather large distances from the access provider. The solution for this could be found in a local switch closer to

the subscribers. This would lead to a reduction in fiber use, but requires an active component in the field that needs to be powered, which might be expensive to maintain. The most attractive option is the Passive Optical Network (PON,

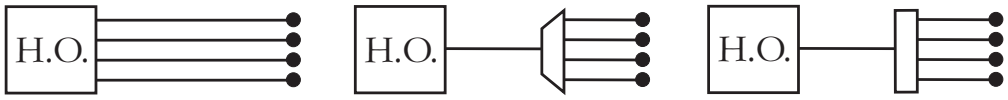

FIGURE 1.3: Schematic drawing of different FTTH network; point-to-point (left), active star (middle) and passive splitter (right)

right picture in Figure 1.3). This layout requires no active switching or routing in the network or any of its components (hence passive). An optical splitter is used to divide the data stream, thus creating a point-to-multipoint network. The end user will be equipped with a transceiver, capable of switching to a certain channel. This could be done by wavelength division multiplexing (WDM) or time division multiplexing (TDM), sharing the same connection by either separate wavelengths or time slots for each transceiver. All the active equipment will be localized in the head-office (H.O.), allowing easy maintenance.

Until now FTTH deployments, especially the PON layout, does not meet its expectations. Although a lot of fiber is brought towards the end customers homes [6], this is mainly facilitated by point-to-point layouts to (newly build) premises. Since the electrical competing technologies like Cable and xDSL can still also meet the bandwidth demands, they have the competing edge of an already present infrastructure. However when the demand for bandwidth keeps rising, FTTH is by many foreseen as the only capable infrastructure [2, 3]. xDSL might even be a driver, instead of a competitor, since the currently large demand for DSL connections lead to more fiber network advancing towards the premises [7].

The key issues in FTTH will be cost and manageability. This thesis will discuss efforts to lower the (component) costs and increase the manageability by integrating complex reconfigurable functions.

1.4 Integrated optics

As was discussed in [8] currently 90% and in future around still 70%, of the costs of optical components is in packaging. Therefore integrating as many functions as possible is desired for low cost components. It is especially attractive when the components can be made with standard processes in mass-production scale. Furthermore a flexible building block is required that can be used for filtering and switching functions and that is suitable for integration. This thesis will discuss the use of integrated optic microring resonators as building block for low cost, highly flexible and high bandwidth optical network components.

1.5 Microring resonator

Microring resonators (MR) represent a class of filters with characteristics very similar to those of Fabry-Perot filters. However, they offer the advantage that the injected and reflected signals are separated in individual waveguides, and in addition, their design does not require any facets or gratings and is thus particularly simple. MRs evolved from the fields of fibre optic ring resonators and micron scale droplets [9–12]. Their inherently small size (with typical diameters in the range between several to tens of micrometers), their filter characteristics and their potential for being used in complex and flexible configurations make these devices particularly attractive for integrated optics or VLSI photonics applications [13–18]. As will be outlined in the following, MRs are used in filter applications, delay lines, as add/drop multiplexers and modulators, while other applications in optical sensing, spectroscopy or coherent light generation (MR lasers) are outside the scope of this thesis. In the following the 4-port microring serving as a wavelength filter is discussed, while the 2-port operation of microrings as is used in [19] is not covered. This chapter starts with the basic principles and the functional behaviour of a single microring resonator which are needed for the understanding of the following chapters.

1.5.1 Fundamental aspects

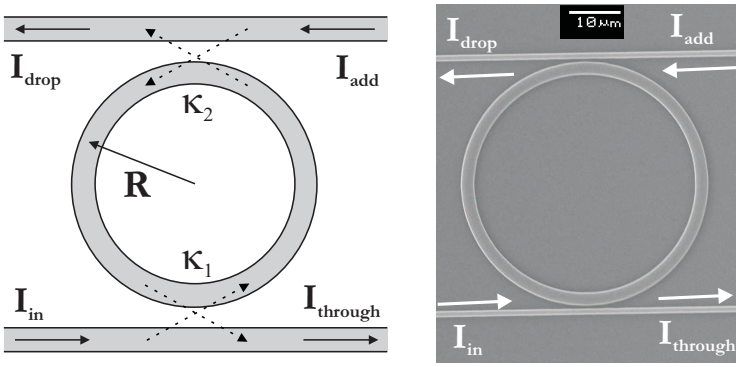

FIGURE 1.4: Schematic drawing of a microring resonator (right) and SEM picture (left) with in- and output port waveguides

A basic schematic drawing of a MR is shown in Figure 1.4. The structure consists of a ring waveguide with radius R and two straight port waveguides. The ring and port waveguides are evanescently coupled; a fraction κ of the incoming power is coupled to the ring. When the optical path-length of a roundtrip is a multiple of the effective wavelength constructive interference occurs and light is 'built up' inside the ring: the MR is ON resonance. As a consequence, periodic fringes appear in the wavelength response at the output ports as is shown in Figure 1.5. At resonance the drop port shows maximum transmission since a fraction κ_2 of the build up power inside the ring is coupled to this port. In the through port the ring exhibits a minimum at resonance. In the ideal case with equal coupling constants, at resonance all the power is directed to the drop port. An additional 180° phaseshift of the light coupled back to the through port after a roundtrip with respect to the light coming directly from the in port, causes at resonance full extraction of the light in this port.

Before coming to a more detailed description of MRs it is worthwhile to introduce a number of key parameters of MRs. The difference in position between two consecutive resonant peaks, see Figure 1.5, is called the Free Spectral Range and can be defined either in the frequency or wavelength domain (FSR_f or FSR_λ,

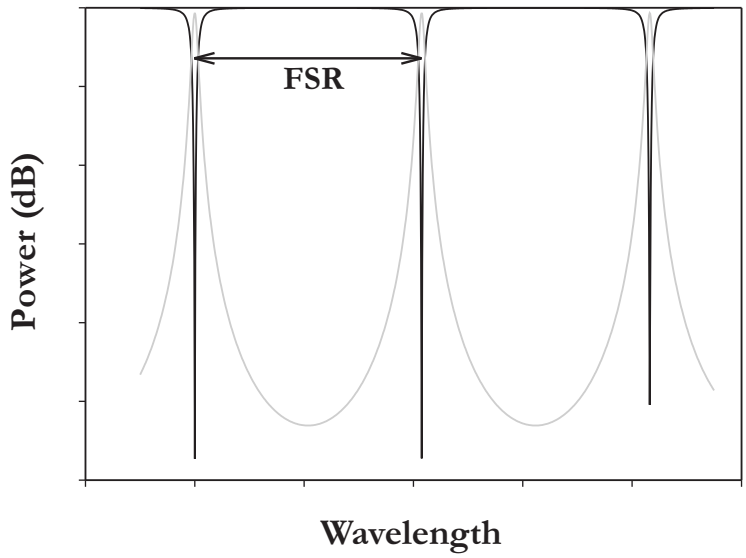

FIGURE 1.5: Simulated response of a MR for the through- (black) and drop port (grey). Also shown is the Free Spectral Range, the distance between two consecutive fringes

respectively):

$$FSR_f = \Delta f = \frac{c}{n_g 2\pi R}, FSR_\lambda = \Delta\lambda \approx \frac{\lambda_0^2}{n_g 2\pi R} \tag{1.1}$$

with n_g the group index [17]

$$n_g = n_{eff}(f_0) + f_0 \frac{dn_{eff}}{df}\Big|_{f_0} = n_{eff}(\lambda_0) - \lambda_0 \frac{dn_{eff}}{d\lambda}\Big|_{\lambda_0} \tag{1.2}$$

With n_{eff} the effective index, R the radius of the ring, c the speed of light in vacuum and f_0 is the center frequency, i.e. the frequency where the length of the optical path in the ring is equal to an integer multiple of the wavelength, also indicated by the resonance frequency of the MR. Analogous λ_0 is defined as the resonance wavelength of a MR. Another important parameter of the MR is the Full Width Half Maximum ($FWHM$) or 3-dB bandwidth, which is a measure for the bandwidth of the device. A quality measure of the microring is the Finesse F

which is the ratio between the *FSR* and the 3-dB bandwidth [20].

$$F = \frac{FSR}{FWHM} = \frac{\pi(X_1X_2)^{1/4}}{1-(X_1X_2)^{1/2}} \tag{1.3}$$

$$X_i = \sqrt{(1-\kappa_i^2)}e^{L_r\alpha} \tag{1.4}$$

With κ the abovementioned fraction of the field coupled to the ring, α the losses per length inside the ring and L_r the length of the optical path in the ring. High Finesse devices have a small *FWHM* and a strong intensity build-up in the ring when in resonance. Therefore high F devices are suitable for applications were high intensities in the cavity are necessary like lasers or non-linear optical (NLO) devices. Instead of the Finesse also the quality factor Q can be used as an absolute measure for the wavelength selectivity of the microring resonator according to:

$$Q = \omega_0/\Delta\omega_{FWHM} = \lambda_0/\Delta\lambda_{FWHM} \tag{1.5}$$

Where $\Delta\omega_{FWHM}$ and $\Delta\lambda_{FWHM}$ are the respectively 3-dB bandwidths in frequency and wavelength domain. The speed of high bit-rate communication is limited by the bandwidth of the optical filters. As this bandwidth in high Finesse MRs devices is becoming increasingly small only medium Finesse devices ($F \sim$ 10 - 20) with relative large coupling constants ($\kappa \sim$ 0.4-0.6) are employed for these applications as will be shown in the next chapter. The *FWHM* is determined by the coupling constants and the loss inside the ring according to [21, 22]:

$$FWHM_f = \frac{c}{2\pi R n_g}\left(\frac{\sqrt{X_1X_2}}{\pi\sqrt[4]{X_1X_2}}\right) \tag{1.6}$$

1.5.2 Bent waveguides

Bent waveguides exhibit radiation losses, which -for a given confinement of the guided wave- increase as the bend radius decreases. On the other hand, for a given bend radius, the bending losses decrease, as the confinement of the guided wave gets stronger, or alternatively spoken, the bending losses decrease, as the (effective) index contrast between the ring and its surrounding/substrate increases.

In the following we will focus on high index contrast rings (n > 0.1), since this is a prerequisite for small footprint devices offering the required integration potential. In relation to the index contrast the term 'minimum bend radius' is used to define the lowest acceptable (technology-dependent!) radius keeping the bend losses sufficiently low. 'Sufficiently low' is dependent of the application and also related to the coupling fractions as this chapter will show. Typically one designs for a bending loss below 1 dB per 360° roundtrip. The minimum bend radius as a function of effective index contrast is illustrated in Figure 1.6. As can be seen, a high index contrast enables extremely small dimensions and thus compact structures, but at the same time puts severe challenges to the fabrication technology. In addition, the stronger the confinement and the smaller the ring dimensions the more polarization related issues become important. On the one hand, polarization dependence is strongly dependent on symmetry in strongly guiding waveguides. However, even if a chosen geometry would exhibit low birefringence in a straight waveguide (i.e. the propagation constants for TE- and TM-polarized light are approximately the same [23]) this is normally no longer true in bends or rings with small radii. In that case, the modes are no longer pure TE- or TM-like, the resonance wavelengths and other filter characteristics become polarization dependent and even polarization conversion can occur [21,24,25]. Thus polarization independence does either require a specific design and an advanced technology [24], or one has to resort to polarization diversity [26]. On the other hand, the polarization behaviour can be used to make polarization converters.

1.5.3 Other MR geometries

The shape of MRs is evidently not restricted to a circle. Nearly any geometrical path that provides optical feedback will act like the microring. An often used geometry is the racetrack [27] which is shown in Figure 1.7. In this geometry the couplers of the resonator are straight waveguides that allow accurate control of the coupling constants at the expense of being somewhat larger and leading consequently to a reduced FSR. Another common shape is the disk [28] instead of a ring as shown in Figure 1.7. A disk is more difficult to make single mode,

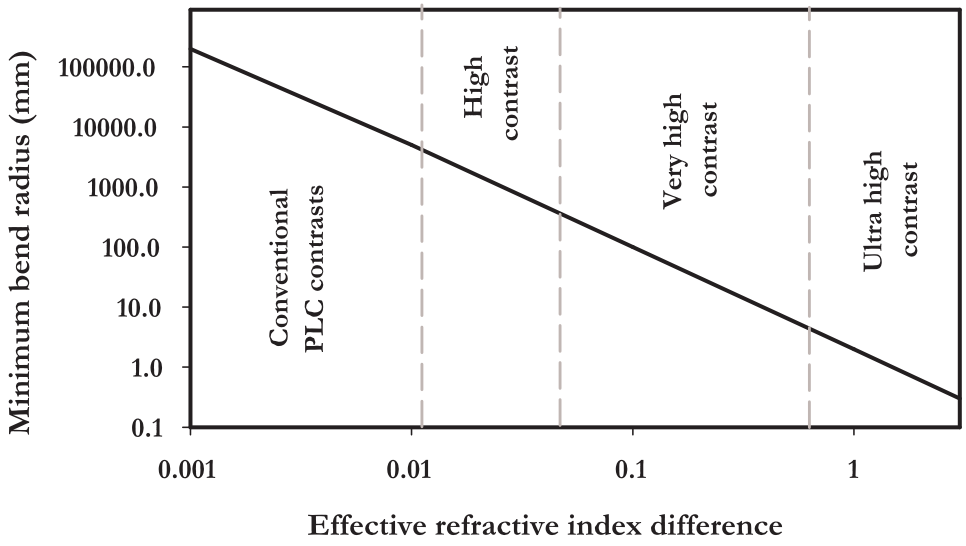

FIGURE 1.6: Effective contrast versus minimum bending radius (< 1 dB/90°).

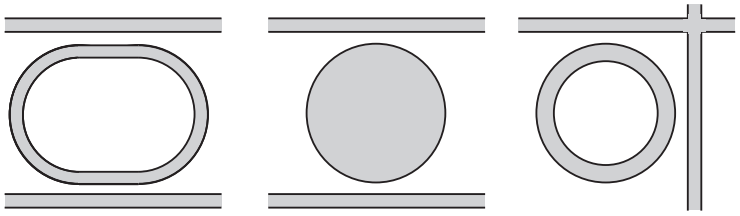

FIGURE 1.7: Other Microring resonator shapes: Racetrack (left), disk (middle) and Manhattan configuration (right)

since the lateral width of the cross section is large. But since the lateral contrast of the disk is higher than the contrast for a ring, potentially lower losses can be obtained. The place of the adjacent waveguides is not important. As can be seen from equation (2.4) only the total roundtrip length influences the response and not the place of the coupling regions. Another common shape therefore is the so called cross-grid or Manhattan [29] configuration as is shown in Figure 1.7. This structure allows for very optimal use of area and is in large extend scalable.

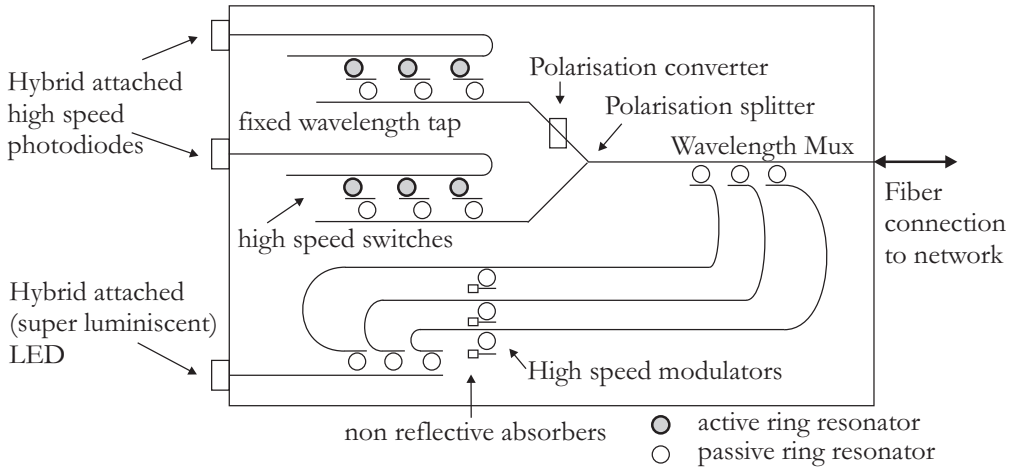

FIGURE 1.8: Integrated subsystem (transceiver) based on active and passive microring resonators

1.6 Projects

This section gives a brief overview of the research projects within which the results described in this thesis were obtained.

EC-IST project NAIS

The EC-funded project NAIS (Next-generation Active Integrated-optic Subsystems) aims to develop existing integrated optical microresonator technology into a robust, densely-integrated active photonic platform, to create an optical subsystem on a chip. The subsystem as is shown in Figure 1.8 combines functions such as high-speed optical switching, modulation, and wavelength multiplexing and filtering, in a scalable manner, to eventually handle hundreds of optical information channels. These functions are becoming increasingly vital to realize fiber optic access networks that provide high-bandwidth telecommunications services to the home or desktop. By using optical microresonator technology and organic electro-optic materials large-scale photonic integration of active functions is feasible. A new generation integrated optic technology is developed that eventually leads to low-power, highly manufacturable and hence low-cost network subsystems on a chip, which can be deployed in optical network nodes. For the realisation of the

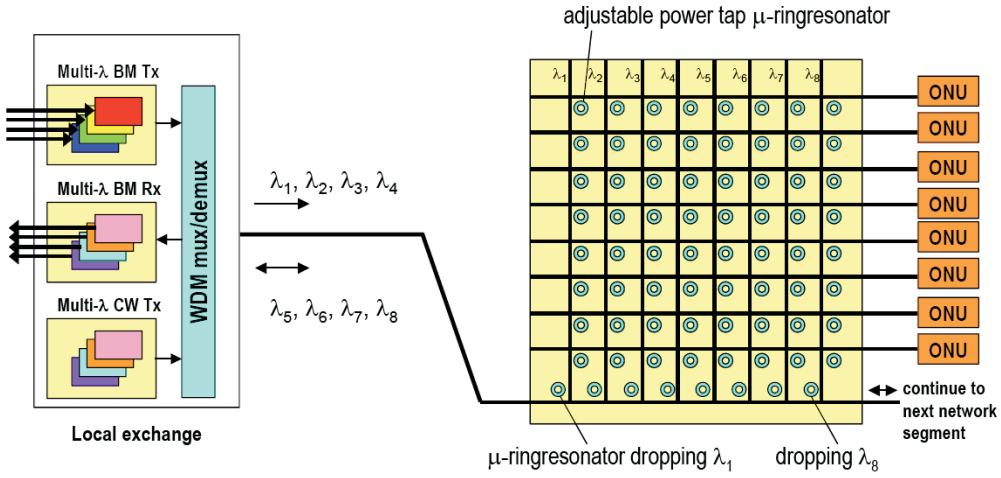

FIGURE 1.9: Integrated wavelength multi-casting router, using thermally tunable micro-ringresonators, applied in a tree-and-branch access network topology

final deliverable, a subsystems with active functions, a chain of activities is carried out that include the study of the materials aspects of special passive and organic electro-optic optical materials, development and application of new design tools, the technological realization and the detailed characterization of devices. Parallel to these activities system studies are performed in order to supply specifications and assure the relevance of the new devices and subsystems. Special attention is given to the manufacturability and a possible route to large scale, low-cost production of the proposed subsystems.

Dutch Freeband Broadband Photonics project

In the Dutch Freeband Communications project "BroadBand Photonics" a dynamically reconfigurable broadband photonic access networks is investigated. The project aims to develop and validate a novel system concept, which will enable to provide congestion-free access to users with traffic demands fluctuating in time and in place. A dynamic network reconfiguration techniques will be explored, based on optical wavelength routing in the optical fibre feeder part of these (hybrid) access networks. The project will approach the goal of a reconfigurable access network along two tracks. First the network topologies and functionalities will be investi-

gated, which provide reconfigurability while minimizing installation and operation costs, enhancing network availability, and facilitating network maintenance. Second the possibilities for advanced integration of the optical and electrical functions will be investigated, yielding more compact, cheaper, more reliable and less power consuming devices; in particular for the most cost-sensitive sites, namely the wavelength routing site and the user site.

One of the parts under investigation is a reconfigurable multicast lambda-router based on thermally tunable MRs as is depicted in Figure 1.9. Using a high level of integration in passive optical integrated circuit technology (silicon oxynitride), the concept deploys micro-ring resonators, which can thermally be tuned to select a specific wavelength for dropping from a waveguide to another waveguide. As shown in Figure 1.9, a matrix of micro-ringresonators is put within a rectangular grid of waveguides, in order to select wavelengths and to partially couple power into outgoing waveguides feeding the Optical-Network-Units (ONU) at the user site. In the same way, upstream signals from the ONU-s are guided by the router via the feeder fibre to the local exchange.

1.7 Outline

This thesis is structured as follows: After the brief introduction of the microring resonator fundamentals in the current chapter, a more detailed discussion will be given in **chapter 2**. In that chapter an application oriented top-down design approach for the microring resonator as wavelength filter will be given. With the aid of a scattering matrix model of a MR, a geometrical design can be made which meets the demands of the network specifications. Finally physical layer simulations of the MR in a network environment will be described which confirm the geometrical design.

In **chapter 3** the thermal properties of a micro ring resonator will be described. These properties allow the filter to be tuned to a specific resonance wavelength. This way switching functions can be implemented. In addition fabrication errors and environmental temperature changes can dynamically be corrected. The

basic properties of thermally tuning will be explained as well as the design and characterization of a thermally tunable single ring will be given.

Chapter 4 describes the use of devices built out of more than one MR to create complex structures. Also a comparison is made with alternative technologies. Examples of fabricated and measured structures based of multiple MRs will be given, like a wavelength selective switch, a Vernier switch and a reconfigurable optical add-drop multiplexer.

To see if multi MR based structures can perform in optical networks, system level measurements have been performed which will be described in **chapter 5**. This chapter describes the system level characterization methods, - setups and the measurements on both single MR as well as multiple MR structures for 10 and 40 Gbit/s datasignals.

Finally in **chapter 6** some conclusions will be given and some relevant issues are discussed. The chapter will be finalized with an outlook to the future of multiple microring resonator structures and presented in a tentative roadmap.

CHAPTER 2

Top-Down Design of Microring resonators

This chapter describes an application oriented top-down design approach for the microring resonator as wavelength filter. With the aid of a scattering matrix model of a MR, a geometrical design can be made which meet the demands of the network specification. Physical layer simulations of the MR in a network environment have been done to confirm this.

Parts of this chapter were extracted from:

Geuzebroek, D.H. and A. Driessen "Ring Resonator Based Wavelength Filters", in *Wavelength Filters For Fiber Optics*, Venghaus, H (edt.), to be published 2006

2.1 Introduction

In an application oriented design of a MR for use as wavelength filter one conveniently follows a top-down approach starting on a high level of abstraction working the way down to geometrical physical parameters. First the MR is modelled at a high level to incorporate the system level requirements as expressed in specifications. In our case this is done by the scattering matrix approach. Once the desired parameters are determined a concrete geometrical design for a specific technology can be made. This is of course not a serial design approach and some iteration is needed, since realizable specifications are limited among others by the technology used. Polarization related issues are not taken into account and are neglected by assuming a single polarization state, or adapting the system by, e.g. polarization diversity.

2.2 Network level parameters

When designing microring resonators as wavelength filters in telecommunication networks, first some network level parameters need to be defined. These parameters are the basis for designing the microring structures used in this thesis. Figure 2.1 gives a brief overview of some important parameters: Crosstalk, Bandwidth, Insertion Loss (IL) and channel spacing. Linear crosstalk can be defined in

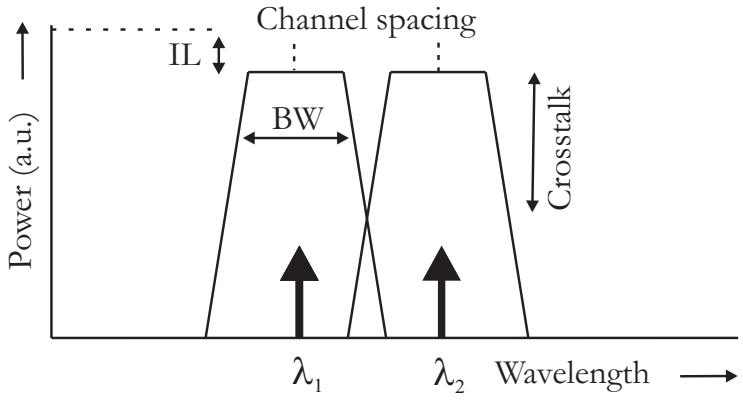

FIGURE 2.1: Parameters of wavelength filter

two categories. When interference occurs from power of a neighbouring channels it is called out-of-band crosstalk. When due to switching and routing two different signals are interfering on the same channel it is called in-band crosstalk. The bandwidth of a filter is defined as the -3dB width of the peak power at the center wavelength. The insertion loss is the decrease in average power in the passband of the filter. The channel spacing is the distance between the center wavelengths of two consecutive filters.

Furthermore some parameters are used to qualify a system carrying information bit patterns. The power penalty is the increase in received optical power needed to compensate for the impairments with respect to the ideal (back-to-back) case. The Bit-Error-Rate (BER) is the average probability of incorrect bit identification [4]

2.3 z-transform

The z-transform is a widely used description in digital filter theory, where filters are constructed with different standard delays. As is done in [17] also optical filters can be described this way. Especially Mach-Zehnder Interferometers (MZI) or MRs can be described by z-transform. For a MZI the filter response is constructed out of different combinations of standard delays in the feedforward paths. For a MR the standard delays are constructed by the optical feedback paths. Using the z-transform has the advantage of simplified mathematical description and the use of standard (digital) filter design techniques.

A MR can be modelled by writing the roundtrip phase in terms of a multiple of unit delay $T = 2\pi R n_{eff}/c = 1/FSR_f$. Then by substituting the z parameter according to

$$e^{-j\omega T} = z^{-1} \tag{2.1}$$

with $\omega = 2\pi f$ the angular frequency. An output field constructed out of N feedback paths can now be described as

$$E_{out}(z) = E_0 + E_1 z^{-1} + \cdots + E_{N-1} z^{N-1} \tag{2.2}$$

2.4 Top-down design model

One frequently chosen way of modelling the response of a single MR without explicit inclusion of polarization issues is the use of a scattering matrix [17,30,31]. In many cases this approach is sufficient for the derivation of concrete geometrical design parameters for different material systems such as III-V semiconductors, SiON etc. The MR is then modelled as two couplers and two delays ϕ_1 and ϕ_2 in-between as is shown in Figure 2.2. The couplers couple a fraction κ_1 or κ_2 of the field over to the cross port and a fraction $\mu_{1,2} = \sqrt{1-\kappa_{1,2}^2}$ to the bar port. $\gamma = 10^{-\alpha L/20}$ is the loss per roundtrip, where αL is the loss in dB for one roundtrip and L the optical path length. The delays in Figure 2.2 are related to the frequency and the optical path-length $L = L_{opt1} + L_{opt2}$ as $\Phi_{1,2} = \frac{\omega L_{opt1,2}}{c}$, which are not necessarily identical to each other. As has been shown in section 1.5.3, the exact position of the couplers does not matter, as long as the total roundtrip phase is the same.

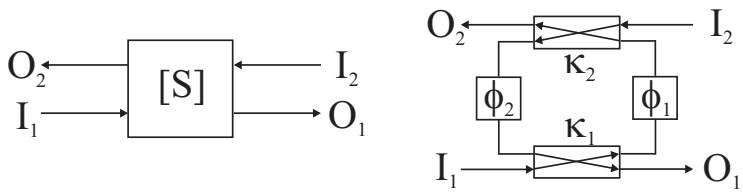

FIGURE 2.2: Scattering matrix model of a microring resonator

When looking at the optical field in drop port (O_2), it is build up out of several roundtrips. First a fraction of the incoming field ($\kappa_1\kappa_2$) is dropped after half a roundtrip (γz^{-1}). Secondly light is dropped going one roundtrip ($\kappa_1\kappa_2\mu_1\mu_2\gamma z^{-1}$). This leads to an infinite sum connecting the drop port to the in port according [17]:

$$O_2(z) = -\kappa_1\kappa_2\gamma z^{-1}[1 + \mu_1\mu_2\gamma z^{-1} + (\mu_1\mu_2\gamma)^2 z^{-2} + ...]I_1(z) \tag{2.3}$$

The transfer function connecting the drop port to the in port is:

$$H_{drop}(z) = \frac{O_2(z)}{I_1(z)} = \frac{-\kappa_1\kappa_2\sqrt{\gamma z^{-1}}}{1 - \mu_1\mu_2\gamma z^{-1}} \tag{2.4}$$

Similarly the one can derive for the field at the through-port as function of the input port field:

$$O_1(z) = \mu_1 - \kappa_1^2 \mu_2 \gamma z^{-1}[1 + \mu_1\mu_2\gamma z^{-1} + (\mu_1\mu_2\gamma)^2 * z^{-2} + ...]I_1(z) \tag{2.5}$$

this leads to the transfer function

$$H_{thr}(z) = \frac{O_1(z)}{I_1(z)} = \frac{\mu_1 - \mu_2\gamma z^{-1}}{1 - \mu_1\mu_2\gamma z^{-1}} \tag{2.6}$$

Deriving the transfer function for every combination of in- and output ports leads to the following scattering matrix connecting al inputs to all outputs:

$$\begin{bmatrix} O_1 \\ O_2 \end{bmatrix} = \begin{bmatrix} S_{11} & S_{12} \\ S_{21} & S_{22} \end{bmatrix} \begin{bmatrix} I_1 \\ I_2 \end{bmatrix} \tag{2.7}$$

Where S_{11} and S_{12} are the transferfunctions from equation 2.4 and 2.6 respectively. For the other matrix elements the following holds:

$$S_{21} = -S_{12} \tag{2.8}$$

$$S_{22} = \frac{\mu_2 - \mu_1\gamma z^{-1}}{1 - \mu_1\mu_2\gamma z^{-1}} \tag{2.9}$$

2.5 Design rules/dependencies MR

By use of the scattering matrix model one can extract from the desired functional behaviour and a given loss and radius, values for the coupling constants. For example, in order to have as much power in the drop port as possible the two coupling constants must be the same [32]. In this case the device is said to be symmetric and has the lowest possible insertion loss in the drop port. Different parameters are found when optimizing the extinction ratio between the drop and through port. In that case the MR must be critically coupled [33], that means $\mu_1 = \mu_2\alpha_r$. Under this condition all power is extracted from the through-port leading to the highest possible extinction ratio.

With the scattering matrix model, also the influence of the loss parameter on the response can be determined. System related design issues like filtering bandwidth, insertion loss, crosstalk and channel separation can be determined in this way. Three examples of this are given in the following. Figure 2.3 shows

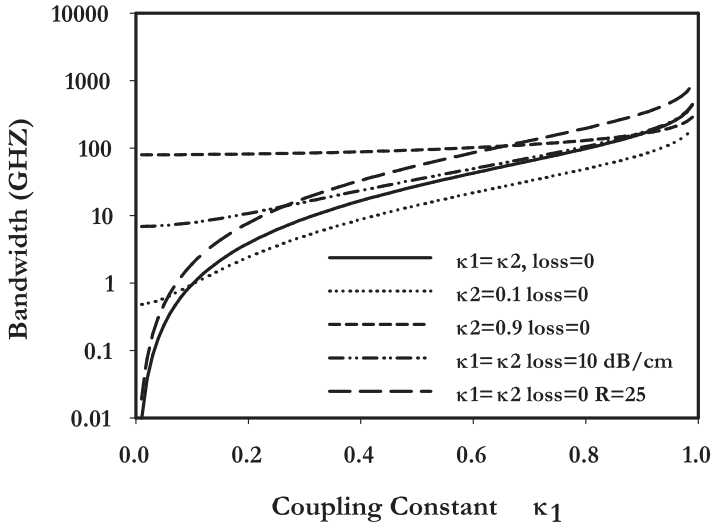

FIGURE 2.3: Bandwidth of a MR as a function of coupling constant κ_1

the 3-dB bandwidth of a microring based filter with radius of 50 μm, as given by Eq. 1.6, dependent on the coupling constant κ_1. The bandwidth increases as the coupling ratio gets higher. Also the effect of asymmetry in coupling is shown in the figure by the lines with a fixed κ_2. Losses do not have a large impact on the bandwidth. Only at the lower coupling constants a difference can be seen. In this region the finesse of the ring is higher and so more roundtrips are made. From the bandwidth dependence of Figure 2.3 one could conclude that having κ_2 fixed to 0.9 is favourable, since it allows for high bandwidths over a long range of κ_1. But when looking at the other specifications, this conclusion might be premature. For example Figure 2.4 shows the insertion loss in the drop port of a microring resonator as a function of the coupling constant κ_1 for a MR on resonance. The

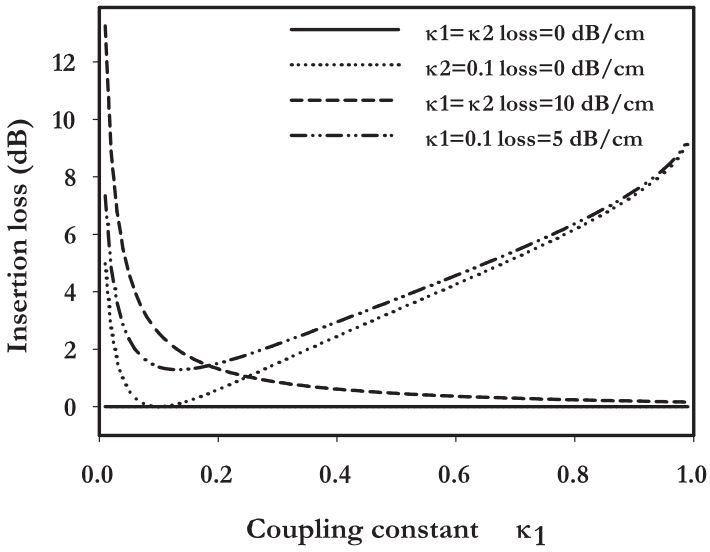

FIGURE 2.4: Insertion loss for signals sent to the drop port as function of the coupling constant κ_1 for a MR on resonance.

insertion loss (IL_{drop}) can be calculated according to: [20, 32]

$$IL_{drop} = -10 \log \left(\frac{\kappa_1 \kappa_2 e^{-2\pi R}}{(1 - \sqrt{X_1 X_2})^2} \right) \tag{2.10}$$

A symmetric lossless device has no insertion loss as can be seen from the solid line in Figure 2.4. When the ring has losses, the insertion loss is increasing, especially at lower coupling constants. Asymmetry in the coupling constants causes the insertion loss to increase, also at large coupling constants. So for low insertion loss devices with bandwidths exceeding 10 GHz, the ring must be designed symmetrically with coupling constants above 0.4. When optimizing for the maximum field inside the cavity as needed, for example, in all-optical switching, totally different specifications are obtained. Then the coupling constants must be in the order of 0.1 as is described in [34] and as can be seen in Figure 2.5. The intra-cavity power ($Pcav$) has a maximum when the coupling constant is symmetric and relatively small (around 0.1). The scattering matrix model comes out to be a good way of designing a single microring resonator, especially when an optimization has to

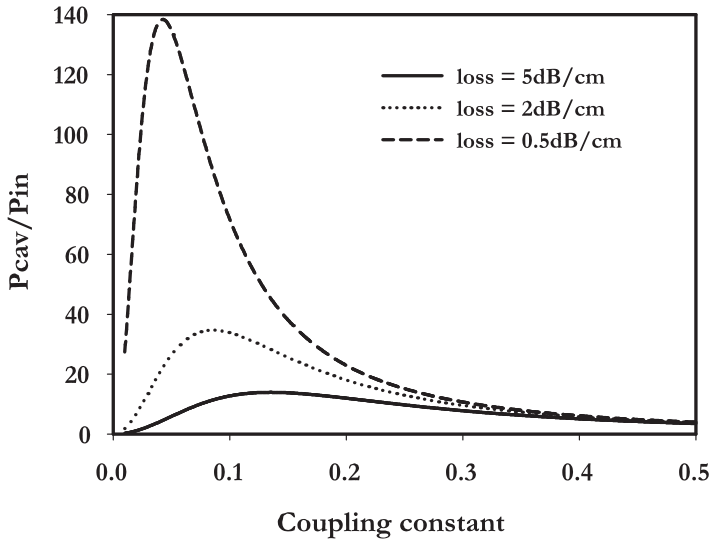

FIGURE 2.5: Power inside cavity as function of coupled fraction assuming symmetric coupling for a ring with radius R=50 μm

be made with respect to a set of specifications. Furthermore, this model allows for extracting 'experimental' parameters by fitting the model to measured data. In doing so, the realized device can be characterized and be compared with the original design. The scattering matrix model can also be used for the design of complex devices. Cascading more than one ring can simply be expressed by matrix multiplication, as will be shown in chapter 4.

A parameter which has not been addressed until now is the ring radius R. This parameter or more precisely, the optical roundtrip pathlength, determines directly the FSR. Also the roundtrip losses and consequently the finesse, are very sensitive to the radius. For telecom applications in the third telecom window, it is useful to have a FSR larger than this window. This implies very small rings $R< 6$ μm, made in a high index contrast technology to avoid excessive bending losses. The trade-off between the FSR and resonator losses can be circumvented by using more than one ring. When two rings of different radii are used, the Vernier effect [35–37] causes the total FSR to be a multiple of the respective single ring FSR according

to:

$$FSR_{tot} = N \cdot FSR_1 = M \cdot FSR_2 \tag{2.11}$$

with N,M integers without common devisor.

2.6 Group delay and dispersion

For applications in telecommunication the time behaviour of the micro ring or alternatively the wavelength response to a time-varying signal is of great importance. Since the filter is a resonant filter, the delay will be dependent on the position with respect to the resonance wavelength. The wavelength dependence of the delay is called the dispersion. Since (pulse) modulated signal have a certain width in their spectrum, different components of the modulated signal have a different delay causing spreading of the pulse in time resulting in Inter-Symbol-Interference. There are different causes for dispersion and can be distinguished into four types: material-, waveguide-, multimode- and structural dispersion [17, 31, 38].

Material dispersion

Material dispersion is caused by the wavelength dependence of the refractive index of the material. Each wavelength component of the pulse will have a different refractive index and therefore travel at a different velocity. The sensitivity of wavelength arises from the displacement of the electrons from their equilibrium being frequency dependent causing a frequency dependent polarization, which in turn leads to a frequency dependent dielectric constant.

Waveguide dispersion

Waveguide dispersion, or intra modal dispersion, is a consequence of the dependence of the propagation constant (β) on wavelength. As β is related to the effective refractive index of a mode travelling through a waveguide. The effective index is wavelength dependent as the mode is more confined for higher wavelengths, increasing the propagation constant. Due to this, each wavelength component of the

pulse will travel at a different velocity.

Modal dispersion

Modal dispersion, also known as inter-modal dispersion, is a result of multi-mode propagation of light where each mode travels with a different group velocity. The modes can be higher order modes of the same polarization, or mode of different polarization (polarization mode dispersion)

Structural dispersion

Structural dispersion, also known as quadratic dispersion, plays a role when light travels through a photonic structure [17]. It is determined by the layout of the device and is the second derivative of the transmission phase-response with respect to the frequency.

It appears that in the case of a MR only the structural dispersion is abound and that the other dispersion aspects can be neglected [17, 31]. Furthermore since the ring and port waveguides are assumed to be single mode, no modal dispersion will be present. Therefore, in the following, dispersion in a MR will be regarded as structural dispersion only.

When $\Phi_z(\omega)$ is the transmission phase-response of a optical structure with transfer function *H(z)*, the normalized group-delay τ_n is the negative derivative of the phase-response (T is the inverse of the FSR) and the dispersion is the second derivative of the phase-response:

$$\tau_n = -\frac{d}{d\omega}\,\Phi_z(\omega) = -\frac{d}{d\omega}\,\arg(H(z))\Big|_{z=e^{j\omega}} \tag{2.12}$$

$$D = -c\frac{T}{\lambda^2}\frac{d}{d\omega}\tau_g(\omega) \tag{2.13}$$

The absolute group delay is given by $\tau_g = T\tau_n$.

Figure 2.6 shows a typical simulation of a group-delay and dispersion response of the drop port of a single ring with radius 50 μm. Figure 2.6 (middle) shows that with decreasing coupling constants (in that case F and Q are increasing) the absolute delay is increasing, since more time is needed to 'build up' the signal.

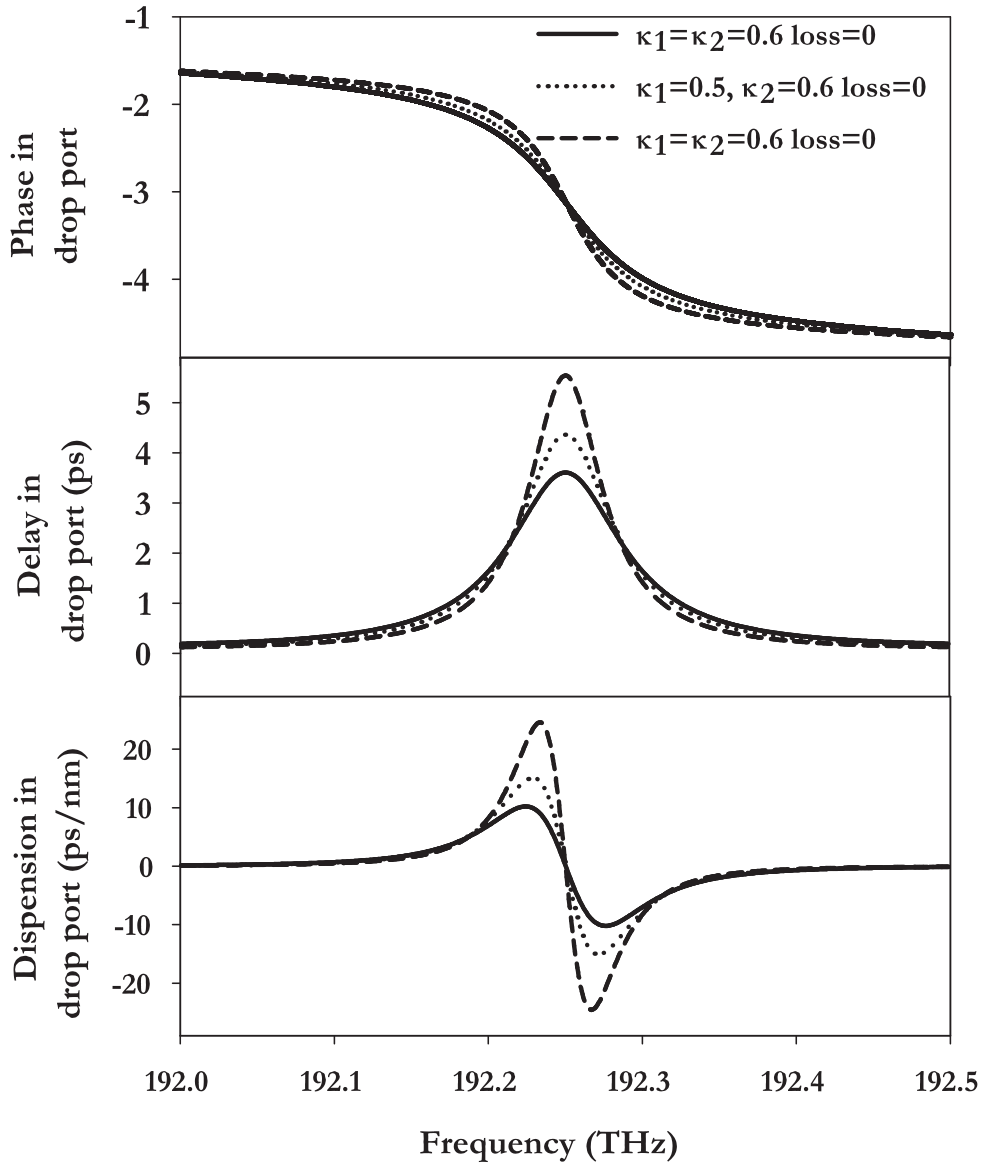

FIGURE 2.6: Simulated phase (top), group delay (middle) and dispersion (bottom) in the drop port of a microring for various coupling constants

Also non-symmetric coupling constants influence the delay as can be seen from the dotted line in the figure. Figure 2.6 (bottom) displays the simulated dispersion in the drop port for various coupling constants and the effect of asymmetry. The

radius of the device influences the delay in that larger rings take longer to time for a roundtrip and so causing higher delays at a given Finesse. When the device is symmetrically coupled the drop and through responses of the dispersion are the same. When however one of the coupling constants is different from the other, responses as given in Figure 2.7 can be found. The figure shows that the drop and through response now differ. Furthermore when switching the asymmetric coupling constants, the drop port remains the same, but the through response is mirrored. The minimum phase filter becomes a maximum phase filter [17]. This effect can be used in filters used to optimize the time domain parameters of a signal i.e. dispersion compensators.

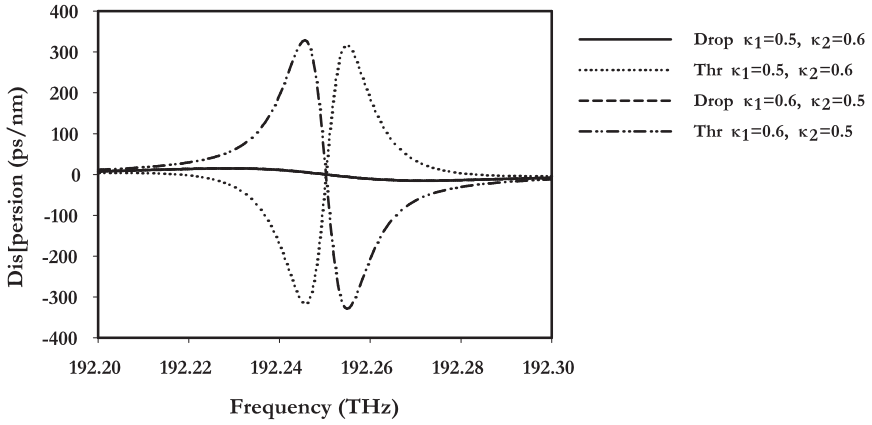

FIGURE 2.7: Dispersion in drop and through port for two different kind of asymmetry

2.7 Geometrical design

When a desired combination of coupling constants, loss and radius is found, a bottom-up design can be made that eventually results in a realistic geometry and composition for a MR fulfilling the given specifications. This geometrical design ends up in a set of masks and processing instructions that allow the realization of the device. Basically three design considerations have to be taken into account for a given set of input parameters: phase-matching, mono-modality and waveguide

losses. In addition, also the tolerances of the technological processes should be considered in order to end up with a fault tolerant design. The choice for the materials system and the available technology offer a set of limits for the materials and geometry related parameters and tolerances which enter in the design of the device

First a choice has to be made between two principal coupling configurations for a MR as shown in Figure 2.8. When the ring and waveguide are structured in the same waveguiding layer the configuration is called 'laterally coupled'. When the ring and the waveguides are in different layers the configuration is called 'vertical coupled'. The vertical coupling configuration has the advantage that the coupling mainly depends on the thickness of the layer in between, which can be controlled very accurate during deposition. This comes at the expense of an additional processing step for the ring layer. The lateral configuration uses only a single layer but needs very accurate lithography and etching processes to open a precise gap between the straight waveguide parts and the ring. Another advantage of the vertical configuration is that the ring and waveguide layers do not have to be the same thickness, increasing the design freedom. The optical modes of the

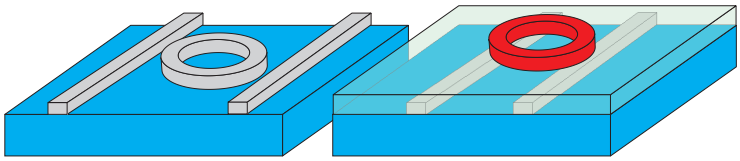

FIGURE 2.8: 3D drawing of ring laterally coupled (left) and vertically coupled (right) to the straight waveguides

straight waveguide cross-section and the bend cross-section can be calculated by use of (Bend-) mode solvers. Since the two modes propagate in structures which differ largely with respect to the z-invariance (z is the propagation direction), they can not be calculated in a single step. In addition, different simulation tools may be needed. The most relevant parameters obtained by these calculations are the effective index, the propagation and bending loss of the modes and the number of higher order modes besides the desired fundamental ones. Figure 2.9 shows an example of a bend mode and straight waveguide mode calculated by a commercial

mode solver [39]. Clearly the deformed modeprofile with a shift to the outer rim of the curved waveguide is visible indicating the effect of the bend on the mode.

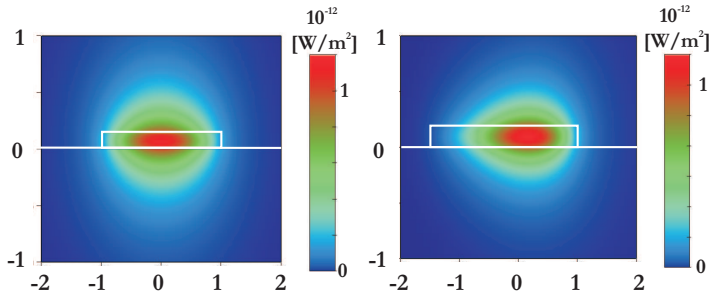

FIGURE 2.9: Optical mode of straight waveguide (left) and bend (right)

An important design consideration, which has to be taken into account, is the phase-matching between the mode that propagates within the ring resonator and the mode of the port waveguides. Ideally the effective indexes of these modes should be the same. In general however, this is not easily achieved because the index of the mode in the micro resonator needs to be relatively high to keep the radiation induced bending losses at an acceptable level. The effective index of the bend mode is therefore generally higher than the index of the straight waveguide which is bound by the condition of mono-modality. The mismatch in phase causes the coupling between the port waveguides and the ring resonator to be less efficient as is shown in Figure 2.10. The figure displays the result of modeling a coupler which consists of a straight waveguide vertically coupled to a bend waveguide as is schematically shown in the right part of this figure. The vertical distance between the two is 1 μm, the lateral offset, the gap, is varied. This calculation assumes waveguides index of 1.97 and surrounding index of 1.45 and a radius of 50 μm The figure shows how the coupling as function of the lateral offset changes for several phase-mismatches. It appears that for large phase-mismatch higher values for the coupling constants can not be obtained.

The minimum acceptable radius of the ring is determined by the radiation losses induced by the bending of the waveguide and is dependent on the index contrast. The width and height of the waveguides are limited on one side by the

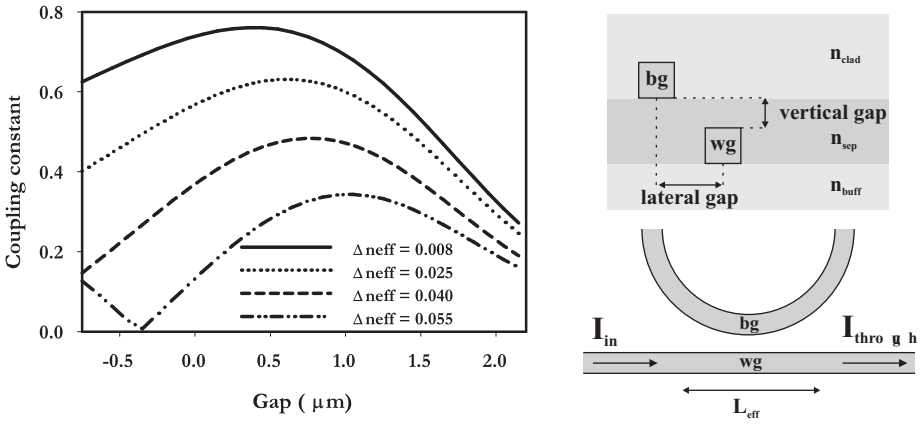

(a) (b)

FIGURE 2.10: (a) Effect of phase-mismatch (Δneff) on the coupling constants as a function of the lateral offsets

need of mono-modal waveguides and on the other side by the available fabrication technology (often lithography issues). Figure 2.11(a) shows one example of the effective index of a bend and straight waveguide. It is obvious that only in the case of vertical coupling phase matching is possible, as then the two layers can be grown independently. The radius of the ring is chosen such that it provides the desired FSR and minimizes the losses inside the ring. The bending losses are dependent on the index contrast as can be seen in Figure 2.11(b), where the effect of a change in the cladding index (n_{clad}) on the bending losses has been calculated for a nitride bend waveguide with $n_{sep} = n_{buff}$=1.45. A pronounced minimum of the bending losses around n_{clad}=1.45 can be observed. Furthermore when contrast decreases the bending losses increase. So higher index contrasts allow smaller radii and so larger FSR. The determination of the gap (lateral or vertical) between the straight and the ring can be done by for example beam propagation modelling (BPM) or coupled mode theory (CMT) [40]. It is important to note that the coupling between a bend and straight waveguide mode is different from the coupling between two straight waveguides with z-invariance. As a consequence the coupling length (L) of the coupler is not a well-defined parameter and should be replaced by an effective coupling length L_{eff}. Typical calculation results of the coupled fraction as function

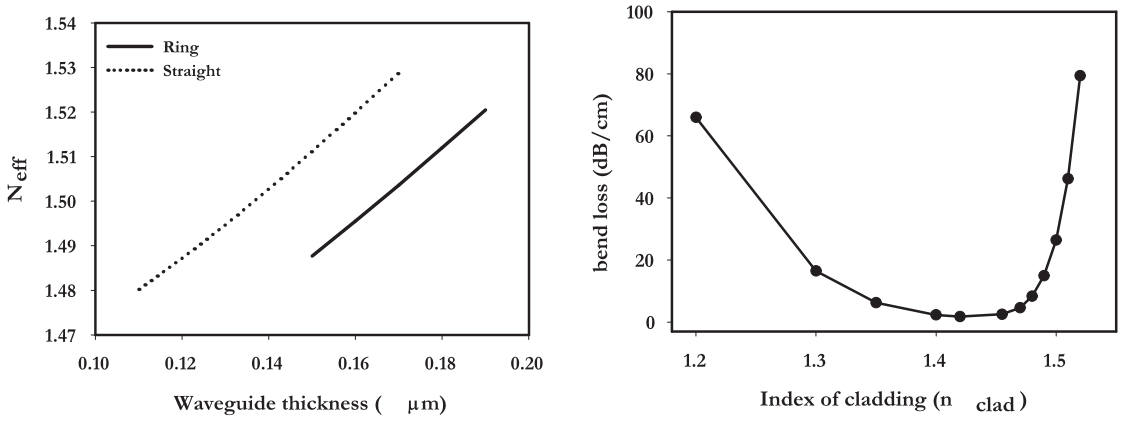

(a) (b)

FIGURE 2.11: (a) Example of effective index of straight waveguide (dotted) and ring for various waveguide thicknesses (b) bending losses of a ring for different cladding indices

of the lateral and vertical gap are shown in Figure 2.12.

2.8 Network level simulations

For simulating the behavior of MRs in network environments physical layer simulation tools were used from *Virtual Photonics Inc.*: VPItransmissionMaker and VPIcomponentMaker. These simulation tools use several models for network components, like lasers, amplifiers and receivers, to predict the behavior of a cascade of components in a network. The tools can also deal with optical feedback loops and so simulate a MR response. When doing so however, the freedom for choosing the simulation parameters for the system level simulations is limited. Therefore the simulations discussed in this paragraph where performed in two steps. First the magnitude and phase response of a MR were calculated given certain parameters of interest ($\kappa_{1,2}$, radius and loss). Second this response was incorporated in higher level simulation as a "measured" filter response.

The simplest simulations are built up out of the following components:

- Transmitter: model of a DFB laser producing a CW optical signal

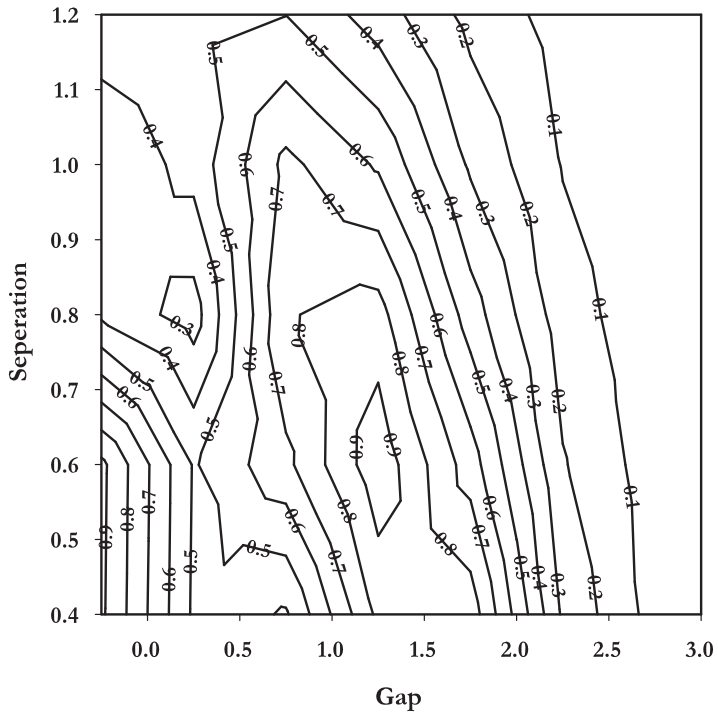

FIGURE 2.12: BPM calculation of coupling constant between straight waveguide and ring (R= 50μm) as a function of lateral and vertical distance.

- Modulator: model of a Mach-Zehnder modulator which can take into account a frequency chirp resulting from the modulator asymmetry
- Device: Simulated magnitude and phase response of a ring
- Receiver: model of a PIN photodiode, including shot noise
- BER tester: Deterministic analysis

Since optical systems are designed for low probability of bit errors, calculating the *BER* by counting the errors might take days. Therefore other methods are used to calculate the *BER*, for example using the Probability Distribution Functions of the received 1's and 0's. The simulation software can handle noise in different fashions. For simulations which invoke nonlinear interaction between the signals and noise, the two are simulated together. However when only linear interaction

between signal and noise is taken into account the signals and noise can also be simulated separately. This reduces the calculation time without distorting the results. The deterministic BER analyzer can analyze the signal waveform, including effects caused by crosstalk, dispersion or non-linear propagation effects. It calculates the *BER* estimate by combining the results of this analysis with the noise power distributions which where calculated separately according to:

$$BER = \frac{1}{2N}\sum_{n=0}^{N-1} erfc\left(\frac{p(n)-D}{\sigma(n)}\right) \tag{2.14}$$

$$erfc(x) = \frac{2}{\sqrt{\pi}}\int_{x}^{\infty} exp(-y^2)dy \tag{2.15}$$

With $p(n)$ and $\sigma(n)$ the mean and variance of bit number n, and D the decision threshold.

A measure for the quality of the data transport along the complete system is the eye diagram. When a pseudo random bit sequence is used to simulate a random bit stream and the received bitstream is plotted every two bit-periods an eye diagram like in Figure 2.13 can be simulated. In this figure the Back-to-Back 40 GHz eye shows clear openings and steep rising and falling transitions. A little noise can be seen due to the thermal noise in the photoreceiver. The right plot in Figure 2.13 is the same signal but now at the drop port of a MR with a BW of 40 GHz. Clearly the effect of dispersion can be seen; the transitions have become less steep. However, since the eye is still open error free detection is still possible. To see when the eye is closing an additional component is added. An attenuator just before the receiver causes it to receive less power. By adjusting the attenuation and measuring the BER for certain received optical powers (ROP), figures like the one in Figure 2.14 can be made. This figure shows the BER vs ROP of the back-to-back system as well as results including the 40 GHz MR. The difference between the two lines is the power-penalty as defined in section 2.2. In this case that is 0.8 dB. The bandwidth of a MR influences the capability of filtering high speed data. To show this, several MRs with different bandwidths were simulated and the power penalty at a BER of 10^{-11} for different modulation speeds is plotted

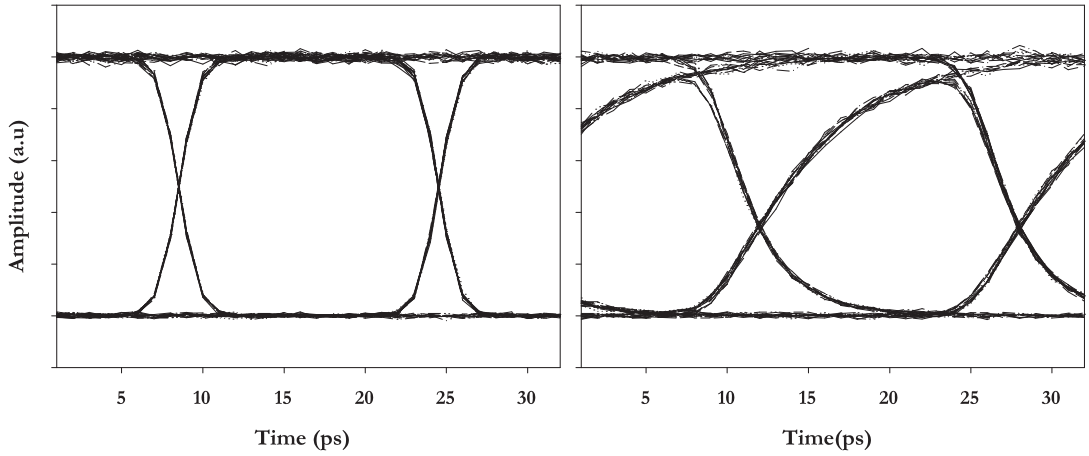

FIGURE 2.13: Simulated Eye diagrams for 40 Gbit/s NRZ signals; the input(left) and after a MR (right) with BW = 40 GHz

in Figure 2.15. The figure shows clearly that when the modulation speed exceeds the bandwidth of the device the power penalty increases exponentially.

When a MR is not tuned exactly to the center frequency of the optical carrier, the signal is influenced in two ways. First the amplitude of the eye decreases since less power is dropped. Second, since the center of the carrier is now located on the side slope of the resonance peak, the dispersion is also different. Figure 2.16 shows the simulated power penalty as function of the de-tuning of the center of the filter with respect to the carrier frequency.

The simulations in this section demonstrate the capability of a MR to filter Gbit/s data with error free detection. In the next chapters a thermal tunable microring will be designed and complex functions with multi MR structures will be investigated.

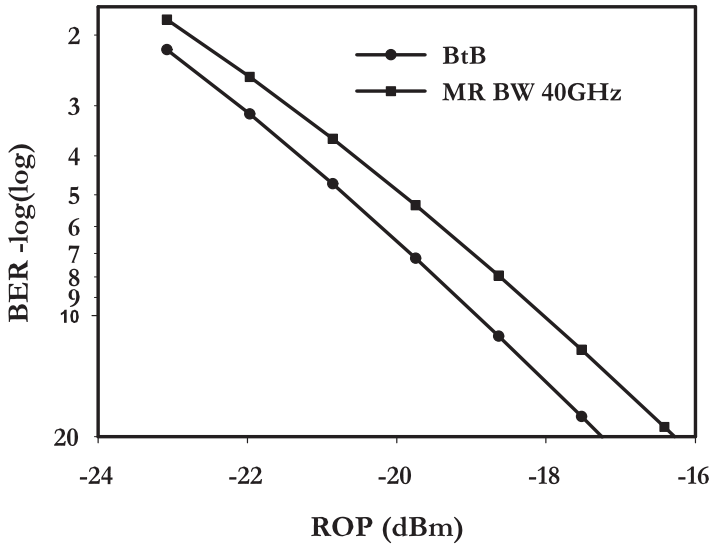

FIGURE 2.14: Simulated BER of transmitter and receiver at 40Gbit/s (BtB) and with MR versus the received optical power

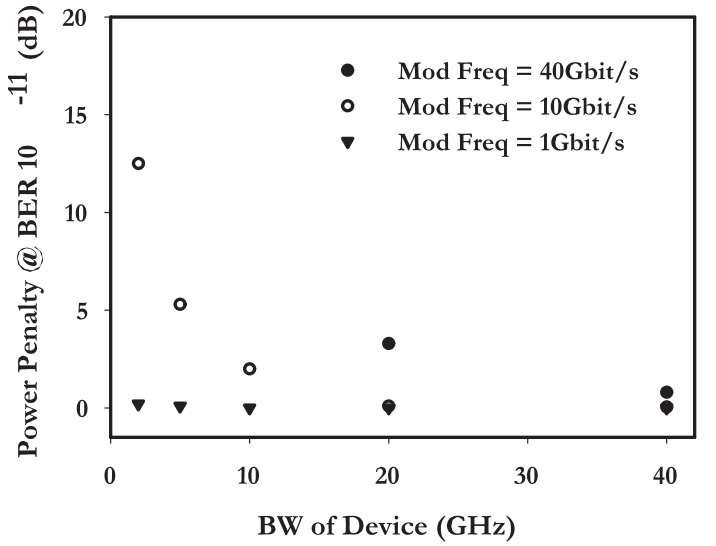

FIGURE 2.15: Bandwidth of device vs Power penalty at BER = 10^{-11} for different modulation speeds

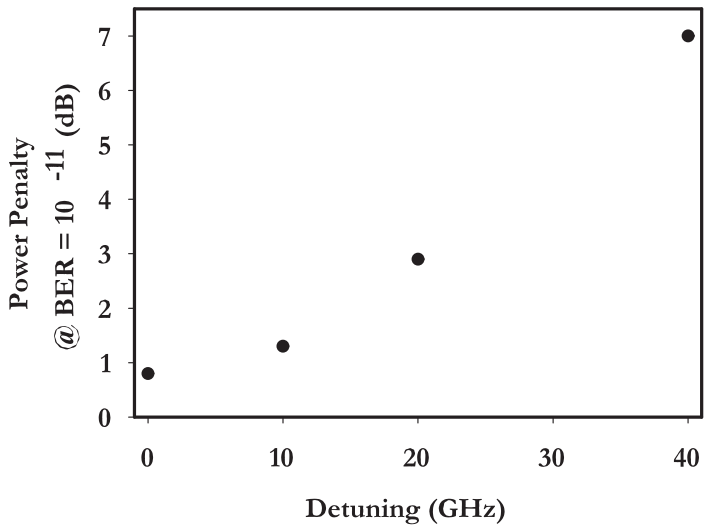

FIGURE 2.16: Simulated Power penalty vs the detuning of the transmitted wavelength with respect to the filter center

CHAPTER 3

Thermally Tunable MR

In this chapter the thermal properties of a micro ring resonator will be described. These properties allow the filter to be tuned to a specific wavelength. This way switching functions can be made and can fabrication errors and environmental temperature changes be corrected. First the basic properties of thermal tuning will be explained. Thereafter the design and characterization of a thermally tunable single ring is given. Finally a method of increasing the switching speed will be described.

This chapter was extracted from:

D.H. Geuzebroek *et. al.*, "Wavelength tuning and switching of a thermo-optic microring resonator" Proc. Europ. Conf. Integrated Optics, 2003, Prague, Czech Republic.

Geuzebroek, D.H. and A. Driessen "Ring Resonator Based Wavelength Filters", in *Wavelength Filters For Fiber Optics*, Venghaus, H (edt.), to be published 2006

3.1 Tuning and modulating

Until now the ring was assumed to be totally passive, i.e. all geometrical and materials parameters being constant in time. To add functionality or to overcome fabrication errors the MR can be made active by varying (tuning) some of the parameters and consequently its wavelength response. Furthermore additional functionality can be added by tuning externally the roundtrip loss or coupling constants of the ring.

Resonant wavelength tuning

The resonant wavelength of a MR can be tuned in several ways. The most straightforward approach is to change the effective index of the ring by any of the following means:

- Thermal Optic effect: by applying heat to the ring the refractive index of the material changes [41]
- Electro-Optic effect: an electrical field causes the change in refractive index [42]
- Carrier injection: by direct charge injection or by optical pumping of the a material above its bandgap energy and generation of electron-hole pairs, the loss parameter and the refractive index of the material is changed [43, 44]
- Changing the material (sensor) [45, 46]
- Opto-Optical effect: the light itself causes through NLO materials a change in index [20]

By one of these processes the effective index can be varied resulting in a shift of the resonance wavelengths, by an amount of $\Delta\lambda$. This shift can be used in filter applications to tune the passband to the desired wavelength. Also statistical errors in the radius during fabrication can be cancelled by post deposition trimming. The principle of tuning is shown in Figure 3.1 (a). The same phenomenon can lead to

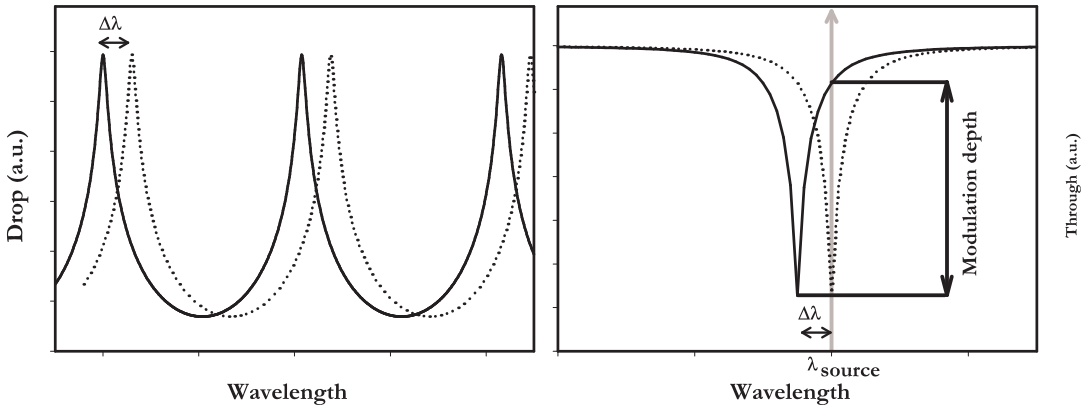

FIGURE 3.1: Tuning the pass-band of a MR filter (right) and modulation by tuning the resonance dip around the source wavelength (left)

an additional function when operating at constant wavelength λ_{source}. By a small change in effective index around the steep flank of the MR response a modulation at λ_{source} with a high extinction ratio can be obtained.

Although being most likely the simplest to be implemented, the thermal optic effect suffers from being slow with a response in the order of hundreds of microseconds. For switching applications this can be sufficient but for modulation other effects must be used. The thermo-optic effect can be used by applying a thin film heater on top of the ring. The heater must be placed as close as possible to the ring to minimize the driving power. On the other hand a minimum distance has to be preserved in order to avoid large additional losses inside the ring due to the presence of the absorbing heater metal. The shift in center wavelength of the ring λ_c is a function of the difference in effective index induced by heating the device, according to:

$$\delta\lambda_c = \frac{\lambda \Delta N_{eff}}{N_{eff}} \tag{3.1}$$

The change in effective refractive index induced by the heater depends largely on the materials used and the distance between the heater and ring. Glass-like materials have a dependence of the temperature on the refractive index (dn/dt) of around 10^{-5}, whereas polymers have a coefficient being an order of magnitude higher [41]. Thermal shifts of 20 pm/mW have been shown for glass based MR [47]. For polymer MR this shift is 1 nm/mW [48] around two orders of magnitudes higher, which can be explained by the larger thermo-optic coefficient and a better conductance of the heat as is described in [49].

The electro-optic effect changes the i-th component of the refractive index n_i as function of the applied electric field E_k according to:

$$\Delta\left(\frac{1}{n_i^2}\right) = \sum_k r_{ik} E_k \tag{3.2}$$

With r_{ik} the eo tensor [50, 51] . This effect is inherently much faster as the thermo-optic effect. In practice now the limiting factor will be the 'build-up' time of the resonance given by

$$\tau_{cav} = \frac{F \cdot R \cdot n_g}{c} \tag{3.3}$$

For well-designed ring resonators it is possible to electro optically modulate light at speeds of several tens of GHz, experimentally demonstrated is up to now 1 GHz [51, 52].

In semiconductor materials, with highly confining waveguides which have a bandgap energy higher than the photon energy, it is possible to change the refractive index by injecting free carriers [53].

For all-optical or opto-optical tuning mostly the Kerr non-linearity of a material is used [20] i.e. the total effective refractive index of the material is dependent on the intensity of the light (I_{eff}) :

$$n_e = n_{e,0} + n_{e,2} I_{eff} \tag{3.4}$$

With $n_{e,2}$ a parameter dependent on the Kerr non-linearity. Recently [44] showed GHz modulation in Silicon-on-Insulator MRs based on this effect.

In the methods described above an active function was introduced by changing the resonant wavelength. When in contrast to that only permanent changes have to be made in order to compensate for fabrication errors other methods should be applied. For example, the effective index of the ring can be altered by locally injecting high optical power by a laser. This so called laser-trimming can be used as a post fabrication process to trim every MR to the proper resonance position [54]. For low-cost mass production, however, the need of trimming should be completely avoided.

Loss parameter tuning

In the previous section several methods of tuning were discussed whereby the optical roundtrip path length was changed resulting in shift of the the resonant wavelength. Alternatively the roundtrip loss can be changed controlling the Q-factor and the shape of the resonance curve. In this way a MR can be used as space-switch, as at the resonance wavelength in high Q weakly coupled MRs practically all power is directed to the drop port, but at low Q to the through port. There are several methods of controlling the Q of the cavity dependent on the materials in the system. In semiconductor devices the Electro-Absorption or Free Carrier Injection can be used to control the loss parameter [53]. Other materials like polymers and glasses allow for doping with rare-earth ions like Erbium [55]. In these materials the losses can be largely reduced by optical pumping. In this way switching of light by light is feasible, i.e. opto-optical switching.

Coupling constants tuning

Finally parameters which can be tuned are the individual coupling constants. This has been done mainly in relatively large racetrack structures where enough coupling length is present to allow for thermo-optic tuning restricted to the coupling sections [56]. Furthermore some more exotic methods have been demonstrated making use of MEMS (Micro Electro-Mechanical Systems) technology [57]. Fleming et. al. changed the coupling between port waveguides and ring by moving the ring, which was attached to a membrane, in a controlled way by electro-static

forces to the evanescent field of the waveguides underneath. In this way light at the resonance wavelength is coupled from one to the other waveguide [58].

3.2 Thermal Tuning

The microrings described in this work are made thermally tunable. This is easy to implement and does not require expensive and exotic materials. Since the microring will be used for switching and routing functions and not in as a modulator, the speed of the relatively slow thermo-optic devices will be sufficient.
The thermo-optic effect is the change of refractive index in a material, caused by a change in temperature. As described in [41], there are two effects that are important:

- a change in refractive index due to a change in density
- a direct change in the refractive index, caused by thermal changes in polarizability

Mathematically this can be described as follows

$$\frac{dn}{dT} = \left(\frac{\partial n}{\partial \rho}\right)_T \left(\frac{\partial \rho}{\partial T}\right) + \left(\frac{\partial n}{\partial T}\right)_\rho \tag{3.5}$$

Where n is the refractive index, T is the temperature and ρ is the density of the material.
The first term in (3.5) for fused silica is only $\sim 0,3 \cdot 10^{-6}$ $[K^{-1}]$, while the second term is much larger $\sim 10^{-5}$ $[K^{-1}]$ [41]. For (glassy) polymers these values are respectively $\sim -10^{-4}$ $[K^{-1}]$ and $\sim 10^{-6}$ $[K^{-1}]$ indicating that for polymers the thermo-optic effect is mainly determined by changes in density. In addition the effect is considerably larger in magnitude and has an opposite sign.

One can distinguish three heat-transport mechanisms:

- Convection: transfer of heat through a fluid (liquid or gas) caused by macroscopic molecular motion;

- Radiation: transmission of energy in the form of electromagnetic radiation;
- Conduction: transport of heat between objects or particles by direct contact.

As discussed in [59–62], the effect of convection and radiation on the temperature profile in the currently considered waveguiding structure can be neglected, and only conduction will be taken into account.

Heat conduction is the transfer of heat from warm areas to cooler ones, and effectively occurs by diffusion. The heat flux is therefore [63]:

$$\Phi_Q \approx \frac{(\text{heat per unit area})}{(\text{unit of time})} \approx \frac{-\rho\ C_p\ \Delta\ T\ d}{\frac{d^2}{\kappa}} = -\rho\ C_p\ \kappa\ \frac{\Delta\ T}{d} \tag{3.6}$$

where

density	ρ	[kg m^{-3}]
mass heat capacity	C_p	[J kg^{-1} K^{-1}]
diffusion distance	d	[m]
thermal diffusivity	κ	[m^2 s^{-1}]

The negative sign denotes that heat flows from areas of higher temperature to areas of lower temperature. Noting that the temperature gradient is $\nabla T = \Delta\ T/d$ and defining the thermal conductivity $K = \kappa\ \rho\ C_p$ results in an equation known as Fourier's law:

$$\Phi_Q = -K\ \nabla T \tag{3.7}$$

The time-dependent heat conduction equation in its generalized form is intuitively given by

(rate of heat change per area) = (heat production per volume per time)

- (heat loss)

$$\rho\ C_p\ \frac{\partial T}{\partial t} \quad = \quad Q + \nabla(\kappa \nabla\ T) \tag{3.8}$$

where Q is the heat production in [W m^{-3}]. When the thermal conductivity is not a function of position, this results in a 2-dimensional heat conducting equation:

$$\frac{\partial T}{\partial t} = \frac{H}{Cp} + \kappa \left(\frac{\partial^2 T}{\partial x^2} + \frac{\partial^2 T}{\partial y^2} \right) \tag{3.9}$$

With H the heat production per unit mass. The 2-dimensional heat conducting equation can be solved in commercial finite difference solvers.

3.2.1 Transient model

Now a one-dimensional transient thermal model of a uniform bar is considered, as presented in [59]. A mathematical description of the transient temperature will be given as well as an electrical circuit equivalent. A uniform bar with length L and cross section area A is considered. The sidewalls are thermally insulated from the environment (adiabatic) and one endface is isothermal at T = 0 K (heatsink). The other endface has a uniform plane heat source of heat flux $Q_s(t)$. Heat inside the bar can be transported only in the z-direction. Using integral transform technique, in [64] the transient temperature solution of (3.9) is then found to be:

$$\begin{aligned} T(z,t) = \frac{2}{L} \sum_{m=1}^{\infty} & \exp(-\kappa\ \beta_m^2\ t)\ \cos(\beta_m\ z) \\ & \cdot \frac{\kappa}{K} \int_0^t \exp(\kappa\ \beta_m^2\ t)\ Q_s(t')\ dt' \\ & m = 1, 3, 5, \ \ldots \end{aligned} \tag{3.10}$$

with all parameters defined as before, and

$$\beta_m = \frac{m\ \pi}{2\ L}, \quad m = 1, 3, 5, \ \ldots \tag{3.11}$$

Note that the solution is independent of the cross section area A. If $Q_s(t)$ is a step function starting at t=0, and a heat generation rate is defined as $G_s = \frac{Q_s}{\rho\ C_p}$

one can derive

$$T(z,t) = \sum_{m=1}^{\infty} \frac{2\ G_s}{L\ \kappa} \frac{1 - \exp\ (-\kappa\ \beta_m^2\ t)}{\beta_m^2} \cos(\beta_m\ z) = \sum_{m=1}^{\infty} T_m(z,t) \tag{3.12}$$

The temperature distribution reaches a steady-state value as t approaches infinity. At the source location z=0, this steady-state temperature is calculated to be

$$T(0,\infty) = \sum_{m=1}^{\infty} T_m(0,\infty) = \frac{Q_s\ L}{K} \tag{3.13}$$

It will turn out to be convenient to rewrite this as

$$T(0,\infty) = P\ R \tag{3.14}$$

with $P = Q_s\ A$ and $R = \frac{L}{K\ A}$

Generally, the heating of a uniform material with a uniform heat source is modelled with a simple parallel RC-circuit, charged by a step current source. It can be shown, however, that this is only correct for the steady-state. The step response of a parallel RC-circuit with resistance R and capacity C, on a current source I_0 is

$$V(t) = I_0\ R\ (1 - \exp\ (\ \frac{-t}{R\ C})), \quad t > 0 \tag{3.15}$$

Substitution of

$$\begin{aligned} R &= \frac{L}{K\ A} \\ C &= \rho\ C_p\ L\ A \\ I_0 &= Q_s\ A \end{aligned} \tag{3.16}$$

and replacing the variable V by T results in

$$T(t) = \frac{Q_s\ L}{K}\ (1 - \exp\ (\ \frac{-t\ K}{\rho\ C_p\ L^2})) \quad , t > 0 \tag{3.17}$$

This equation has to be compared with T(0,t) as found from (3.12)

$$T(0,t) = \sum_{m=1}^{\infty} \frac{2\ G_s}{L\ \kappa} \frac{1 - \exp\ (-\kappa\ \beta_m^2\ t)}{\beta_m^2} \tag{3.18}$$

In figure 3.2 the reponses (3.17) and (3.12) are plotted. The parameters are the same for both lines, and they are chosen such that temperature is normalized to a steady-state value of 1 unit and the time is normalized to a value such that the steady-state value is reached in approximately 1 unit of time. For the steady-state,

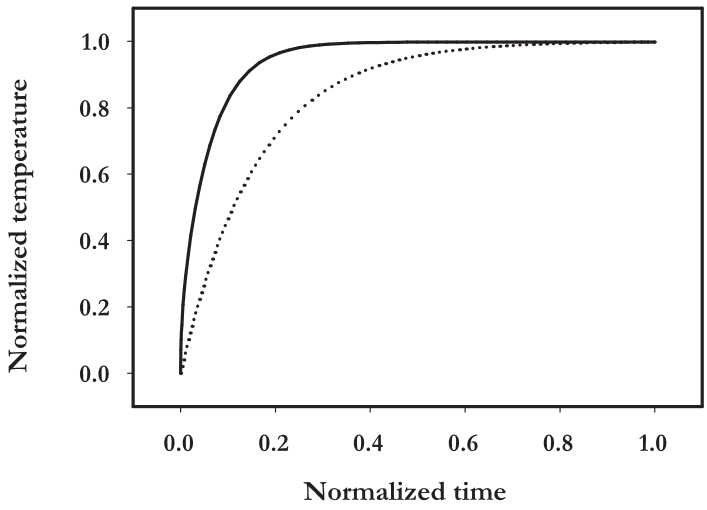

FIGURE 3.2: Comparison step responses of uniform bar model and parallel RC-circuit

the two models yield the same results. The response predicted by the mathematical model, however, is much faster than the response one would expect from a parallel RC-circuit. It can also be shown that the 2 lines cannot be fitted by changing the time-constant of the RC-circuit (not plotted). This shows that the heating of a uniform material with a uniform heat source cannot be modelled as a simple parallel RC-circuit [59].

A correct model is obtained by looking at the elements T_m that are summed in (3.12). The transient temperature can be modelled by a network consisting of

an infinite number of parallel RC circuits ('stages'), connected in series. Note that these stages do not indicate a physical part of the bar, this should already be clear from the fact that the number of stages is infinite. The values of the resistances are found from (3.12) by looking at the elements that are summed to calculate the steady-state temperature at the source location. Each element (and therefore the value of the resistance in each stage) is described by

$$T_m(0,\infty) = \frac{8\ Q_s\ L}{\kappa * \pi^2\ m^2} \tag{3.19}$$

According to (3.14), dividing the temperature by the total power yields the resistance

$$R_m = \frac{T_m(0,\infty)}{Q_s\ A} = \frac{8\ L}{K\ A\ \pi^2\ m^2}, \quad m = 1,3,5,\ \ldots \tag{3.20}$$

Finding the value of the capacitance in each stage is slightly more complicated. First, the parallel RC-circuit is considered, for which the response is calculated in (3.15). It can be shown that

$$\frac{dV}{dt}|_{\ t=0} = \frac{I_0}{C_m} \tag{3.21}$$

Next, (3.12) is considered and it is calculated that

$$\frac{dT}{dt}|_{\ t=0} = \frac{2\ Q_s}{\rho\ C_p\ L} \tag{3.22}$$

By comparing these two, ignoring the dummy-variables T and V, and noting from (3.16) that $I_0 = Q_s\ A$ it is found that for every stage

$$\frac{Q_s\ A}{C_m} = \frac{2\ Q_s}{\rho\ C_p\ L} \tag{3.23}$$

and solving this equation yields the (desired) result

$$C_m = \frac{1}{2}\ \rho\ C_p\ L\ A \tag{3.24}$$

The model described in this section will be used in the heater driving optimization

in section 3.6.

3.3 Design of a Thermally Tunable MR

This section describes the choices made in the design of a single thermally tunable MR. Before complex structures with many rings can be implemented, a single ring device is investigated to asses the design strategy and to investigate the thermal properties of the MR. The design choices will be discussed in three areas: materials system, geometrical design and heater design.

Materials System

First a materials system has to be chosen which suits the demands for thermally tunable MRs, especially with the road to complex MR structures in mind. As stated in chapter 2, when low loss devices with small ring are desired, an index contrasts larger than 0.1 is needed. Furthermore, the condition to keep the devices potentially as low in costs as possible, excludes exotic materials. The losses of the materials must be small allowing cascading many rings. Finally, since the devices need to be thermally tunable, the materials system must be thermally stable, so that reproducible device behavior can be expected.

The abovementioned criteria lead to the choice of silicon-nitride (Si_3N_4) waveguiding channels embedded in silicon-oxide (SiO_2). The index difference (1.97 to 1.5) is sufficiently high to allow small rings. Furthermore, the losses in this materials have shown to be low (< 0.2 dB/cm) [65] in the third telecom window. With this technology high Finesse MRs with air cladding have been demonstrated [34, 66]. The technology is very stable since the glass like materials do not suffer significantly from external influences. The thermo-optic coefficient of these materials are not that high (in the order of 10^{-5} K^{-1}) especially in comparison with, for example, polymers which have a order of magnitude higher effect. But since the melting point of the material is very high, also large temperatures, increasing several hundreds degrees can be allowed, of course at the expense of higher driving power. All in all, the Si_3N_4/SiO_2 combination looks promising for for devices made

based on thermally tunable multi-MR structures and will therefore be applied for the devices discussed further.

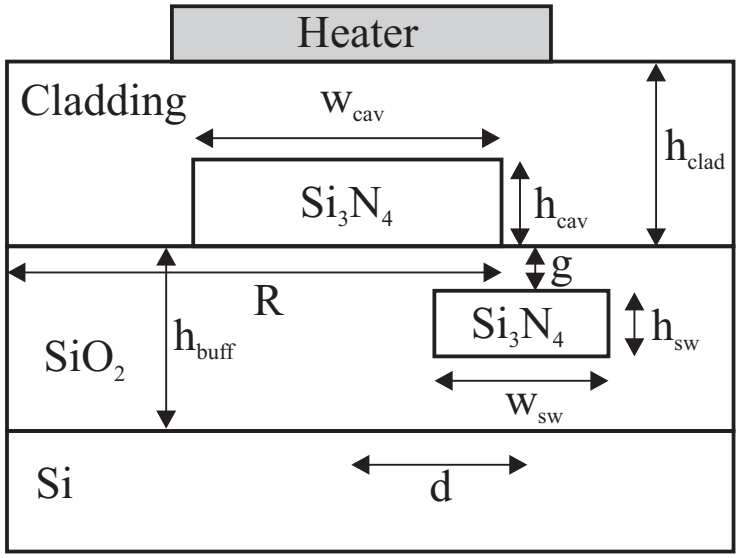

FIGURE 3.3: Cross section of MR

Geometrical design

A cross section of a single MR is shown in Figure 3.3. As discussed above, the MRs described in this work will have Si_3N_4 waveguide channels embedded in SiO_2, vertically coupled to the Si_3N_4 ring with radius R. The buffer layer is thermally grown SiO_2 and the intermediate layer is a TEOS SiO_2 layer, which will be discussed in more detail in the fabrication section (section 3.4). For thermal tuning and switching a cladding layer as depicted in Figure 3.3 is favorable since it allows optical isolation from an efficient local heating structure on top of the resonator. The rings have a radius of 50 μm since that allows for phase-matching as was discussed in chapter 2 and still allows for a FSR of over 4 nm with bending losses below 5 dB/cm. Since the aim for these MR filters is to filter high bit-rate signals, the bandwidth of the devices have to be set accordingly. Therefore coupling constants in the range of 0.4 to 0.7 have been chosen and the lateral and vertical gaps are chosen accordingly. A vertical distance (g) of 1 μm was chosen to be able to

TABLE 3.1: Parameters values for thermally tunable MR

Parameter	Abbreviation	Value
Radius	R	50 μm
Ring height	h_{cav}	180 nm
Ring width	w_{cav}	2.5 μm
WG height	h_{sw}	140 nm
WG width	w_{sw}	2 μm
Buffer thickness	h_{buff}	8 μm
Cladding Thickness	h_{cladd}	3 μm
vertical gap	g	1 μm
lateral gap	d	0.5 to 1.7 μm

have several offsets to reach the desired coupling constants. Lateral distances d, ranging from 0.5 to 1.7 μm, were applied to reach the desired coupling constants. Table 3.1 shows the design parameters for the rings which will be discussed further in this work. The thicknesses and widths of the ring and the waveguide where chosen such that the waveguide is single mode (higher order modes are below cut-off or have significantly higher losses) and have still effective indices as close to each other as possible. With the parameters from table 3.1 the calculated phase mismatch is 0.012.

Heater design

In this section, the thin film heaters that are used for device tuning will be considered. There are three main requirements in the design process of the heater [67].

- First the heater should not introduce additional losses in the microring resonator. Since the heater is made of a metal which introduces losses to optical fields, the distance between the ring and the heater should be sufficiently large.

- Second the heater should operate at low power. This leads to a contradiction with the first requirement since for this the heater has to be placed as close as possible to the ring. Furthermore materials must be used that have a high electrical resistivity allowing efficient heating at low current.

- Third the heater should be reliable: its characteristics should not vary over time. This has direct implications for the materials used and the maximum applied power and consequently for the maximum tuning range of the device.

In order to meet these requirements, several geometries have been studied in [67]. Finally an omega geometry as shown in Figure 3.4 was chosen because of efficiency expectations and its relatively straightforward design. Chromium was chosen as the heater material because of its very good adhesion properties to silicon oxide, wide usage, high thermal resistance and ease of use.

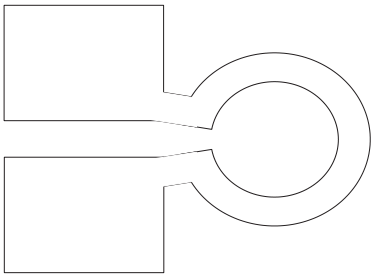

FIGURE 3.4: Geometry of an omega heater

Other design parameters include the width of the heater, the lateral heater placement and the cladding width. The width of the heater is 10 μm, because for a wider heater, the relatively small increase in N_{eff} would not outweigh the additional power consumption. The cladding layer thickness is 3 μm, because simulated losses in the ring due to the presence of the chromium heater are negligible, see figure 3.5. The heater is placed centered above the ring, although a small offset would be beneficial due to the asymmetry of the mode that is propagating in the ring. This effect however, is too small to be of practical use.

If a high current is sent through the heaters, they will generate more heat and the heating of the channel can be done faster. However, the magnitude of the driving signal is limited by the heaters that eventually will break down if too much power is dissipated. In order to be able to predict the break down power of the heaters, some initial measurements have been performed on test structures. Note that it is assumed that the Ω-heaters break down because of overheating and not because of sparking between the leads, the so-called dielectric breakdown. When

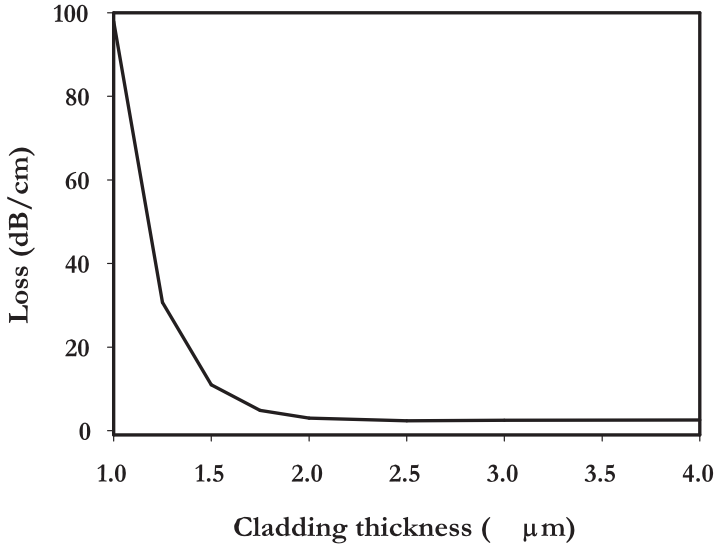

FIGURE 3.5: Losses in a 50 μm ring as function of the thickness of the cladding

the dielectric strength of air of 3 10^6 V/m is taken into account and a designed gap of 10 μm between the leads, dielectric breakdown might occur at a voltage of 30 V. This leads together with the resistance of the heater of 200 Ω to a power dissipation of 4.5 W. As experiments have shown the heater has been overheated at power levels long before dielectric breakdown can occur.

The heater structures on the test wafer were also used for examining the temperature dependence of the heater resistance. Knowledge about this temperature dependence is useful since a direct way of measuring the temperature of the heaters is extremely difficult. Through the use of the temperature dependence of the resistance however, the temperature can be determined indirectly by measuring the resistance of the heater if its resistance for a specific temperature is already known. By measuring the resistance of the heater at a certain power dissipation in the heater it is then for instance possible to link the power dissipation directly to the temperature of the heater. The temperature dependent resistance of the chromium heaters was determined from the measurement of a resistance testing structure at increasing temperatures. The test wafer with this structure was put

on a metal plate with a thermal conducting compound put in between to improve heat conduction. The metal plate with the wafer was placed on a hotplate of which the temperature could be controlled. The temperature was measured using an infra-red (IR) thermometer. The resistance was measured through the use of probing pins and a multimeter. The result of this measurement is shown in Figure 3.6(a). The resistance in this figure was normalized to the resistance measured at room temperature. The figure shows two runs. After the first run the resis-

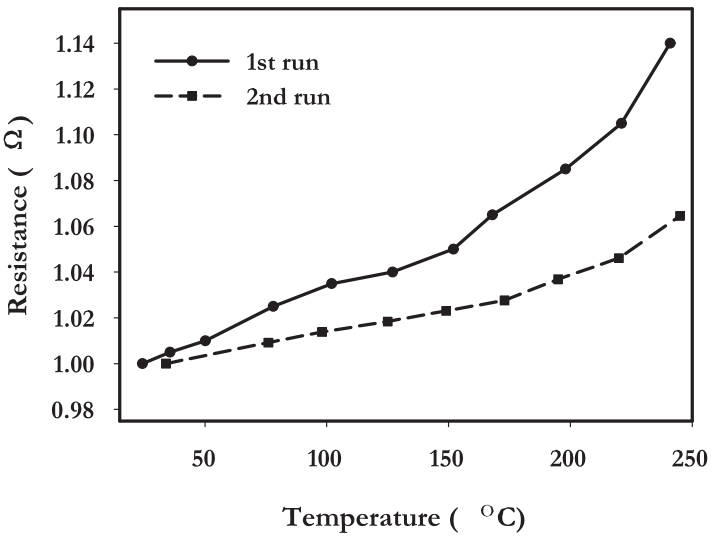

FIGURE 3.6: Resistance of the compact Ω-heater as function of temperature

tance at room temperature has changed. This is a common response for metal thin film resistors where in the first run different impurities are removed increasing the resistance. The second and following runs remain stable and can be used as reference for determining the temperature of the heater in normal operation. To investigate at which driving power the heater breaks down, some destructive test where performed on the test heaters. An increasing current was applied while measuring the resistance. The results are shown in Figure 3.7(a). The power was increased in several runs shown in the figure. The initial resistivity (at P=0) has increased after the first run as already could be seen in Figure 3.6. This first run

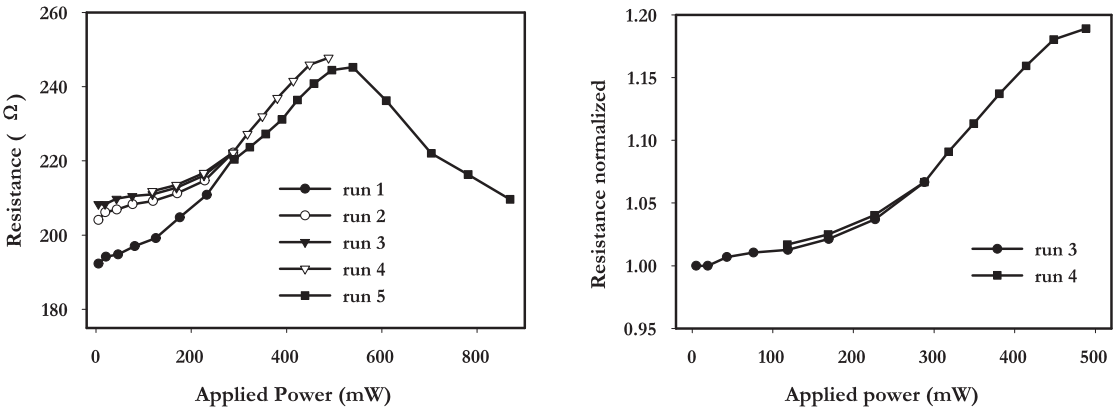

(a) (b)

FIGURE 3.7: Heater test; Measured (a) and normalized (b) Resistivity against applied power

is called passivication of the heaters. The second and third run start around the same value. Until an applied power of around 300 mW the heater remains stable on the line of the third run. When increasing the power above this value, the heater is in an area where the response becomes unstable again, dependent on the number of runs and duration of these runs. When the power is increased above 500 mW the heaters are really destroyed resulting in a lower resistance and at some point (870 mW in this case) the heater breaks down.

Two pictures of Ω-heaters after a destructive test are shown in Figure 3.8. It shows that the heated power is distributed evenly across the heater. The heater has deliberately been broken by an excessive heater current at a point where most of the heat is dissipated, in the case of Figure 3.8 (a) at a random position in the Ω-shaped structure, in the case of Figure 3.8 (b) near the leads. Simulations have been performed to find the response of a microring when applying a heater as described above. By using a commercial Finite Difference Solver for thermo-optical problems [39] the temperature profile of the used layer stack can be simulated and also the change in refractive index of the layers induced by the temperature rise. Figure 3.9 shows such a temperature profile of the layer stack mentioned before.

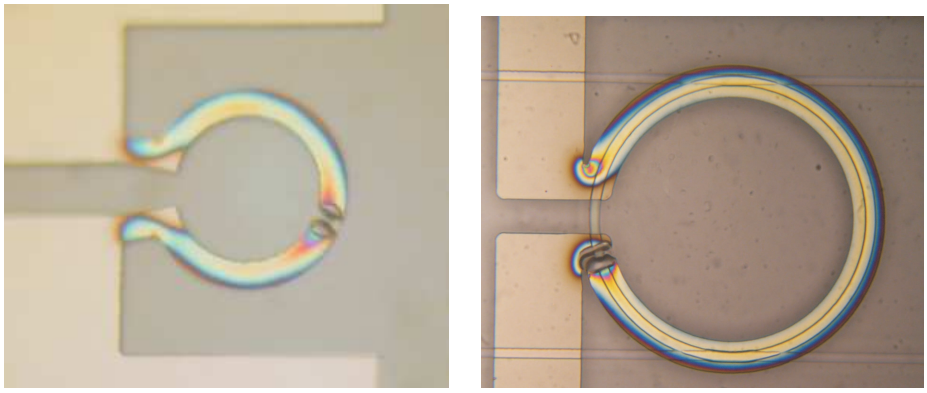

(a) (b)

FIGURE 3.8: Ω-heaters after destructive tests with two type of leads

TABLE 3.2: Material parameters for temperature profile simulation

Material	Thermo-optical coefficient	Specific heat	Thermal conductivity
SiO_2	$1.15\ 10^{-5}$	$1.75\ 10^{6}$	1.4
Si_3N_4	$1.15\ 10^{-5}$	$2.2\ 10^{6}$	30.4

This temperature profile leads to a change in refractive index of the layer stack. When the optical mode is again simulated with the changed layer stack, an optical mode is found with a slightly different in effective index. This can be done for several heater temperatures and leads to a temperature dependence of effective index of the guided mode. By using equation (3.1) the expected temperature dependence of the center wavelength of a microring can be calculated. As a result Figure 3.10 is obtained, where a ring of 50 μm radius with a 3 μm cladding is assumed. Together with the measured power-temperature dependence of Figure 3.6 the slope of the graph leads to a center wavelength dependence $d\lambda/dP$ of 9 pm/mW. In table 3.2 the material parameters for the temperature profile simulations are given. For this simulation the Si wafer is regarded as a perfect heat sink.

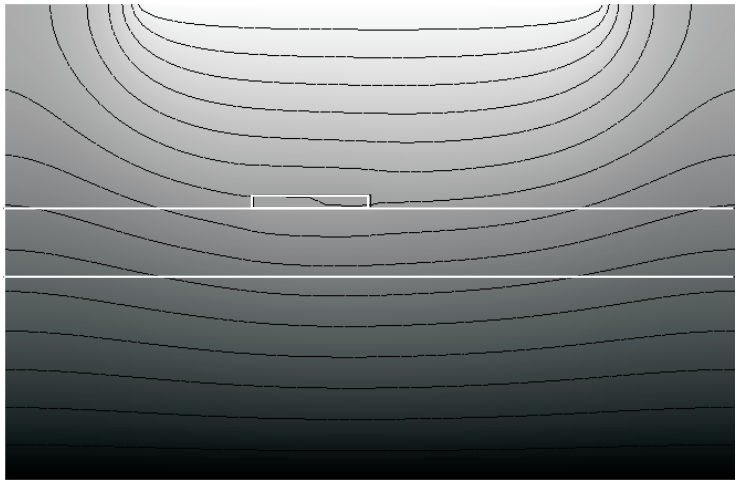

FIGURE 3.9: Simulated temperature profile of a crossection with 10 μm heater width and 3 μm cladding

3.4 Fabrication

The MRs are made with the use of standard cleanroom fabrication technology. The processing starts with a silicon wafer with 8 μm thermally grown SiO_2 as a buffer layer. This thickness is enough to isolate the waveguides from the silicon substrate. A layer of Si_3N_4 is grown on top of this using Low Pressure Chemical Vapour Deposition (LPCVD). By photolithography and Reactive Ion Etching (RIE) the waveguides core layer is structured. The buffer layer of SiO_2 is deposited with a TEOS (Tetra-Ethyl-Ortho-Silicate) LPCVD process. TEOS does not have a mushroom-like shape overgrow of channels occurring in PECVD SiO_2, which causes voids near the waveguide increasing losses and disrupting the coupling between the waveguide and the ring [68]. The ring layer is again a LPCVD Si_3N_4 layer patterned by contact lithography and RIE. The cladding layer is fabricated by depositing a Plasma Enhanced CVD (PECVD) layer of SiO_2. TEOS can not be used now, since a layer thickness higher than 1 μm causes severe stress. After this the layer stack is annealed at 1050° for 1 hour to remove the hydrogen inside the layers and decrease the materials losses. Finally the heater layer is deposited by sputtering a chromium thin film and patterned by photolithography and chromium wet-etch. The typical layer dimensions used are stated in table 3.1. In Figure 3.11 a realized

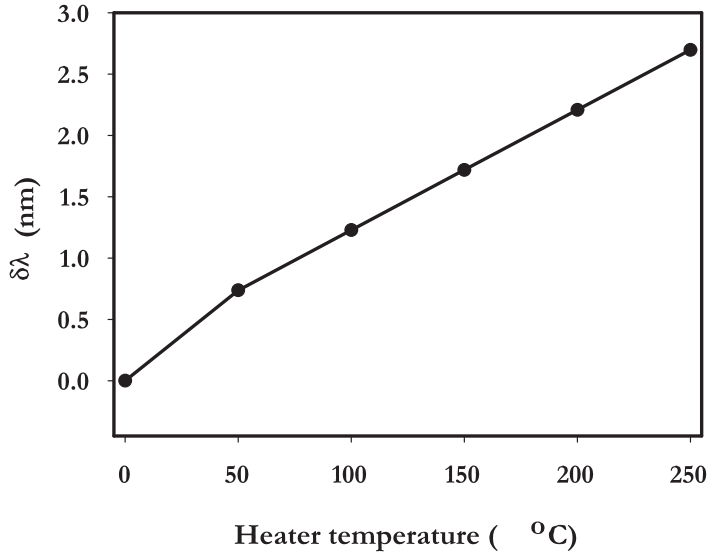

FIGURE 3.10: Simulated change in center wavelength ($\delta\lambda$) as function of temperature for a ring with 50 μm radius and 3 μm cladding

MR with and without a heater are shown. Appendix A shows a more detailed process flow of the realized rings.

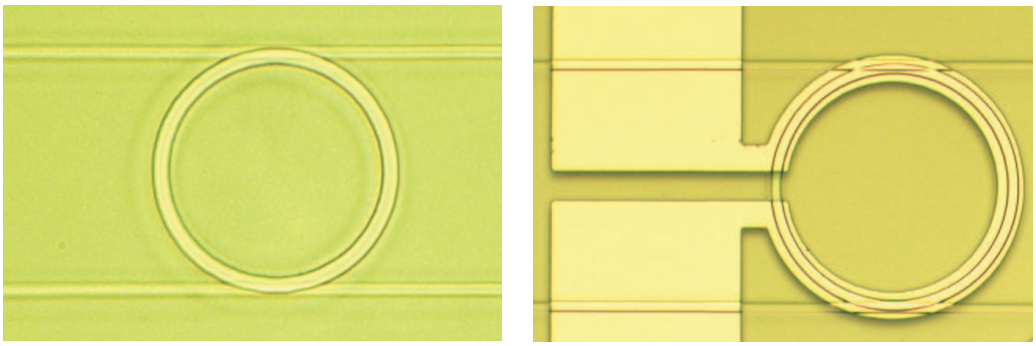

(a) (b)

FIGURE 3.11: Photograph of realized microring with and without heater with a radius of 50 μm

3.5 Characterization of a single MR

For a complete test of MRs with respect to design parameters and system specifications pigtailing and packaging is needed. For rapid feedback stand-alone characterization of the bare diced wafer pieces is often sufficient. The single MR is mostly placed in a typical set-up as shown in Figure 3.12. Light is coupled into the device by either butt coupling a fiber or through a system of lenses. The source can be a broadband source (EDFA ASE) or a tunable laser. The filtered light is then detected by either a spectrum analyser or a photo detector. Especially for high index-contrast devices the demand on the micromechanical positioner (xyz table) is high, as positioning is needed with submicrometer precision with negligible drift in time during a measuring sequence of tens of minutes.

Typical measured responses of a single MR are shown in Figure 3.13 where the throughport of a 50 μm radius ring is measured and fitted to the scattering matrix model of chapter 2. The fitted parameters are κ_1=0.7, κ_2=0.6 and 10 dB/cm loss which are in good agreement with the designed parameters in the case of the coupling constants. The slight asymmetry is caused by an error in alignment between the port waveguide and ring layers. The increase in loss with respect to the simulated 5 dB/cm might be due to scattering losses which were not accounted for in the design. Since this ring has high coupling constants, the

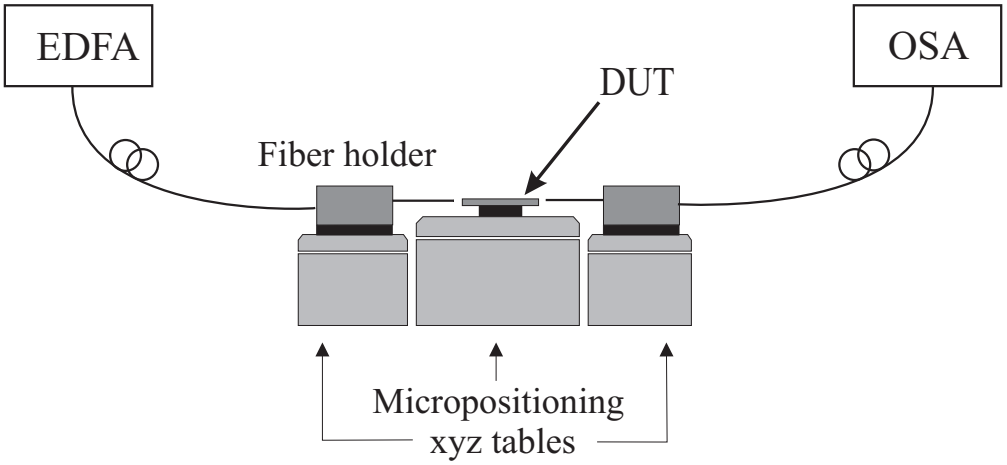

FIGURE 3.12: Characterization Setup

additional losses can be overcome and still good responses are measured. The exact center wavelength of the ring is determined by the fabrication technology. Small errors in ring diameter caused by lithography limitations or small changed in thickness of the deposited layer causes the wavelength to shift.

$$\delta\lambda \approx \frac{\lambda \Delta R \Delta N_{eff}}{R N_{eff}} \tag{3.25}$$

Where $\Delta R \Delta N_{eff}$ is the change due to differences in radius and effective index. When the assumption is made that the effective index does not change, a 10 nm change in radius causes the ring to shift 0.3 nm. Figure 3.14 shows the response of two different rings on a wafer separated by about 1 mm. The rings show a difference in center wavelength of 0.6 nm, indicating that the radius can be controlled down to ~ 20 nm. Devices with different lateral distances between port and ring waveguides were realized in order to determine the influence on the coupling constants and the filters response. Figure 3.15 (left top and bottom) show the through and drop response of rings with lateral distances ranging from 0 to 1.6 μm. In the right part of this figure the fitted coupling constants are plotted against the lateral offset. Both the through- and drop responses were fitted. Clearly a change in coupling constant can be observed for varying lateral offset. The coupling is the strongest when the optical modes of the waveguide and the ring are closest together as was

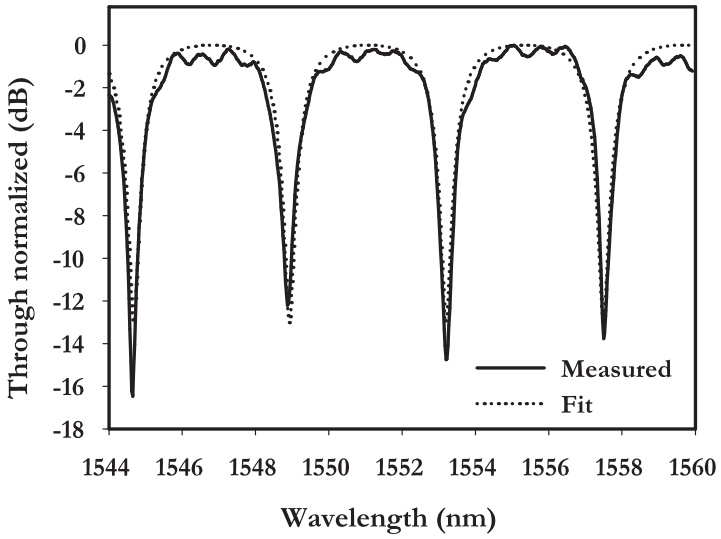

FIGURE 3.13: Measured and fitted response of 50 μm radius ring with κ_1=0.7, κ_2=0.6 and 10 dB/cm loss

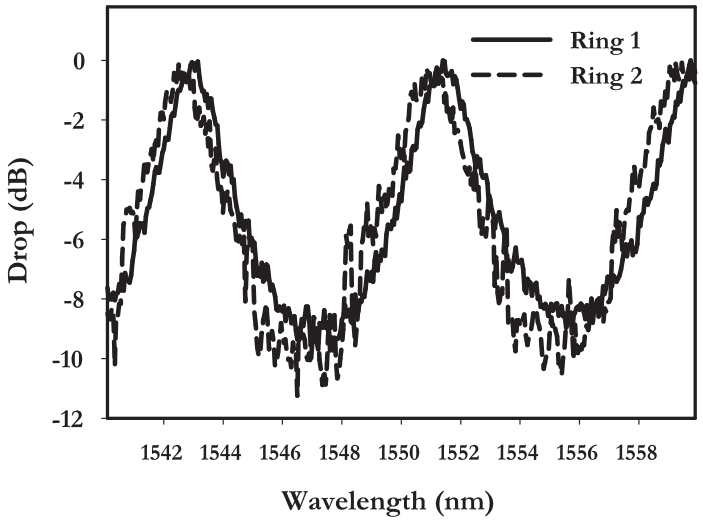

FIGURE 3.14: Measured drop response of single MRs showing good reproducibility for a 25 μm radius ring

predicted in Figure 2.10. The values extracted from the fitted through and drop response coincide except for the offset 0 μm, where fitting was very difficult due to the unpronounced dip. The offset where κ_1 reaches its maximum is slightly different from the offset for maximum κ_2, around 0.8 and 0.4 μm respectively. This can be explained when Figure 2.10(a) is taken into account. The effective index difference for the measured rings are around 0.005. Figure 2.10(a) shows that the maximum coupling is reached at an offset of 0.6 μm. Apparently there was a slight alignment error causing the ring to shift towards the first coupler. That way the coupling for the first coupler was increased, while the coupling for the second one was decreased.

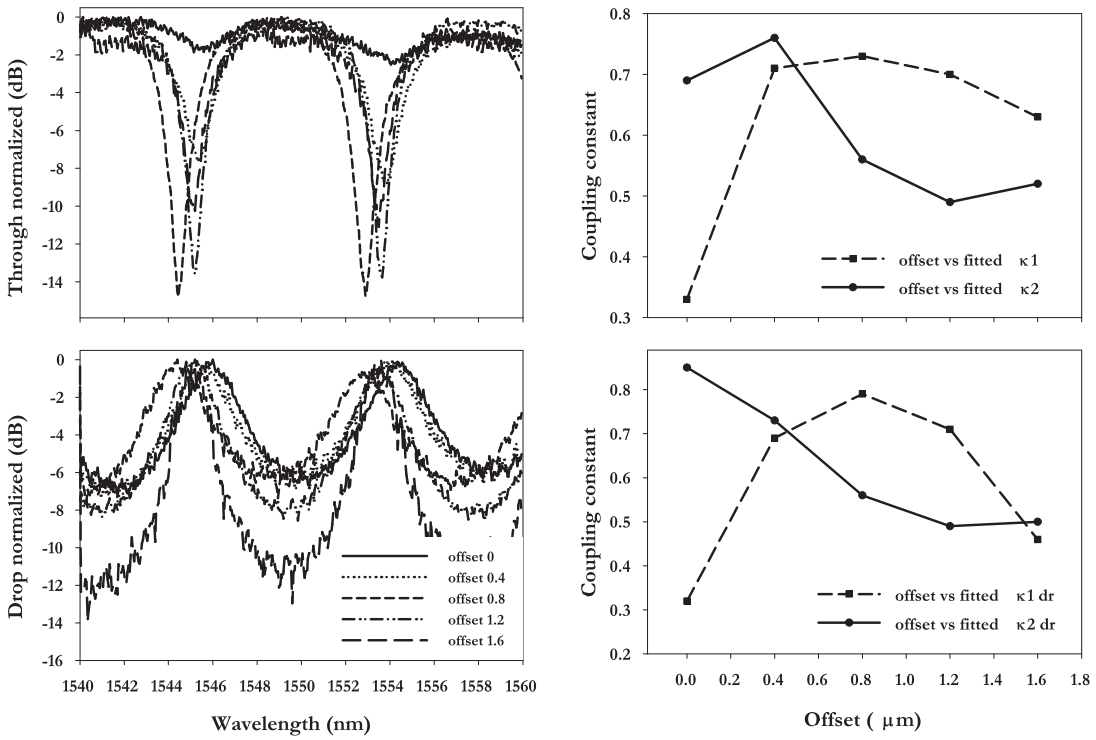

FIGURE 3.15: Through and drop responses for different offsets and the fitted coupling constants for 25 μm radius rings

3.5.1 Measurements on Thermal Tuning

Measurements were performed on a MR with a 4 μm PECVD SiO_2 cladding and chromium heaters. The results are shown in Figure 3.16(a), which gives the resonant dips in the drop-port as a function of applied power. The right part of this figure shows the measured relative shift in resonance wavelength as a function of the dissipated power for three different rings. When a linear dependency is assumed a relative resonance shift of 20 pm/mW can be found for the ring with radius 25 μm and 3 μm cladding. For the ring with a 25 μm radius and a cladding of 4 μm cladding this is slightly lower: 16 pm/mW. Finally the ring with 50 μm radius and 4 μm cladding has a dependency of 11.3 pm/mW. This last number is in good accordance with the simulated value from Figure 3.10 being 9 pm/mW. The difference can be explained by the fact that the simulated value is for a strip heater and not an Ω-shape one. It is nice to mention that the maximum achieved shift for the 50 μm ring is 4.3 nm, which outreaches the FSR of the ring of 4.2 nm. This way any wavelength can be addressed by tuning, which is a very important feature for use as part in optical network equipment.

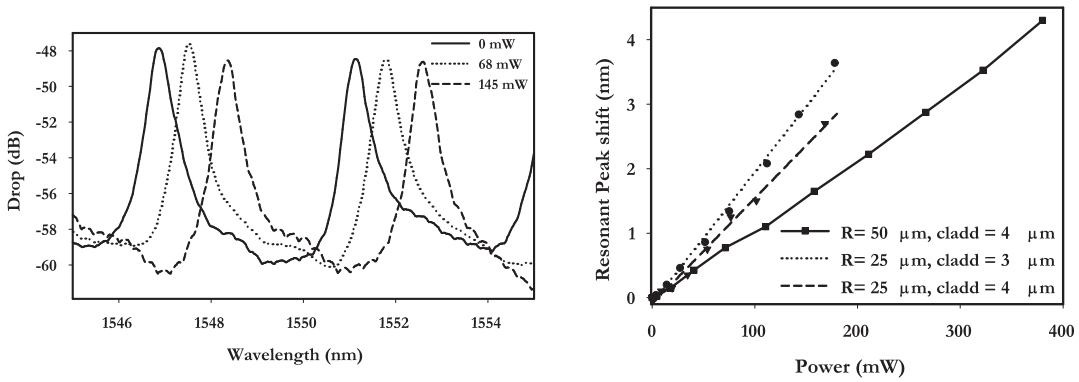

(a) (b)

FIGURE 3.16: (a) Shift of drop response as function of applied power and (b) relative shift vs applied power for three different rings

3.6 Tuning Speed optimization

Thermal tuning is not a very fast method of tuning, but it can be optimized. First, the material properties and geometry of several parts of the device structure could be optimized. The heat capacitance and resistance of the layer between the heater and the distance of the heater to the ring are parameters which influence the behaviour directly. The material and shape of the heater structure influence the speed as well. Secondly, the shape and amplitude of the driving signal can be optimized to increase the speed of the response with low driving powers. In this section the focus is on optimizing the driving signal, since the materials choice and geometry are in most cases optimized or a compromise was made with other design issues.

The amplitude and the shape of the driving current determines the speed and the magnitude of the heating. The application of a larger current will enhance the generated heat and therefore the increase in temperature, but this will also take more time. Furthermore, the final resulting modulation will not be perfectly linear with the power, because the resonance peak that is used for the modulation can only be locally approximated by a linear function. Note that this also depends on the modulation depth, i.e. the amplitude of the current.

The shape of the driving signal is also of great importance. By applying an overshoot the heating can be made faster. This means that at the start of the driving pulse, a higher current than is needed for the desired steady-state temperature is shortly applied. Just before the desired temperature is reached, the current is changed to a level that results in the desired temperature.

So far, only the possibility of speeding up the heating of the material is discussed. The cooling down of the structure is equally important, though. Enhancing the speed of the cooling down process might be done by active cooling, but this would require major adaptations to the device and the low cost low power principle would not hold anymore. A much easier way to do this is biasing. In biasing, a DC-current is applied, that will result in a relatively small change in temperature, refractive index and therefore resonance wavelength. To heat the device, the overshoot current is applied, to cool it down, a reverse overshoot is ap-

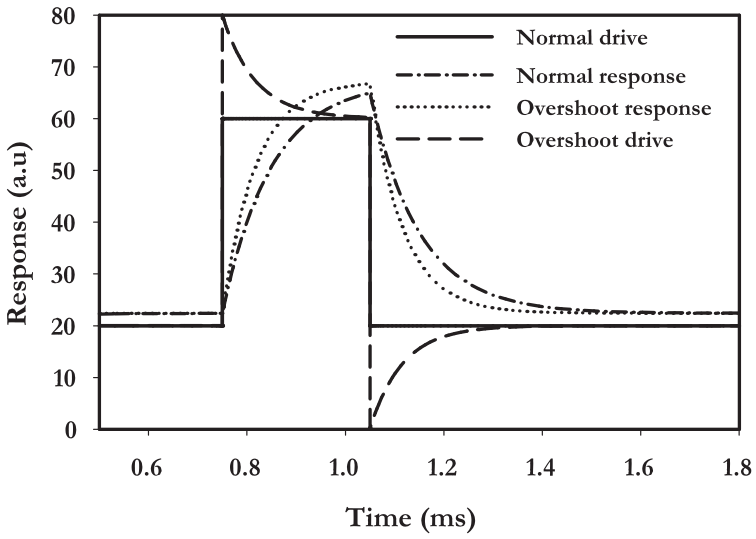

FIGURE 3.17: Simulated result of modulated output driven by normal block wave and overshoot-and-bias signal

plied. See Figure 3.17 for the simulated behaviour of overshoot and bias driving. The maximum current that can be applied is limited, due to the destruction of the heaters at high powers. The use of a bias will therefore cause a smaller modulation depth, but the modulation will be faster, since the time needed for cooling down is reduced. Figure 3.17 shows that the overshoot-and-bias driving signal causes a faster response in both heating and cooling. Measurements have been done on a single MR based on SiO_2/Si_3N_4 with a chromium heater. A modulating signal was applied to the heater. The wavelength of the incoming light source is chosen such that it is placed on the slope of the resonator response. Figure 3.18(a) shows the measured responses of the system with and without the overshoot in the driving signal at 500 Hz. The overshoot response reaches its maximum value faster and the slope is steeper for the rising case. The rise-time is improved from 0.93 ms to 0.54 ms, an improvement of 42%. The response in the falling slope did not change since in this case no overshoot was applied for the falling slope. Furthermore the steady state value of the overshoot driving signal is less then the normal driving signal, so the same modulation depth in output response was reached with 44%

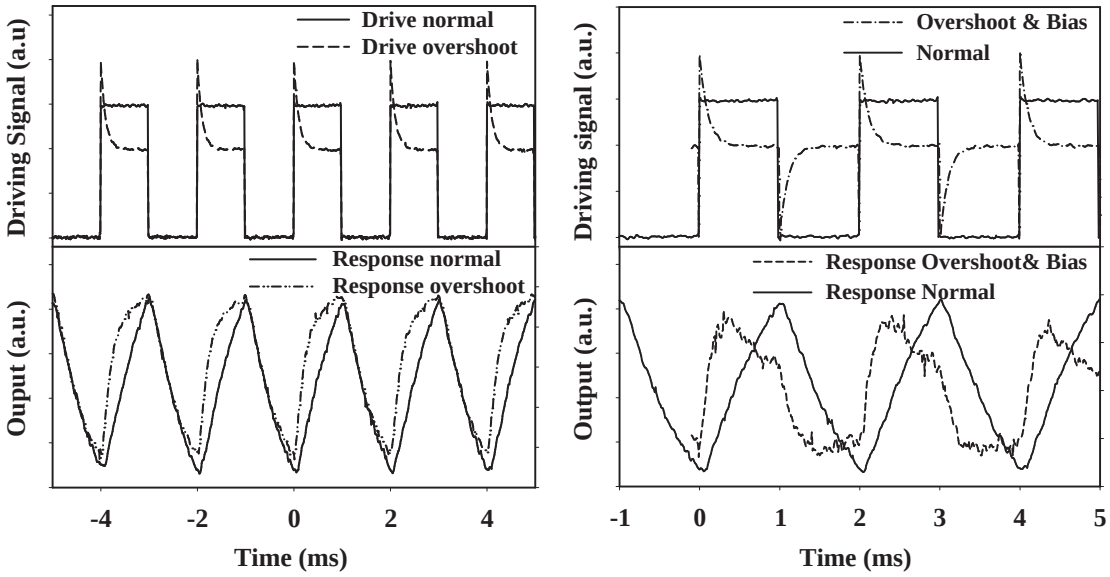

FIGURE 3.18: (a) Measurement of response with normal and overshoot drive (b) Measurement of response with normal and overshoot-and-bias drive

less power. The measurement shown in Figure 3.18(b) shows the result of the use of a bias in the driving signal. Now an overshoot has been applied on the falling slope as well. It can be seen that not only the rising slope is steeper than the normal response, but the falling slope as well. The modulation depth in this measurement is somewhat reduced, since the steady-state values for high and low were chosen the same, to investigate only the effect of the overshoot and bias on the slope behaviour.

By using the optimized driving signals, modulation frequencies up to 10 kHZ were measured, resulting in thermal switching speeds in the order of 0.1 ms.

CHAPTER 4

Multiple MR Structures

This chapter describes the use of devices built out of more than one single MR to create complex structures with enhanced functionality. The multiple MR structures will be compared to their competing technologies. Some examples of fabricated and measured structures based on multiple MRs will be given; a wavelength selective switch, a Vernier switch and a reconfigurable optical add-drop multiplexer.

This chapter was partly extracted from:

Geuzebroek, D.H. *et. al.* "Compact Wavelength-Selective Switch for Gigabit Filtering in Access Networks" Photon. Technol. Lett., Vol. 17, No. 2, pp. 336-338, 2005

Geuzebroek, D.H. *et. al.*, "40 Gbit/s Reconfigurable Optical Add-Drop Multiplexer based on Microring Resonators" invited at Europ. Conf. Optical. Comm. 2005 Glasgow UK

4.1 Introduction

Microring resonators combine wavelength selecting, switching and tuning capability in a single ultracompact element. Their application therefore, can lead to flexible implementations for a number of keycomponents in optical networks like optical cross-connects (OXC), reconfigurable optical add-drop multiplexers (R-OADM) and optical network units (ONU).

This section describes the use of multiple MRs in filter applications. As will be shown below, the use of multiple MRs allows to improve substantially the specification of the devices and to enrich the functionality of the filter structures. As was demonstrated in the previous section, the performance of filters based on MRs for application in a telecommunications network can be specified by network level parameters like insertion loss, channel separation or inter channel crosstalk. Since the attainable specifications for these system requirements are limited for a single MR, an attriactive option is to use more than just one ring. This is possible as a single ring occupies only a small chip area. When more than one ring is used, several new structures can be created which can be divided into three groups:

- Higher order filters
- Devices with improved specifications
- Devices with a more complex functionality

Higher order filters employ multiple rings to create multiple feedback paths. By using more than one ring in the filter device the specifications can be improved. Finally complex functions can be created by cascading (active and passive) rings in complex fashions to create a richer functionality than just plain filtering.

Higher order filters

Higher order MR filters are filters where several feedback paths are available to generate the response of the filter. Figure 4.1 shows two different setups, in literature known as the serial cascade [69–73] and the parallel cascade [74–80]. In both cases, the additional feedback paths result in an improved filter response, i.e.

a more flat-top response in the pass-band and a steeper roll-off at the pass-band edges. The design of a serial cascade is extensively described in [17], where a top-down approach is used based on the z-transform. In this way the desired filter responses can be linked directly to the parameters of the serial MR cascade.

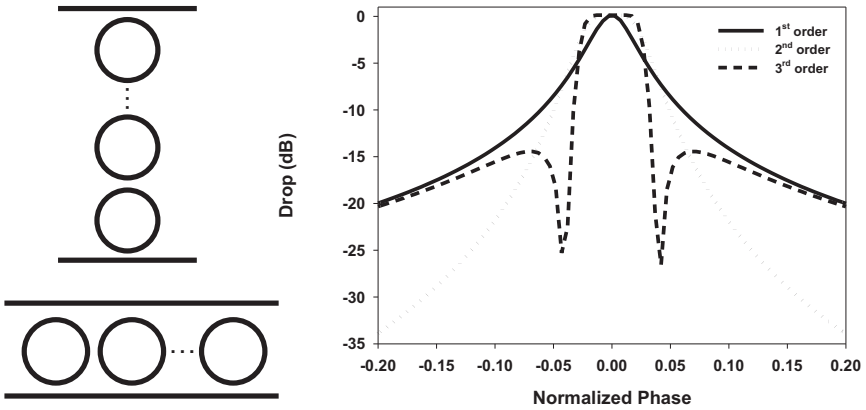

FIGURE 4.1: Higher order MR filters: serial cascade (top-left), parallel cascade (bottom-left) and simulated responses of parallel cascade filters of different orders.

The parallel cascade also offers improvement of the response. These filters can be designed by using the formalism as used in [77, 79] who consider the cascade as a generalization of a Distributed-Feedback (DFB) grating. Another approach is to describe the filter in terms of a prototype filter as known in the microwave domain [74]. Also scattering matrix descriptions are given for the parallel cascaded devices [76, 78] Recently, the z-transform descriptions of these filters has been applied [81] to make a top-down design possible like in the serial cascades . In the serially cascaded structure it is necessarily to control the resonance wavelength of each ring in the filter accurately. In the parallel cascade the distance between the rings must be controlled well with sub-wavelength precision. In both cases the filter responses can be further improved by special designs of all the coupling constants in de cascade [79]. By apodizing the coupled constant, for each individual ring along the array, the filter shapes can be improved even further.

Specification improvement

By using multiple rings also the resulting specifications will improve largely. There are configurations where MRs are solely used for cleaning up channels and improve specifications like the cleanup filters in [82,83] or the Vernier filters [37,77]. Adding rings to a device in order to obtain improved specifications puts severe demands on design and technology, as any additional losses or shift in resonance wavelength will deteriorate the overall performance. But the technological effort of reaching these specifications with a single ring might be even larger. These type of filters differ from the higher order filters in that no additional feedback paths are used, just more rings to improve the specifications.

Complex functions

By employing more than one ring in a device, higher complexity and increased flexibility can be added giving rise to a new functionality. In the following part of this chapter this principle will be extensively shown with examples like a wavelength selective switch, a vernier switch and a reconfigurable optical add-drop multiplexer.

4.2 Complex functions

Since a single MR occupies only a small area, applying more than one MR to create extended functionality is an interesting option. This is especially attractive when with these multiple MRs functions can be created which until now suffered from problems with integration and scaling. In the following, arguments will be given in the advance of multiple MR structures for complex functions. Figure 4.2 shows schematically the rich functional behaviour which can be obtained by a cross-grid or matrix arrangement [84] of MRs requiring only a few mm^2 of chip area as will be explained in the following. The component has N inputs, M outputs and can handle Λ wavelengths. The first stage consists of a tunable WDM demux for each incoming fiber, where every wavelength channel can be tuned separately. Tuning each wavelength separately is a key characteristic since it allows for

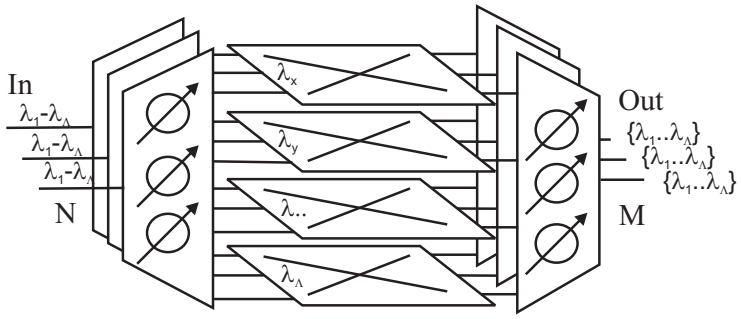

FIGURE 4.2: Functional scheme of a fully reconfigurable and scalable switch matrix with N = 3 input and M = 3 output fibers, each with Λ wavelengths.

grid-independent and reconfigurable devices. In addition, low-cost non-stabilized laserdiodes with thermal drift become acceptable. Second a plain of space switches for each wavelength and output fiber makes it possible to connect any wavelength to any output channel. The third stage is a set of tunable multiplexers allowing unique distribution of wavelengths as well as broad- and multicasting. The cross grid based arrangement of tunable MRs have the potential to combine the optical functions given in Figure 4.2 in a compact device. To show some of the capabilities three examples will be given an R-OADM (reconfigurable optical add drop multiplexer), an OXC (optical cross connect) and an ONU (optical network unit).

Optical crossconnect

An OXC connects two or more networks with each other by a constant or varying number of different, sometimes in time changing wavelength channels. Figure 4.3(a) shows a possible implementation of an OXC with a matrix of tunable MRs having the same functionality as depicted in Figure 4.2. The horizontal dimension is the tunable WDM demux, the vertical dimension the cross plain. Two of these plains are needed to ensure that each wavelength can be switched to any of the attached network. In this setup each wavelengths splitting plain must have different allocations of wavelengths, avoiding wavelength blocking. Since each ring can be tuned separately to any wavelength this is possible. For optical cross connects it is important that high speed data can be switched and filtered. As will be shown

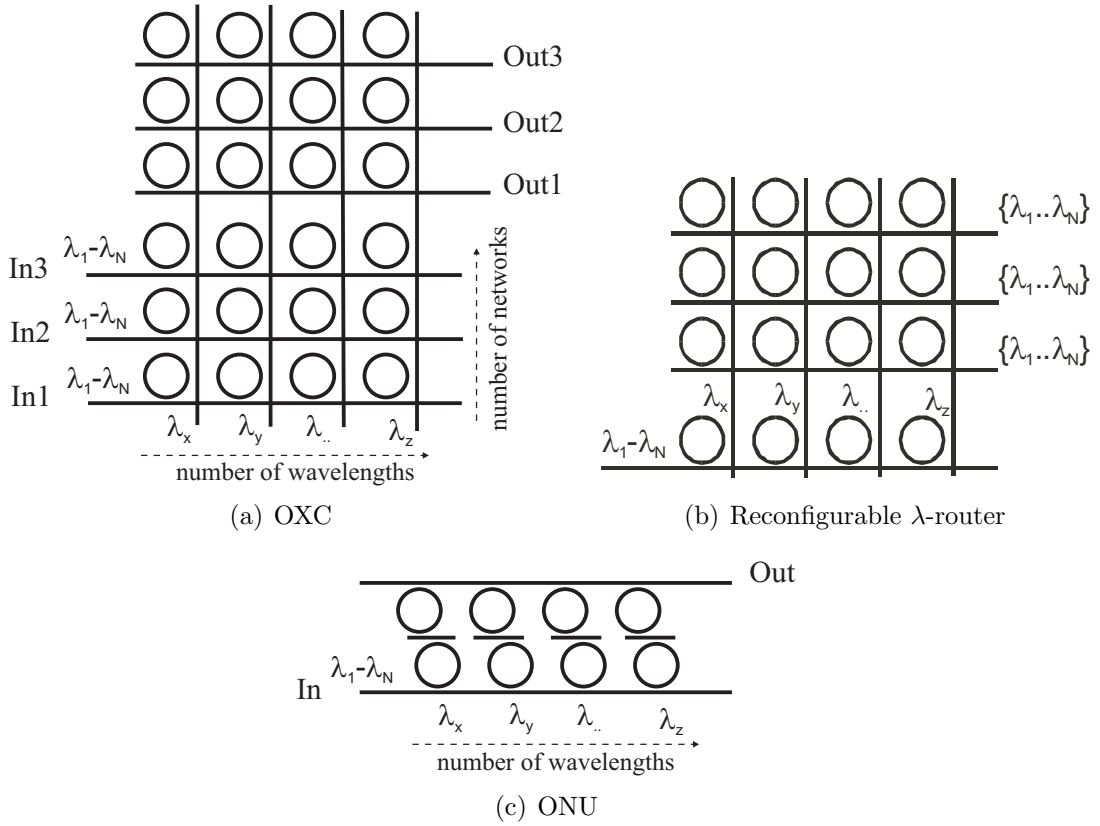

(a) OXC

(b) Reconfigurable λ-router

(c) ONU

FIGURE 4.3: Possible implementation of an OXC, λ-router and ONU based on tunable MRs

later in this chapter, in a pigtailed and packaged test structure consisting of 4 tunable MRs arranged as the lowest row in Figure 4.3 (a), error free filtering and routing of data signals with a speed of 40 Gbit/s has been demonstrated.

Reconfigurable λ-router

In access networks the functional component just described changes in that sense that only one input is used. Still several outputs are used for end-users. The key functionality in this component is the reconfigurability. Figure 4.3(b) shows an implementation of this reconfigurable λ-router in a cross grid structure. The device consists of a single input port and one horizontal plain of wavelengths. The switching matrix is needed to ensure that every end-user can be supplied with

any set of wavelengths. Only this allows multi- and broadcast services as well as flexibility in bandwidth allocation.

Optical Network Unit

In an optical access network, most likely a Passive Optical Network will be the most economical and therefore most attractive implementation. Especially when also at this level WDM is introduced, full use of bandwidth can be made in combination with the Reconfigurable λ-router on the head-end. An ONU needs to be placed in the customer's premises. MRs can be used in this equipment since they allow integrating the complex functions needed for WDM-PON systems onto a mass-producible scale. Furthermore, since the MRs can be actively tuned, changes in the wavelength of the channel or changes in temperature can be overcome by a simple and inexpensive feed-forward control. Figure 4.3(c) shows the schematic drawing of a MR switch based ONU enabling the reception of multiple wavelength channels, both dedicated and multicast ones. The MR based wavelength switch will be discussed further in section 4.4.

4.3 Alternatives

A functional component as the one given in Figure 4.2 can also be made with other technologies besides the microring resonator. Table 4.1 gives an overview of some switching and some wavelength multiplexing technologies. [56, 85, 86]

Multiplexing alternatives

Currently the main component used for wavelength filtering is the Arrayed Waveguide Grating (AWG) [87–89]. It is very suitable for (de)-multiplexing a number of wavelengths into an array of output waveguides. It is a mature technology which attracted a lot of interest in the last decade. The drawback of the device however, is the temperature instability and the fact that the AWG cannot be tuned for each channel separately. The largest disadvantage is that the principle of the device

TABLE 4.1: Alternative switching and (de-)multiplexing technologies

Switching Technology	Switch type	Advantages	Disadvantages
Thermo-Optical	DOS	Mature technology	Scalability, Power consumption, size
Thermo-Optical	MZI		
MEMS free-space	mirror	Low insertion loss, Scalability,	Packaging, multicasting
MEMS planar	waveguide		
Electro-Optical $LiNbO_3$	DOS	High speed	Insertion loss
Electro-Optical SOA	waveguide	Loss compensation, high speed	Noise, distortion, technology
Liquid Crystal	Fiber optic	Insertion loss	Temperature sensitivity

(de-) Multiplexing technology	Type		
AWG	planar	mature technology with high wavelength selectivity	High IL, Not tunable per channel
TFF	planar	High selectivity, low IL	highly dispersive, low tenability, difficult integration
Diffraction Grating	3D assembly	mature technology with high wavelength selectivity	High IL, difficult assembly
Fiber Bragg Grating	fiber	mature technology with high wavelength selectivity	ports not separated
MZI	planar	mature technology with high wavelength selectivity	larges cascades requires large area

is a delay between the branches of the waveguide array. For this some length is needed, consuming chip area.

Switching alternatives

A switch matrix as shown in Figure 4.2 is currently constructed by either a plain of Digital-Optical-Switches (DOS), Mach-Zehnder-Interferometer switches [90–92] or by a matrix of Micro Electro-Mechanical System (MEMS) based mirrors [85, 93]. Although the switch matrix is relatively easy to make, the disadvantage is the large area it consumes and the scalability. The most promising switch architecture for large matrices is the MEMS based mirror. It has shown very low losses and is scalable to higher port counts, however since the technology differs from the planar waveguide approach, packaging might be an issue. Furthermore a MEMS mirror does not allow for multicasting.

When a component like the one in Figure 4.2 needs to be made with AWGs and DOS matrices the following estimate can be given of the area needed for a component with N input, M outputs and Λ wavelengths:

$$A_{total} = N \times A_{AWG\ (1\times\Lambda)} + M \times A_{Switch\ (\Lambda\times M)} + M \times A_{AWG\ (\Lambda\times 1)} \tag{4.1}$$

where $A_{AWG\ (1\times\Lambda)}$ and $A_{AWG\ (\Lambda\times 1)}$ are the areas of an AWG with 1 input and Λ output ports and Λ input ports and 1 output port respectively. $A_{Switch\ (\Lambda\times M)}$ is the area of a DOS switch matrix with Λ input and M output ports. In comparison, a MR based implementation like the OXC from Figure 4.3(a) will occupy an area according to:

$$A_{totalMRs} = (N \times \Lambda + M \times \Lambda) A_{MR} \tag{4.2}$$

where A_{MR} is the occupied area of a single ring. Table 4.2 gives for a 4×4×16 architecture a comparison of the occupied area for an AWG/Switch plain combination on the one hand and the MR implementation on the other. The areas for the AWG and switch plain are extracted from literature and an index contrast technology comparable with the MR technology used in the thesis (Δn = 30%) is assumed [88, 89]. As can be seen the area improvement factor is in the

order of 50 times. Since the MR is in fact a wavelength selective space switch and

TABLE 4.2: Occupied chip area of a OCX for AWG/Switch-plain combination and a MR implementation

	Element area	Total area 4 × 4 × 16
A_{AWG}	2 mm × 2 mm	151.2 mm^2
A_{switch}	0.5 cm × 0.5 cm	
A_{MR}	150 × 150 μm	2.88 mm^2
improvement factor		52.5

thus combines both switching and filtering, the occupied area will be less than in comparable implementations in the same index contrast. To improve the specification of single rings, more rings can be used per wavelength-switching element. Although this will cost additional chip area, the area improvement in comparison with the alternatives, offers enough room to sacrifice some area for specification improvement. The chip area consumption will not be limited by the number of rings, but by the number of fibers attached. When standard fiber arrays are being used, the fiber spacing of 250 μm between two fibers will have a large effect on the area consumption.

To show the capability of multiple MR structure to create complex functionalities, some examples will be given in the remaining of this chapter. The examples, a wavelength selective switch, a Vernier switch and a reconfigurable optical add-drop multiplexer, are all made with the 30% index contrast SiO_2/Si_3N_4 technology.

4.4 Wavelength Selective Switch

An example of using more than one ring to create an extended functionality is the microring based switch shown schematically in Figure 4.4(a). A typical calculated response of the two-stage switch in ON and OFF state is shown in Figure 4.4(b). The first stage of the switch (MR1) selects a certain wavelength band. By tuning the centre wavelength of the second stage (MR2) to overlap the centre wavelength of the first stage, the wavelength band is switched to the drop port (ON state). In the OFF-state the centre wavelength of the second stage does not overlap and

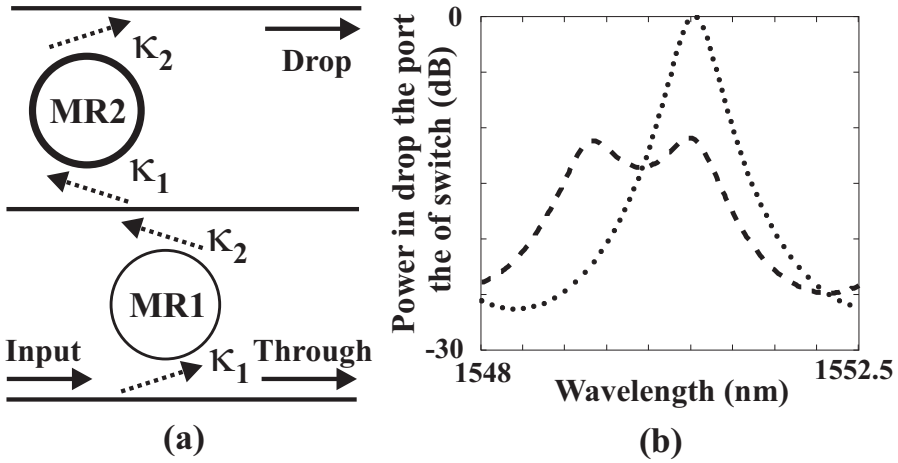

FIGURE 4.4: (a) Schematic drawing of a switch based on two microring resonators and (b) simulated responses of Switch in ON-state (dotted line) and Switch in OFF-state (dashed line)

.

the light dropped by the first ring is not used. The individual stages can be made out of higher order filters to increase the ON/OFF ratio as is described in [29, 32]. Simulations show that ON/OFF ratios of 30 dB can be reached with tuning powers of 30 mW when using parallel cascaded stages and a tunability of the center wavelength of 20 pm/mW [47]. The SiO_2/Si_3N_4 MRs are thermally tunable by means of a heater on top of the cladding. Driving the MRs thermally is fast enough for switching applications where sub-ms responses are sufficient. Switching is possible up to several kHz as is described in chapter 3 by optimization of the driving signal. For applications in an access network the switch is especially useful as it allows to select just one specific wavelength band and to disregard the others. This is a useful function in Passive Optical Network (PON) architectures. The selectivity of the switch can be improved by using two different radii of the rings in the switch. In that case the Vernier effect accounts for an increase in the total Free-Spectral-Range up to 36 nm [94]. The switch can be a building block for even more complex structures like an array of switches [18] which can switch different wavelengths bands simultaneously.

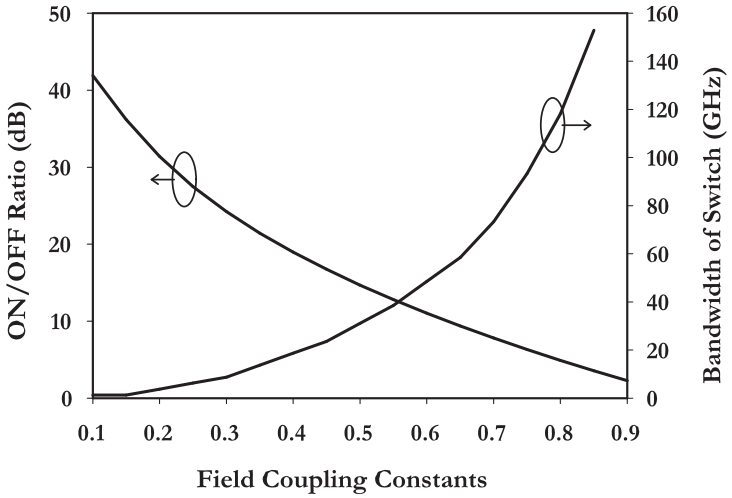

FIGURE 4.5: Effect of coupling constants on the ON/OFF ratio and the 3dB bandwidth of the switch. Both the coupling constants are assumed to be equal; the ring losses were 5 dB/cm and the radius 50 μm.

4.4.1 Design Issues

The main issues in the design of a MR based switch are related to the ON/OFF ratio, the channel separation, the bandwidth and the on-chip insertion loss of the switched channel. The ON/OFF ratio is influenced by the shape of the filter function (steepness) and the thermally induced shift to switch between ON and OFF state. Since the switch is made out of two rings its response exhibits already an increased steepness in comparison to a single ring. A steeper filter shape also reduces the driving power of the switch since smaller shifts are needed for the same ON/OFF ratio. The channel separation of the switch is determined by the Finesse of the device. The bandwidth and insertion loss are determined by the losses inside the individual rings and the coupling constants κ_1 and κ_2, i.e. the fraction of the field that is coupled from the waveguide to the ring and vice versa. In order to have as much power as possible in the drop port, the losses must be low and the

coupling constants of the two coupling regions must be matched to the losses in the ring [32]. The highest extinction ratio (difference between power in drop port and power in through port) can be reached when the individual rings are designed to be critically coupled as described in [33]. The microrings of the described switch have a radius of 50 μm. The effective refractive index of the ring is matched to that of the waveguide underneath the ring. By setting the thickness of the separation layer and the horizontal distance between the ring and waveguide, the coupling constant is controlled.

To ensure a certain 3dB bandwidth the coupling constants of the ring are determined according to Figure 4.5. For a 3dB bandwidth of the switch of 50 GHz and a loss of 5 dB/cm in the rings the coupling constants should be chosen around 0.6. To obtain the desired coupling constants a commercial 3D BPM simulation program [39] was used to determine the corresponding lateral and vertical distances between ring and port waveguides. Figure 4.5 also shows that the ON/OFF ratio will in this case be around 12 dB. To improve this ratio with the current parameters the bandwidth must decrease. For the current device optimization of the bandwidth is chosen above ON/OFF ratio.

4.4.2 Spectral Measurements

A microring resonator based switch has been realized in SiO_2/Si_3N_4 technology [34, 65]. The switch was made out of two microring resonators which are vertically coupled to the port waveguides. The port and ring waveguide dimensions are 2 x 0.140 μm and 2.5 x 0.180 μm respectively. The vertical separation between port and ring waveguide is 1 μm. Omega-shaped chromium heaters were applied on top of the device. The measured spectral responses of the switch in both ON and OFF state are shown in Figure 4.6. The responses are normalized to the measured power in the through port of the device while OFF-resonance and give consequently the on-chip IL in the drop port. The measurements are in close correspondence with the simulated response in Figure 4.6(b). The switch has a measured ON/OFF ratio of 12 dB and a channel separation (difference between ON and OFF resonance) better than 20 dB. The on-chip IL in the drop port of the switch is around 6 dB.

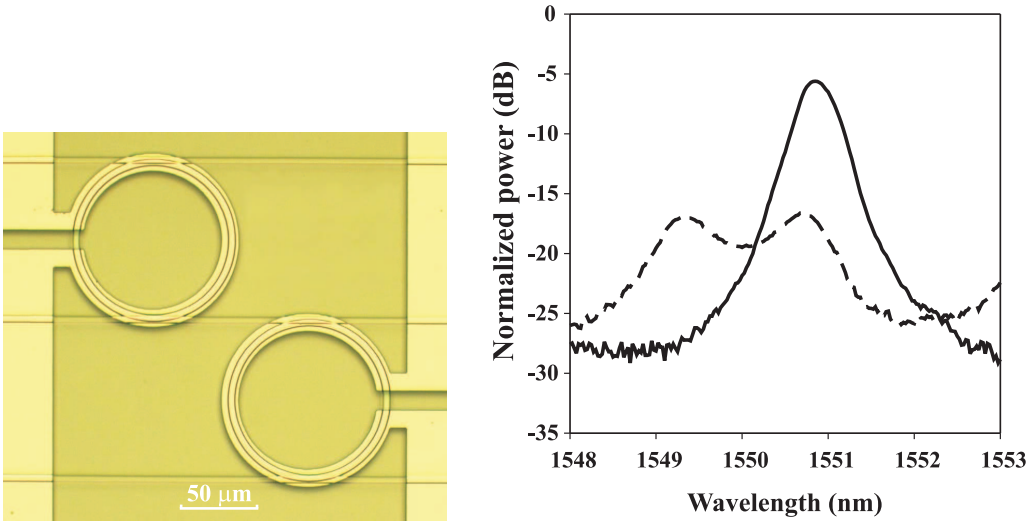

(a) (b)

FIGURE 4.6: (a) Microscope photograph of a realized switch based on two MRs (b) Measured response of Switch. Solid line: ON-state, Dashed line: OFF state.

The device was switched between ON and OFF using 225 mW of electrical power. This implies a shift in centre wavelength of 6.5 pm/mW. Also single rings with the same specification have been characterized. The measured responses were fitted to analytical models to extract the loss in the ring and the coupling constants. The loss inside the ring was found to be about 5 dB/cm, corresponding to 0.16 dB/roundtrip. The measured field coupling constants of 0.6 are in good agreement with the designed values. The propagation losses inside the straight waveguides are lower than 1 dB/cm. The on-chip IL in the drop port of a single ring is about 3 dB which is in accordance with the 6 dB IL in the switch. The rings in the switch show high drop efficiency even after being dropped by two rings. The fit to the measured response shows that the coupling constants for the two coupling regions for both rings are almost identical, which explains the high drop efficiency. Figure 4.6 shows a photograph of a realized switch. The two omega-shaped heaters on top of the two rings and the port waveguides are clearly visible. The size of the switch itself is about 200 x 200 μm^2 excluding the pads to wire the heaters.

In conclusion a compact wavelength-selective switch based on two SiO_2/Si_3N_4 microrings has been designed and realized. Measurements show an ON/OFF ratio of 12 dB and a channel separation of 20 dB. The measurements are in close correspondence with the calculated responses. In chapter 5 measurements on a single MR identical to those employed in the switch will be described. As a result a filtered 10 Gbit/s NRZ modulated signal could be demonstrated without degradation. The measurements show the potential of multiple rings to reach an advanced functionality. To improve the specifications of the switch even more rings can be used. Either as higher order filter stages or as cleanup ring as described in [82]. By using polarization diversity the polarization dependency of the device can be solved. To increase the ON/OFF ratio and lower the power consumption while keeping first order stages, the ring radii have to decrease by a factor of two.

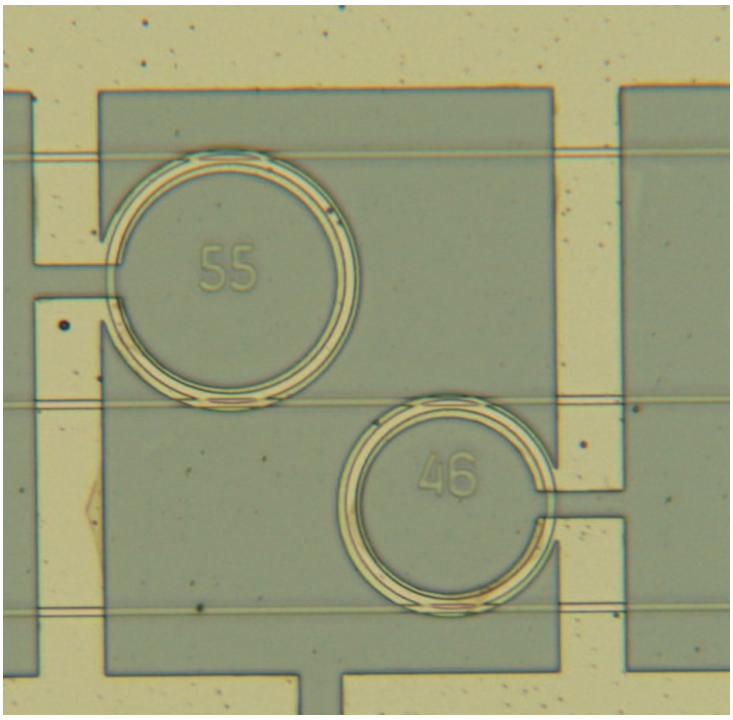

FIGURE 4.7: Picture of realized Vernier switch based on two microrings with different radii of 46 μm and 55 μm

4.5 Vernier switch

To increase the selectivity of the MR based switch the Vernier effect can be used. If the switch is made out of two rings with different radii, the FSR of the switch will be a combination of the FSR of the two rings according to:

$$FSR_{Switch} = N \cdot FSR_{R1} = M \cdot FSR_{R2} \tag{4.3}$$

where N and M are integers. Although the selectivity is increased, additional intermediate side-lobes can cause undesired effects like additional crosstalk. A

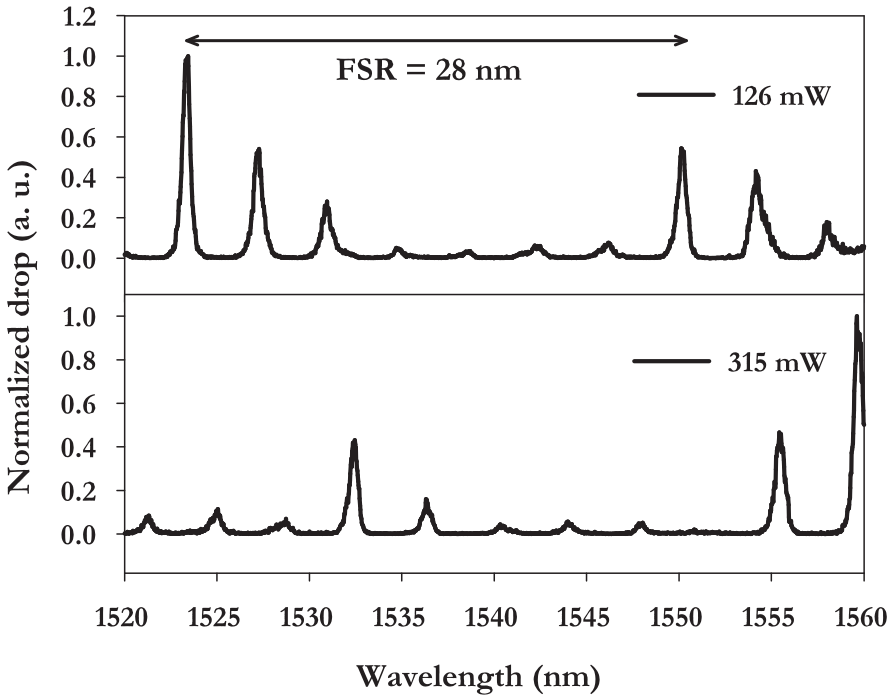

FIGURE 4.8: Measured response of the Vernier switch with total FSR = 28 nm. (Top) 126 mW, (Bottom) 315 mW driving power to only the larger ring

Vernier switch has been realized with ring radii of 46 and 55 μm, which have a FSR of 4.66 and 4 nm respectively. These values where chosen because the FSR

of the switch can now be extended to 28 nm. Furthermore differ the radii of the Vernier switch not too much from the radius of the standard switch (50 μm) so that no redesign of the layer structure was needed. The phase-matching conditions are slightly different in comparison with the standard switch, but still enough coupling could be reached. A photograph of the realized Vernier switch is shown in Figure 4.7, where the difference in radii is obvious. Measurements on this Vernier switch show a total FSR of 28 nm as is shown in Figure 4.8. By tuning the larger ring the place of the main peak can be moved across 7 nm. By applying a current to both rings, any wavelength within the total FSR can be addressed since the tuning range of the rings is at least equal to the FSR of the individual rings.

4.6 R-OADM

As was stated in the introduction of this chapter a reconfigurable Add-drop multiplexer (R-OADM) would be an interesting component to base on microring resonators as it can be a building block for OXC [95]. Furthermore a R-OADM like the one schematically drawn in Figure 4.9 is a good device to demonstrate the capabilities of multiple microring structures. Besides the schematic drawing in Figure 4.9 also a photograph of a realized R-OADM based on MRs is shown. The device is built out of four identical MRs, each able to drop a particular wavelength. Since the thermo-optic tuning range of the ring outreaches the free spectral range (FSR) of 4.2 nm of the ring, any wavelength within the FSR can be addressed. The rings can be tuned separately, making the device grid independent enabling to be very flexible in bandwidth allocation schemes. Besides the general input and output port (In, Out) the device has four add-ports and four drop-ports (Add_1-Add_4, $Drop_1$-$Drop_4$). The device with in total 10 input/output ports and 4 heaters is completely pigtailed and packaged. The individual rings were designed to have a bandwidth around 50 GHz as is described in the previous chapter and [96], by choosing the proper coupling constants ($\kappa = 0.5$) and MR losses (< 5 dB/cm). Very important for obtaining proper drop and add power is the couplers of the MR being as symmetric as possible [32].

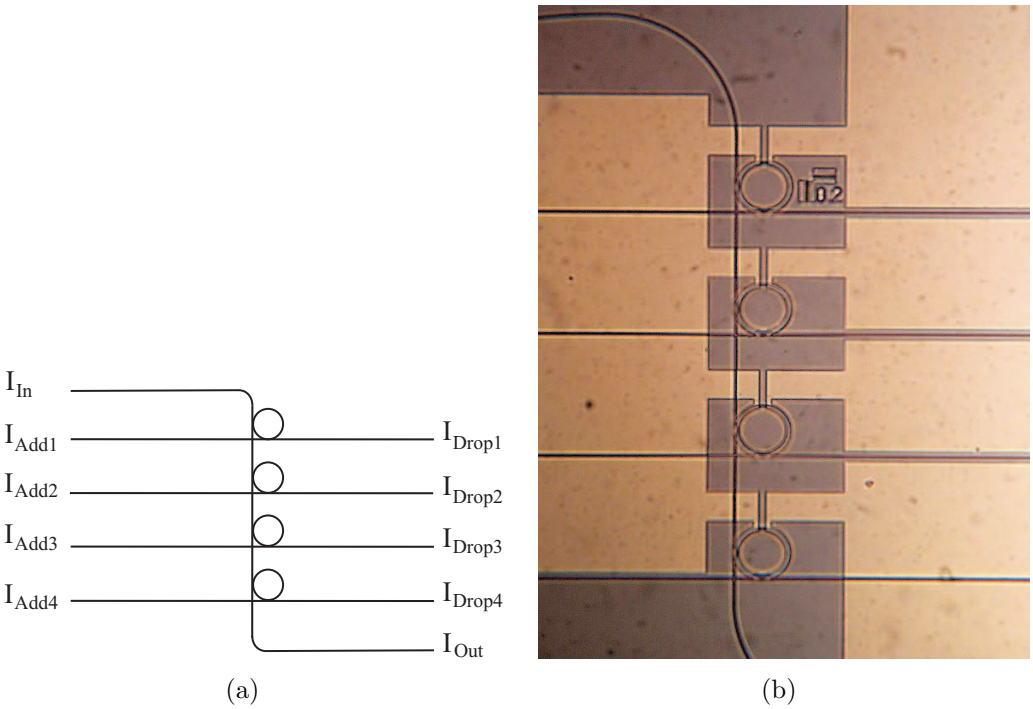

FIGURE 4.9: Schematic lay-out of the MR-based R-OADM and microscope picture of the realized device

4.6.1 Pigtailing and packaging

To be able to perform network level tests on the R-OADM, it is necessary to fully package the device. In- and output fibers have to be attached to the optical chip and it needs to be electrically connected to a controlling unit.

The R-OADM already was designed to facilitate butt-fiber coupling of the in- and output channels to two arrays of fibers. For this purpose the spacing between the input waveguides was set to be 250 μm which is a standard for optical fiber arrays. Furthermore, to make the alignment more easy a waveguide was added which was returned to the same facet as is shown in the left side of Figure 4.10. By launching light on one side and measuring the output power in the other, all intermediate channels are aligned. This eases the alignment procedure at the expense of using an array which includes two additional fibers.

When the fiber array and the optical chip are aligned they need to be fixed

to ensure the alignment. This has been done by a photo-curable epoxy. In this way standard MT (mechanical transferable [97]) fiber array connectors with single mode fibers were attached to the optical device. The pigtailed device was mounted

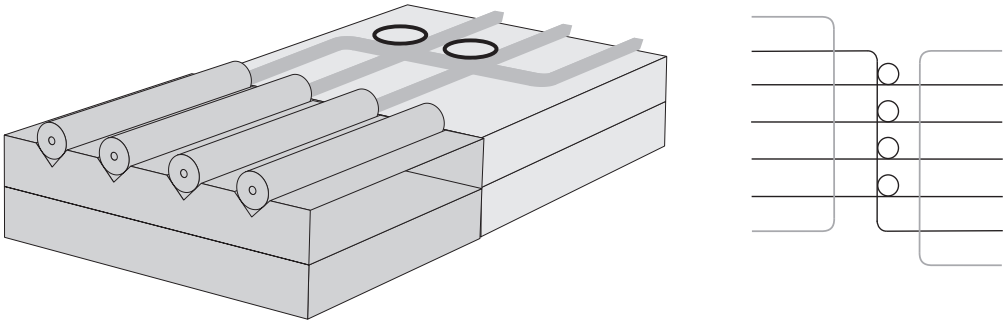

FIGURE 4.10: Schematic of fiber array coupled to optical device (left) and schematic drawing of device with additional alignment waveguides drawn in gray

and wirebonded with Aluminium wires into a standard DIL (Dual In-Line) ceramic package. This was then placed together with some driving electronics in a plastic housing. Figure 4.11 shows a photograph of the pigtailed and wired bonded device. It shows the chip containing 4 R-OADMs, of which only a single one was wirebonded and attached to MT fiber arrays. Appendix C shows the device in its full housing.

The device is butt-coupled to standard single-mode fibers (SMF). Since the optical mode of this fiber does not match the mode of the channel waveguides, losses will be introduced. Table 4.3 shows the calculated loss per fiber-chip coupling for a SMF and a fiber with a small core (SC) to a channel with 2 μm width and 1.5 μm width. The first waveguide is the standard channel, the second one is the smallest possible taper which can be made with the current lithography. A structure tapering from 2 μm to 1.5 μm was used in the R-OADM to optimizes the fiber to chip coupling a little. For the calculations only horizontal tapering is assumed. As can be seen from this table the fiber to chip losses are still high. By applying better lithography, allowing smaller lateral dimensions, together with applying tapers in the vertical dimension [98], fiber to chip couplings can be decreased to 1 dB.

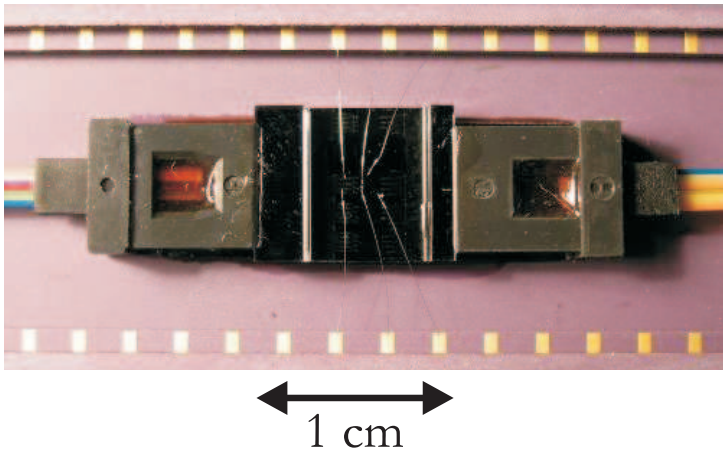

FIGURE 4.11: Picture of pigtailed and packaged R-OADM based on MRs

TABLE 4.3: Simulated fiber to chip losses for channels with height 140 nm

	Modal waist fiber μm	Waveguide μm	Coupling dB
SC	4.5	2	1.9
SMF	9	2	6.6
SC	4.5	1.5	1.7
SMF	9	1.5	6.2

4.6.2 Spectral measurements

Figure 4.12 shows the wavelength scan measurements of the through, add and drop ports, when each ring is addressed to one specific wavelength. This figure shows the capability to drop and add four channels at any desired wavelength within the FSR. The individual rings show an insertion loss in the drop port of 2 dB.

The pigtailed R-OADM was measured using a broadband source and an optical spectrum analyzer with a resolution of 0.1 nm. The top figure in Figure 4.12 shows the response measured at the through-port when the broadband source was connected to I_{In}. The four dips represent the powers extracted from the I_{In} port and switched to the four drop ports. A total heater power of 446 mW was required to set the MR resonance frequencies on a 100 GHz ITU Grid (spaced at

0.8 nm). The minima of the individual MR through responses are 12dB below the normalized input power level. A fit of the individual MR responses to a theoretical MR model showed field coupling constants κ_1 and κ_2 of 0.56 and 0.44 respectively with ring losses of around 1.5 dB/cm. The measured FSR and Finesse were 4.2 nm and 10 respectively, giving a FWHM of 0.4 nm ($\approx$ 50 GHz). It is also possible to let the four rings filter the same wavelength, as is shown in the measurements from Figure 4.13. This figure shows the response measured by an optical spectrum analyser, when all four rings are tuned to different wavelengths (four channel configuration) with a 100 GHz channel spacing. In the single channel configuration all the MRs are tuned to the same wavelength, demonstrating the cleanup effect of using more rings to extract unwanted power in a certain port. Placing the four MR on to one wavelength channel is necessary for multicasting purposes as will be shown in the next chapter. This configuration could be set while dissipating only 20 mW due to the fact that the MRs already had resonance frequencies within 0.1 nm of each other, showing good fabrication uniformity. The change between configurations could be made in $<$ 1 ms. The middle and lower picture from Figure 4.12 show the normalized responses for the adding and dropping configuration. In the Add configuration the MRs select a channel from the add ports and directs it to the waveguide channel leading to I_{out}. The minima of the individual MR drop responses are 17dB below the normalized output power level. The effects of the adjacent MRs on an add channel can also be observed, for instance in the add response of the first resonator. Here the three other MRs, drop power from the main channel which shows up as dips in the response. Using the parameters obtained from the fit to the responses the channel crosstalk of the device was calculated to be -11.7 dB. The drop configuration shows responses similar to those of of the add configuration. Now the power is extracted from I_{In} to the individual drop ports. The dips in the spectrum, caused by the other MRs, are deeper than those seen in the add configuration which is due to the asymmetry in the coupling constants that give a different through response depending on which waveguide is used as input- or drop port.

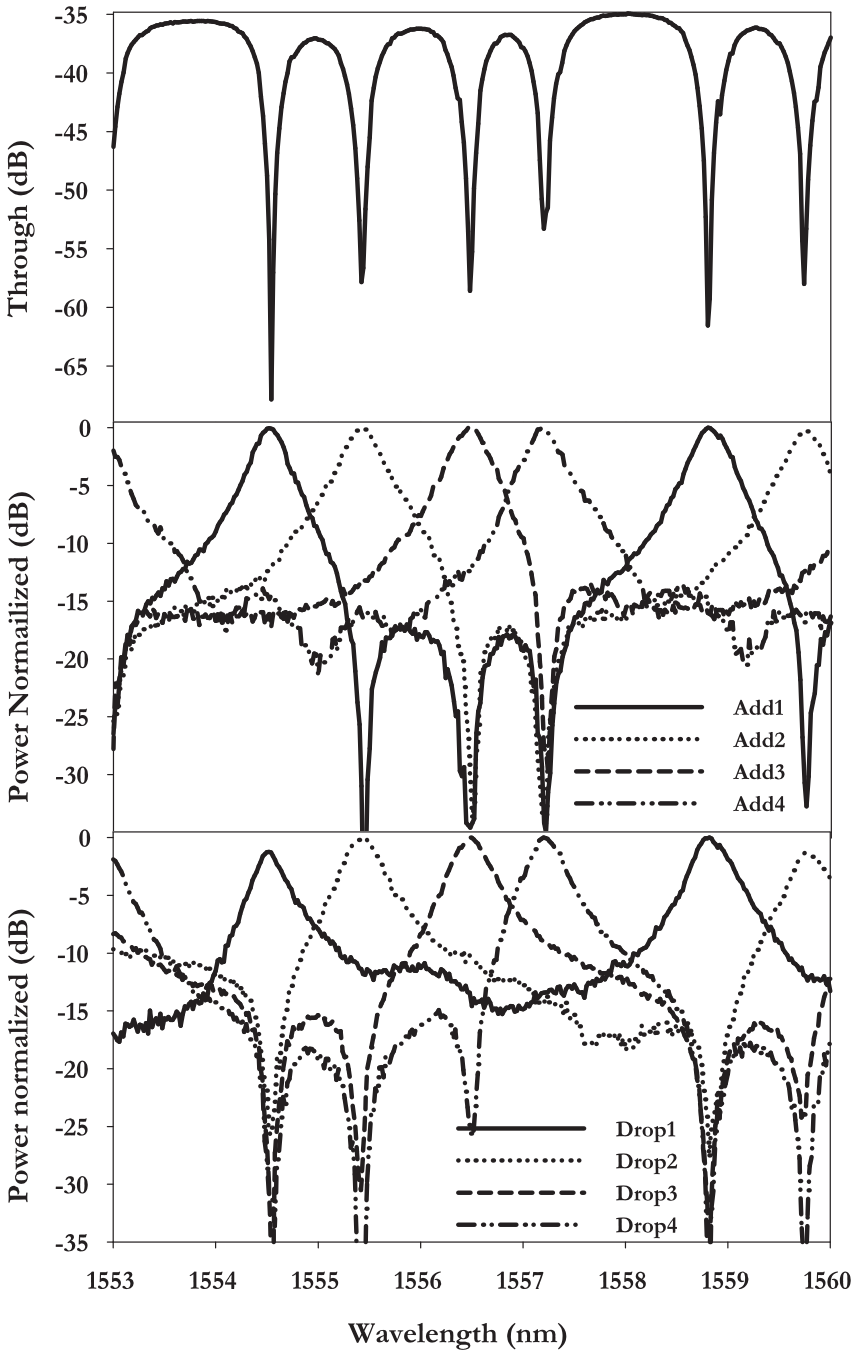

FIGURE 4.12: Measured response of all the ports of the R-OADM with the MRs set on the 100 GHz ITU grid; (top) throughport, (middle) add ports, (bottom) drop ports

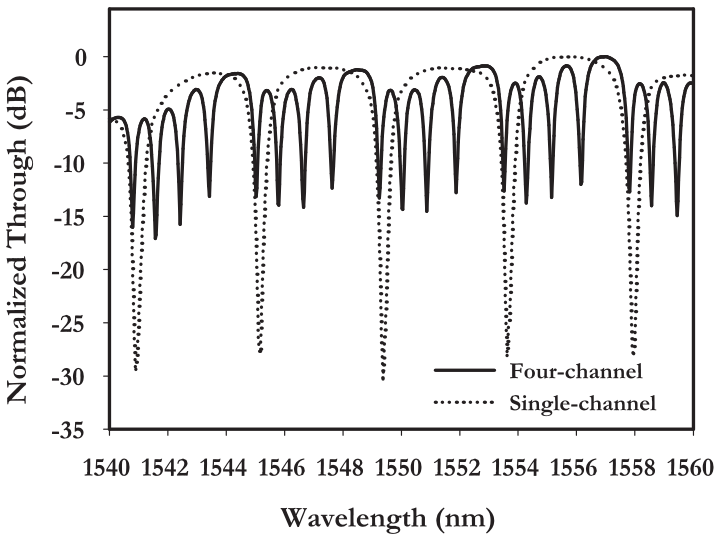

FIGURE 4.13: Measured responses of through-port in four channel and single channel configuration

Insertion loss

The insertion loss of the device was determined by analyzing a number of measurements. A tunable laser was set at a wavelength were all the rings are OFF resonance. This power was coupled into the device by standard single mode fiber butt-coupling. The power in the through port was measured to be -34.8 dBm. Then the same was done for a plain straight waveguide (without the rings) of the same dimensions and from the same place on the wafer. The power now was measured to be -24.8 dBm. Finally the power was measured fiber to fiber without any device. This turned out to be -7 dBm. The following conclusions can be drawn from these data. First the fiber to chip coupling loss is 24.8 - 7 = 17.8 dB. This includes the waveguide propagation loss. When this is assumed to be 1-2 dB, the fiber to chip coupling losses are 8 dB per facet. This is in accordance with the simulated values from table 4.3. Furthermore the 'on-chip' insertion losses of the device are 10 dB (34.8-24.8). This originates from 6 X-crossings with a simulated loss of 0.2 dB and 4 rings with a simulated insertion loss of 0.25 dB, leading to a simulated IL of 2.2 dB. The large discrepancy between simulated and measured

values can be explained by either increased losses of the X-crossings or additional losses in the rings. In the model for the ring, no losses where assumed inside the coupling region. This might have strong effects on the IL as will be discussed later.

4.6.3 Thermal crosstalk

Normally in thermal tuning the Si wafer and the package are regarded as an ideal heat sink. However since the four rings of the R-OADM are so close together (spacing of 250 μm) and since high temperature driving is needed for larger shifts, the wafer and package do not act as ideal heat sinks anymore. This can be seen in the effect of thermal crosstalk, where heating of one ring causes another one to shift.

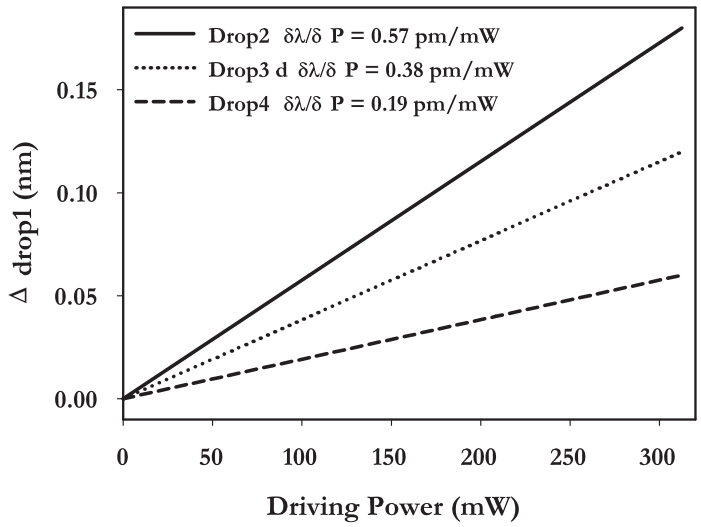

FIGURE 4.14: Measured thermal crosstalk between the rings in the R-OADM

The thermal crosstalk was measured by applying different driving powers to the second, third and fourth ring and measuring the shift at the first one. The measured thermal crosstalk becomes less when the distance increases as is to be expected, respectively 0.57, 0.38 and 0.19 pm/mW as can be seen in Figure 4.14. The tunability of the first ring itself is 9.6 pm/mW so that the thermal crosstalks

are respectively 6%, 4% and 2 %. For the placement of the drop response this is not a big issue since the bandwidth of the rings are broad (3-dB bandwidth of about 0.4 nm). However when in the throughport the highest effect of extraction is needed, the sharp peak needs to be placed with accuracy below 0.02 nm. But since the effect of thermal crosstalk is now known, it can be circumvented by driving the individual heaters with an adapted power. Or, in future devices, trenches will be etched reducing largely the thermal crosstalk.

4.6.4 λ tracking

For telecommunication components, especially in networks closer to the end-user, cost is an important issue. Therefore it is undesirable if a component needs lots of surrounding equipment to stabilize the operation. The R-OADM has the advantage in this respect that every filter component can be tuned individually. Through single feedforward or feedback loops made in the, already present, driving electronics, ambient temperature changes or drift in transmitter wavelengths can be overcome. This way expensive elements like Peltier coolers can be avoided and inexpensive (less stable) transmitters can be used. To show the capability of the R-OADM for stable operation even with a drifting transmitter, a feedback control was used. The output of a drop channel was measured while the wavelength of the transmitter was slightly changed. Since the heater of the R-OADM are controlled by a PC, a control could easily be applied. The computer control was slightly sweeping the heaters temperature in order to detect the maximum in output power. When the transmitter wavelength is drifting, the position where the output is maximized chances. The computer control will look for this new position and will use this as new driving point for the heater. To avoid instability of the control loop, a hysteresis was applied. Figure 4.15 shows experimental results of the stabilization. When no thermal control is applied, the output power is reduced by 4 dB when the wavelength of the transmitter has a drift of 0.22 nm. By applying thermal control the output is stabilized within 0.4 dB. The output of the thermally controlled measurement is actually slightly increasing.

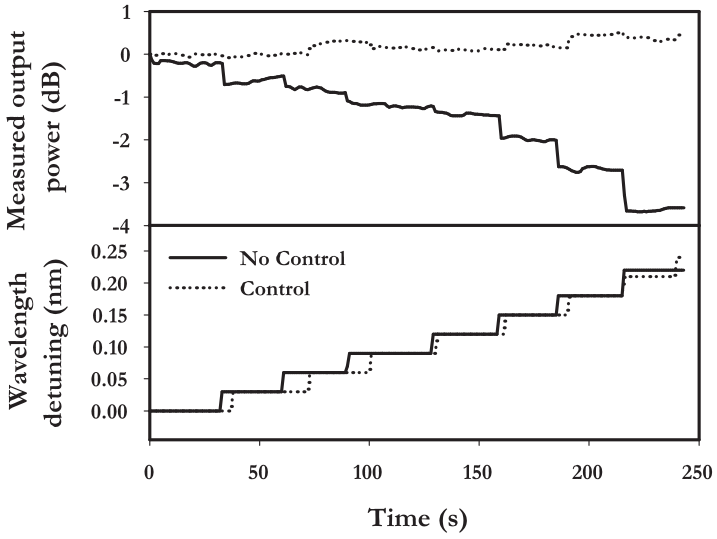

FIGURE 4.15: Measured output stabilization when transmitter is drifting

CHAPTER 5

System level measurements

In order to assess the performance of multi MR based structures in optical networks, system level measurements have been performed. This chapter describes the system level characterization methods, - setups and the measurements on both single MR as well as multiple MR structures for 10 and 40 Gbit/s datasignals. The results will be discussed and compared with the measurements described in the previous chapters.

This chapter was partly extracted from:

Geuzebroek, D.H. *et. al.* "Compact Wavelength-Selective Switch for Gigabit Filtering in Access Networks" Photon. Technol. Lett., Vol. 17, No. 2, pp. 336-338, 2005

Geuzebroek, D.H. *et. al.*, "40 Gbit/s Reconfigurable Optical Add-Drop Multiplexer based on Microring Resonators" invited talk at ECOC'05 (Europ. Conf. Optical. Comm.) Glasgow UK

5.1 System Characterization setup

Two experimental setups will be discussed, Eye patterns and BER measurements and determination of delay. Both allow characterization of the MRs when high speed datasignals are being filtered or routed and have been used in the measurements discussed further in this chapter

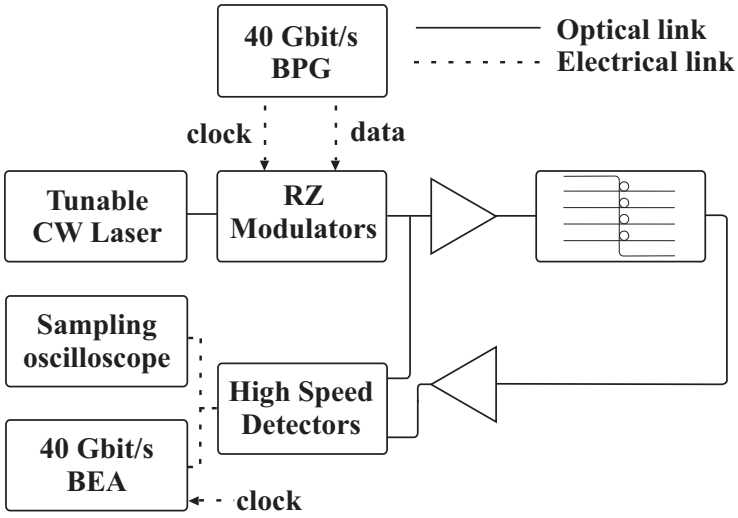

FIGURE 5.1: Measurement setup for 40 Gbit/s RZ analysis of the R-OADM

5.1.1 Eye patterns and BER

As was stated in section 2.8 the eye diagram and BER plots are useful methods for characterizing the response of single and multiple rings to high speed datasignals. Figure 5.1 shows the setup for determining the eye diagrams and BER curves. The high speed data is generated by a Pseudo-Random-Bit-Sequence (PRBS) generator (BPG). This signal is transferred to the optical domain by a high speed optical modulator, which modulates the output of a cw tunable laser. To generate a 40 Gbit/s RZ signal both PRBS data and clock are feeded to the Electro-Absoption (EA) modulators. The high speed optical signal is then fed to the device-under-test (DUT). If necessary the optical signal can be pre- and post-amplified by an Erbium-Doped-Fiber-Amplifier (EDFA). The signals from the DUT are transferred

back to the electrical domain by a high speed photodetector and then visualized on a oscilloscope in case of the Eye diagrams, or processed in the Bit-Error-Analyzer (BEA) in case of the BER measurements. The BER analyser compares the incoming data stream with the one send and counts the errors.

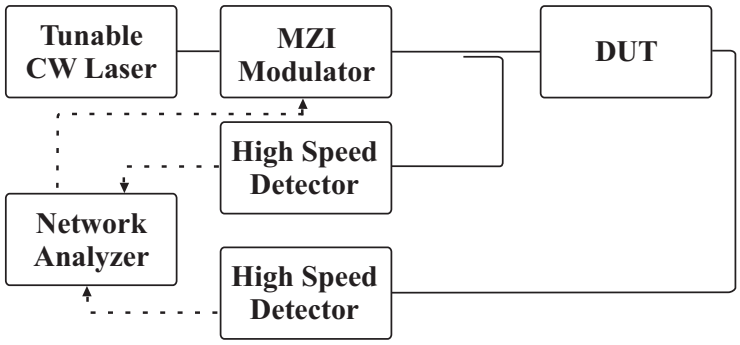

FIGURE 5.2: Measurement setup for the determination of the groupdelay by the Phase shift method

5.1.2 Delay

In the time domain the ring can be characterized by use of the setup shown in Figure 5.2 known as the phase shift method [38]. Monochromatic light from a tunable cw laser is modulated with an RF frequency by a high speed MZI modulator. The signal is then split into two different paths. One is fed to the device under test and then to a detector, the other is fed to the reference path directly to a second detector. The network analyser measures the phase difference of the RF signal in the two paths as a function of wavelength. Knowing the phase difference $\Delta\Phi_{meas}(\lambda)$ and the modulation frequency f_{mod}, the group delay can be calculated according to:

$$\tau_g = \frac{\Delta\Phi_{meas}(\lambda)}{2\pi f_{mod}} \tag{5.1}$$

Only the influence of the MR is of interest in this measurement, i.e. the additional delay between ON and OFF resonance caused by the MR. Therefore, in this case, there is no need to know the exact length of the reference path. The modulation frequency used in this method is a tradeoff between the accuracy of

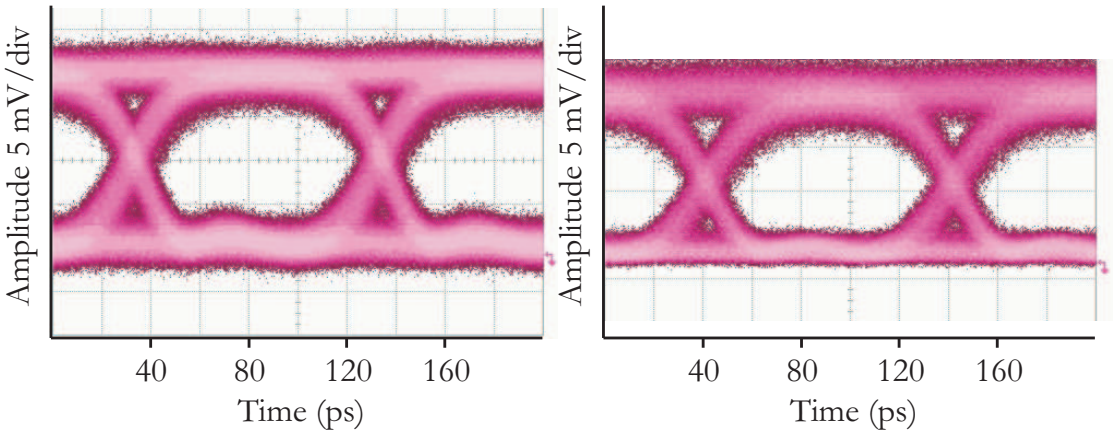

FIGURE 5.3: EYE diagrams of 10 Gbit/s NRZ signals of modulator output (left) and after being filtered by a microring resonator (right)

the delay measurement and the resolution of the measurement in wavelength. The network analyser measures phase differences, so for higher frequencies it can measure smaller delays. However, high modulation frequencies use more bandwidth in the wavelength domain and so lose resolution for a wavelength dependent measurement.

5.2 10 Gbit/s Microring Resonators

Measurements were performed on a single microring resonator with 50 μm radius and $\kappa \approx 0.5$ like the one discussed in section 3.5. A setup like in Figure 5.1 has been used with a $LiNbO_3$ Mach-Zehnder modulator driven by a 10 Gbit/s PRBS generator to see the influence of the filter on the modulated NRZ signal. The measured 10 Gbit/s modulation signal with a bit length of 100 ps is shown in Figure 5.3 where the EYE responses are shown. The left EYE diagram is obtained directly after the modulator, the right one after being filtered by the ring. As this figure shows the ring does not degrade the modulated signal significantly as could be expected since the bandwidth was designed to be 50 GHz. The transitions are still the same and only a decrease in EYE amplitude is seen. The measurements even show some signs of dispersion compensation, since the zero level in the right

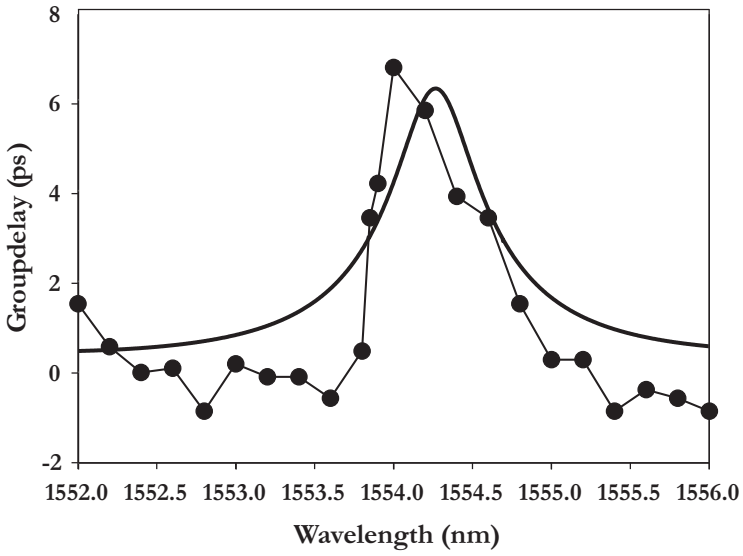

FIGURE 5.4: Measured and simulated groupdelay of a single ring

figure is cleaner than the one in the left figure. The right figure also shows an increased amount of noise at the '1' level. This is an effect caused by the EDFAs, which introduce power dependent noise.

The capability of filtering 10 Gbit/s data without large disruptions can also be seen when looking at the group delay. The group delay of the MR, described above, was measured by using the phase shift method as is given in Figure 5.2. The cw laser was modulated with a RF frequeny of 2.9 GHZ, since at this point the signal-to-noise ratio of the measurement system was maximum. The experimentally determined group delay in the through-port of the device can be seen in Figure 5.4. This figure shows that, at resonance, the measured relative group delay is 7 ps. The maximum group delay difference (between ON and OFF resonance) is much smaller than the duration of a single bit (100 ps), confirming the high speed filtering capability. Only when the modulated signal is larger than the bandwidth of the MR filter, Inter-Symbol-Interference can be seen as is experimentally demonstrated in [99]. It is therefore expected that this single MR can have error free performance at least up to 50 Gbit/s [4]. The measured Q factor of the EYE diagram of the filtered signal as defined in [4] is about 7.5, leading to a theoretical BER of $<10^{-12}$

according to:

$$Q = \frac{I_1 - I_0}{\sigma_1 + \sigma_0} \tag{5.2}$$

$$BER = \frac{1}{2} erfc\left(\frac{Q}{\sqrt{2}}\right) \tag{5.3}$$

Where I_1 and I_0 are the received intensities of the '1' and '0' bit respectively. σ_1^2 and σ_0^2 are the variances of the noise distribution of the '1' and '0' bit, assuming the noise distribution to approach a Gaussian.

5.2.1 10 Gbit/s Switch

The 10 Gbit/s measurements have not been performed on a MR based switch. But some word can be said about the behaviour of a switch at this speeds, since the switch is made out of two identical microrings. Therefore the groupdelay of the switch is twice the amount of the single ring. In the two-ring device, where the rings are arranged in a serial configuration, the 3dB bandwidth is reduced by approximately $\sqrt{2}$. For a 10 Gbit/s modulation signal the enhanced groupdelay and reduced 3dB bandwidth are still acceptable. The IL of the switch is also twice the IL of a single ring as can be seen in Figure 4.6. This means that the EYE opening and the Q factor will decrease. For a switch it is important to reduce the IL of the individual rings as much as possible.

5.3 40 Gbit/s R-OADM

40 Gbit/s measurements were carried out for the R-OADM described in chapter 4 to see the performance of multi microring resonator structures in metro network applications. A measurement setup as shown in Figure 5.1 has been used. At first the performance was investigated for adding and dropping of 40 Gbit/s optical signals by EYE analysis using a wide-bandwidth (70GHz+) oscilloscope (Agilent 86100B) with a precision time base reference module. An optical 40 Gbit/s PRBS return-to-zero (RZ) data signal with a bit word sequence of 2^{31}-1 was encoded

via modulators on a wavelength tunable laser. The signals injected into the R-OADM as well as the received output signals at the drop ports were amplified by EDFAs and converted to electronic signals by high speed photodetectors (U2T). Figure 5.5 shows the measured EYE pattern directly after the modulator (top) and

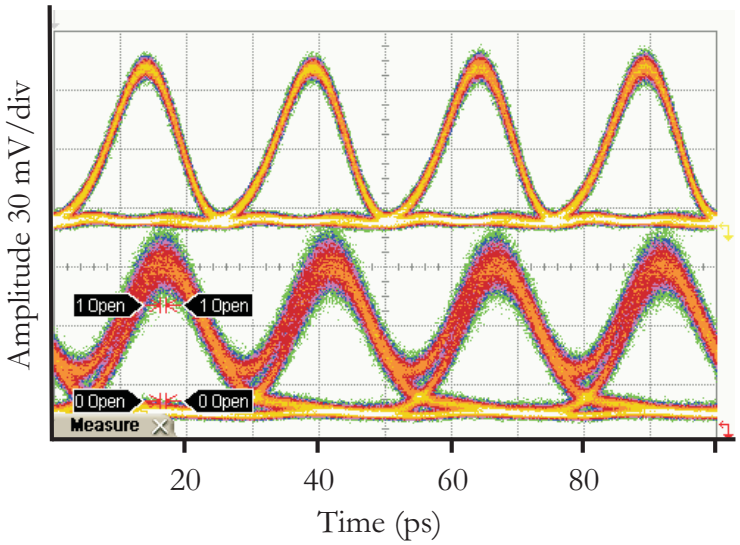

FIGURE 5.5: Measuered EYE patterns of 40 Gbit/s incoming signal (top) and Drop_1 port (bottom)

from the Drop_1 port (bottom) while the MR was tuned to the wavelength of the tunable laser. Clean EYE openings can be seen allowing error free detection. The Drop_1 response shows an increase in noise caused by the EDFAs. Furthermore, at the crossings some inter-symbol-interference (ISI) can be seen, but the EYE stays open enough for error free detection. All other ports, both drop and add, showed similar responses demonstrating the full add/drop capability of the device. The measured EYE patterns of all ports can be found in appendix B. An additional groupdelay at resonance of 6 ps with respect to the off resonance signals was measured at is shown in Figure 5.6. The bitpattern is shifted 6 ps between ON and OFF resonance caused by the additional delay of the filter. This is in close agreement with the values obtained on the single ring measurements by the phase shift method shown in section 5.2. The difference in the EYE amplitude between ON and OFF resonance is 11 dB which agrees with the wavelength spectrum of

the device.

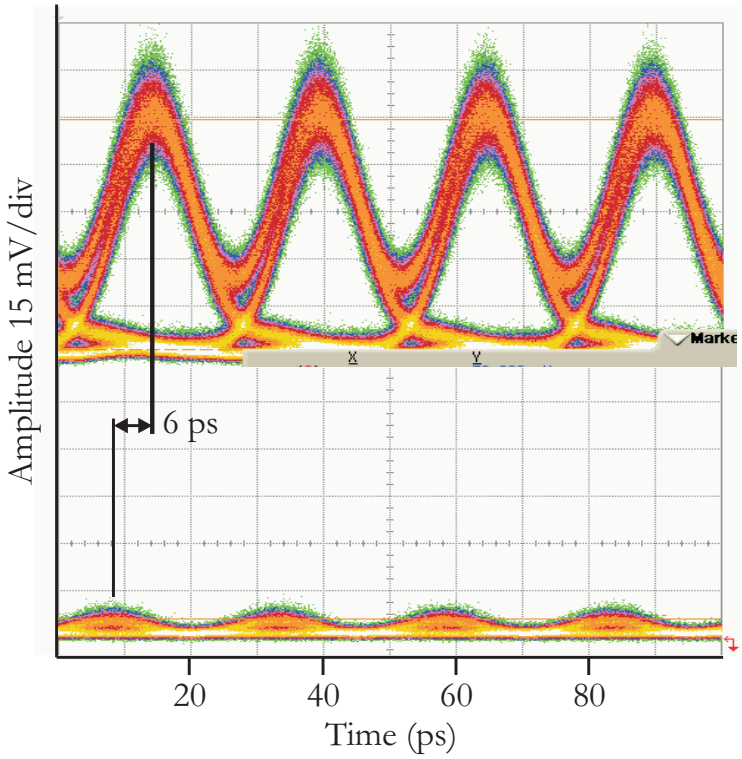

FIGURE 5.6: Measured EYE patterns of a 40 Gbit/s signal at the drop-port; ON resonance (top) and OFF resonance (bottom) showing the additional delay.

5.3.1 BER measurements on R-OADM

To validate the results of the EYE analysis, BER-measurements at 40 Gbit/s have been performed. Figure 5.7 shows the back-to-back BER ratio of the transmitted signal without DUT and the corresponding BER ratio measured at the Drop_1 port of the R-OADM. The latter shows error free detection down to 10^{-9} with a minor power penalty of 1 dB (increase in received power needed to compensate for the impairments with respect to the back-to-back case). The slight error floor in the figure is based on the additional ASE noise of the applied EDFAs. It can be improved by integrated mode transformers resulting in a significant reduction of the

actual fiber-chip coupling losses (currently 8 dB). However EYE analysis and BER-measurements confirm the potential of the R-OADM in high speed applications.

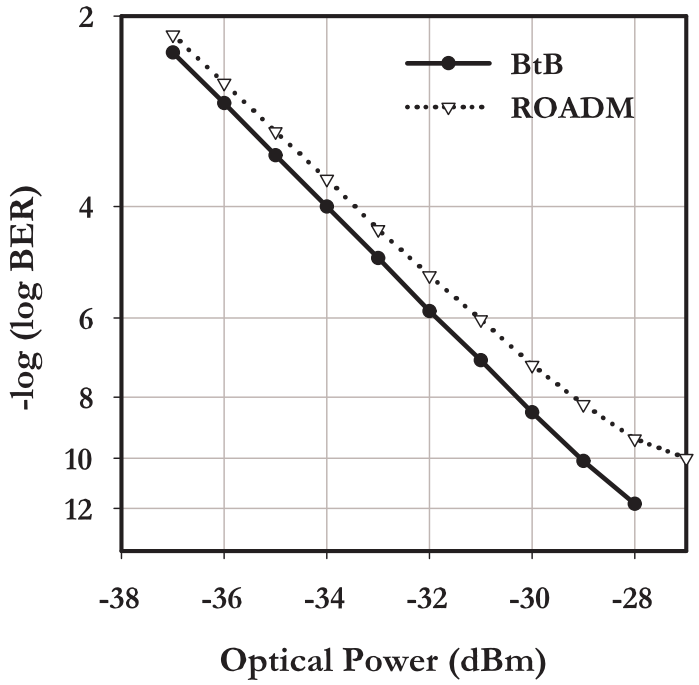

FIGURE 5.7: Measured BER vs received optical power at 40 Gbit/s showing a power penalty at BER = 10^{-9} of 1 dB

5.3.2 Crosstalk

The most crucial test for the evaluation of the ROADM is the measurement of the crosstalk, i.e undesired wavelength still present in a particular port. For this measurement we set the MRs on a ITU grid of 100 GHZ (0.8 nm) spacing between neighbouring channels. We used two 40Gbit/s modulated RZ data signals at λ_1 (1550 nm) and λ_2 (1555 nm). Because of the FSR of 4.2 nm these wavelengths fit exactly the resonance condition of the first and second MR respectively. The crosstalk was determined by use of an optical spectrum analyzer. The results are

summarized in Table 5.1. The first MR ($Drop_1$) was tuned to filter out λ_1 and the second MR ($Drop_2$) was tuned to filter out λ_2. The two other rings ($Drop_3$ en $Drop_4$) where tuned to have the same spacing (100GHz). The results of dynamic crosstalk measurements show good agreement with the wavelength scans, see e.g. Figure 4.12. Higher order filters with steeper roll-off factors can improve this. [73].

TABLE 5.1: Measured crosstalk (dB) for two 40 Gbit/s modulated wavelengths: λ_1 is droped by $Drop_1$, λ_2 by is droped by $Drop_2$

	$Drop_1$	$Drop_2$	$Drop_3$	$Drop_4$
λ_1	-	18.35	21.25	20.63
λ_2	15.43	-	20.21	27.15

5.4 Multicasting

An important feature for a R-OADM in METRO networks is the ability to multicast, i.e. distributing a particular signal wavelength to more than one output channels. The principle of multicasting for the R-OADM based on microring resonators is shown in Figure 5.8. In this case the center of the filter of the first ring is slightly shifted with respect to the signal wavelength. This way only part of the power is being dropped and another part can be filtered by the second MR, which is aligned to the signal wavelength. To experimentally show the capability for multicasting the first MR was tuned such that only part of the power was filtered to $Drop_1$. Being tuned to the signal wavelength the second MR could direct the remaining signal to the $Drop_2$-port. Figure 5.9 shows the EYE patterns of the simultaneously measured responses of $Drop_1$ (top) and $Drop_2$ (bottom). A clear EYE opening can be seen for both drop channels, demonstrating the multicast capability. The amplitude of these EYEs is less than the one measured in Figure 5.5 since the first ring is not tuned to full resonance and the second ring has less input power due to the extraction of the first. This however, causes a reduced ISI in the first ring, since the dispersion is lower when tuned slightly off-resonance.

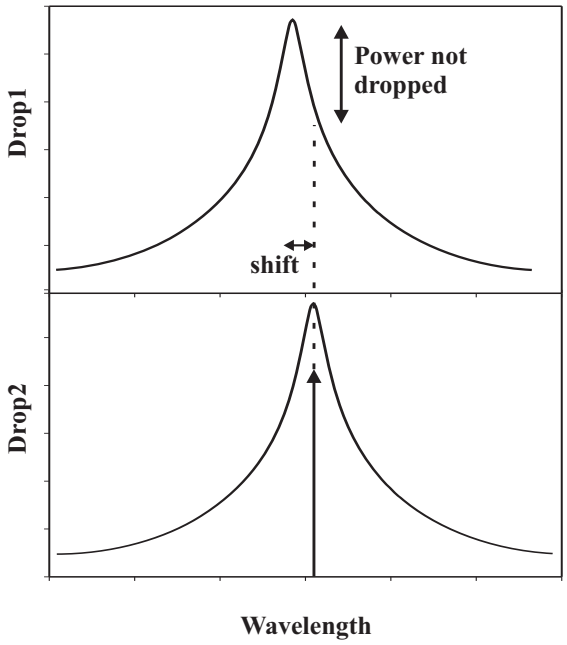

FIGURE 5.8: Principle of multicasting with a R-OADM based on microring resonators

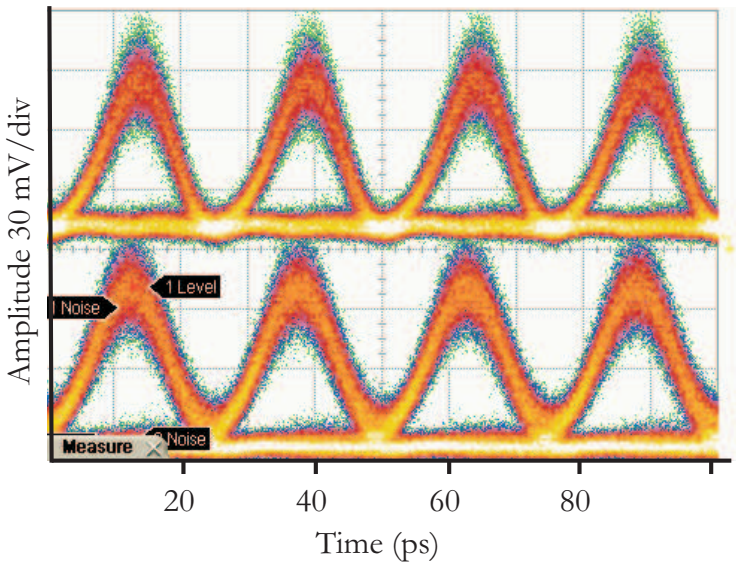

FIGURE 5.9: Simultaneously measured multicast response: 40 Gbit/s EYE patterns in Drop_1 (top) and Drop_2 (bottom) tuned to the same input wavelength channel.

5.5 Discussion

The measurements showed in this chapter demonstrate that multiple MR structures can be used as tunable high bandwidth filters and switches. The measurements are in close agreement with the simulation results. It is important to notice that this can only be reached by designing the ring specifically for this application. The finesse of the rings has to support the desired 3-dB bandwidth. High finesse rings are appropriate for lasing and non-linear optical applications, but for high bandwidth filter applications in telecommunications network, the bandwidth of the filters is of primary importance in design parameters.

Furthermore, the measurements in this chapter demonstrate the good performance of multiple microring resonator structures. By using more than one ring very flexible components can be made, which are desired in today's telecommunication networks.

CHAPTER 6

Discussion and Conclusions

In this final chapter a discussion is given of the results presented in this thesis and of the use of MRs in optical telecommunication components. This discussion will lead to the main conclusions from this thesis. Finally an outlook will be presented recommending future research for multi MR structures in optical telecommunications components. For this also some brief comments on recent picosecond pulse measurements will be given.

6.1 Summary

The previous chapters presented some work concerning the use of multiple densely integrated microring resonators in flexible optical network components.

An introduction of the fundamentals and a top-down design approach of a MR was given in chapters 1 and 2 respectively.

Chapter 3 demonstrated that it is possible to design a MR in SiO_2/Si_3N_4 technology that has sufficiently high coupling constants to support a bandwidth of several tens of GHz. Furthermore it was shown that a MR, with 50 μm radius, could be realized and characterized that is thermally tunable, using an Ω-shaped heater, with a tuneability of $\approx$ 11 pm/mW.

In chapter 4 it was shown that structures made of multiple MRs have great advantages. A MR based switch has been realized and characterized that demonstrated the extended functionality of cascading multiple rings and showed an ON/OFF ratio of 12 dB with a switching power of 225 mW. Also the improvement of specific parameters has been demonstrated by the Vernier switch, where the FSR was increased by a factor of 7. Finally the possibility of using densely integrated MRs was demonstrated by a fully pigtailed and packaged R-OADM consisting of four individually thermally tunable MRs. The MRs in the R-OADM could be tuned across the complete FSR of 4.2 nm of the individual rings. A four-channel 100 GHz spacing filter could be configured by applying 446 mW power. A single-channel configuration, suited for multicasting, could be obtained by applying only 20 mW.

Chapter 5 showed that the realized MRs are capable of filtering high bitrate datasignals. A single MR, with a designed bandwidth of 50 GHz, demonstrated the capability of filtering 10 Gbit/s NRZ data signals with a theoretical BER below 10^{-12}. The MRs in the R-OADM were capable of filtering 40 Gbit/s RZ datasignals with a power penalty of 1 dB at a BER of 10^{-9}. All drop and add ports demonstrated this capability. Furthermore the R-OADM proved able to allow multicasting the 40 Gbit/s RZ signals to two drop ports simultaneously.

6.2 Important issues

This section describes some important issues related to the design and realization of microring resonators. It concerns polarization dependence, the gap between the ring and waveguide, the center wavelength and losses in the coupling region.

Polarization depencence

A serious issue for a microring resonator is its polarization dependence. Since the resonance frequency of a MR depends strongly on the effective index of the mode, there will always be a difference in behaviour for TE and TM modes inside the ring. Also the coupling constant between the ring and waveguides will differ for both polarizations. Only a careful design and a precise technology with tight tolerances will be able to compensate the materials birefringence by a geometry-induced polarization dependence [100]. In practice, this polarization independence can only be reached for cavities with relatively low index contrast [73]. Currently this issue is often solved by polarization diversity, see, e.g. [26], were the incoming signal is split into two orthogonal polarization modes. The polarization of one branch is then converted to allow a single MR design to filter both branches.

Definition of gap

The fabrication of microring resonators is limited by the tolerances of the lithography and the etching processes. For the realization of the gap between the ring and straight waveguide in a lateral configuration one needs in high index contrast structures nanometer precision which can only be obtained by direct e-beam writing, Focused Ion Beam milling or state-of-the-art deep UV wafersteppers. In the vertical configuration this problem is circumvented as the coupling is now determined by the deposition process where a nanometer precision can be obtained more easily. In this case, however, alignment (within 100 nm) will be an issue as ring and port waveguides are structured in two separated lithographic steps. This is especially important when symmetrical coupled devices are desired. The use of a cross-grid architecture even put more emphasis to the alignment, since the

coupling is now critical for two directions.

Resonance wavelength

The resonance wavelengths of the MR is determined by its radius and effective index and is very sensitive for changes in the radius: an additional 3 nm on a 50 μm ring gives a shift of 0.1 nm in wavelength. Astonishingly, even with laser written masks and a contact mask aligner, the reproducibility of the radius for MRs on the same wafer can be below 20 nm. The controlled positioning of the resonance wavelength asks for a very good lithography, controlled deposition of layers and precise etching methods. These problems can be solved by tuning or trimming the device afterwards [54], at the expense of increased driving power or fabrication complexity respectively.

Coupler losses

Finally it is worthwhile to mention another parameter influencing the wavelength response of a microring, namely the loss inside the coupler region. As is described in [101] these losses can be modelled by extending the scattering matrix. The losses can occur when air enclosures or other disruptive elements are present in the coupling area. By this, an asymmetry in the wavelength response is induced where one side of the resonance peak will be less steep than the opposite side. The IL of a MR will also be affected by losses in the couplers.

6.3 Conclusions

The main conclusion that can be drawn on basis of the previous chapters can be expressed as follows. It is possible to design and realize multiple MR devices allowing high bitrate optical network components with reconfigurable functions. For components in METRO network applications, especially the ability of the multi MR devices to filter high bitrate datasignals is very attractive. Furthermore the reconfigurability of multi MR devices places added value over its competitors. In Access networks, lower bitrates are needed, so the main advantages of multi

MR structures in this case are the reconfigurability and the ability for integrating a large number of functions at decreasing costs. For use in end-users equipment the main focus is the cost aspect. Since standard technologies are used and mass-production is feasible also here the multi MRs structures have a great potential. Although the need for very complex, densely integrated functions, might be a little too complicated and unnecessary for this application in the near future. However the need for complexity will emerge towards the end-user as long as the costs does not rise.

6.4 Outlook

This thesis only shows a certain stage in the process of improving specifications of multi MR devices. Looking into the future some word can be said about the effort which need to be taken to overcome or bypass some of the issues mentioned before.

To really extend the potential of multiple MR devices the losses must decrease. Waveguide losses (propagation and scatter), fiber to chip losses and losses in the ring (propagation, scatter and coupler losses) can be improved with technological improvements. Using ultra-low loss waveguide technology together with tapering in both lateral as well as vertical directions will decrease losses into large extend. Better lithography, by e.g. a wafer stepper, allows for lower scattering losses and improves the alignment.

Lots of these technological steps are already being addressed in upcoming project and collaborations. To give a short overview of my view about the future device, a roadmap is given in Figure 6.1. This figure gives a short history of published realized MR devices as well as upcoming devices with increasing complexity, all within the SiO_2/Si_3N_4 range of technology.

The improvement mentioned above are all in the field of technology. However, when the complexity of the devices increases, also the design and characterization of the devices need more attention. Software tools predicting the behaviour of complex devices are necessary to get a grip on these complex questions with many

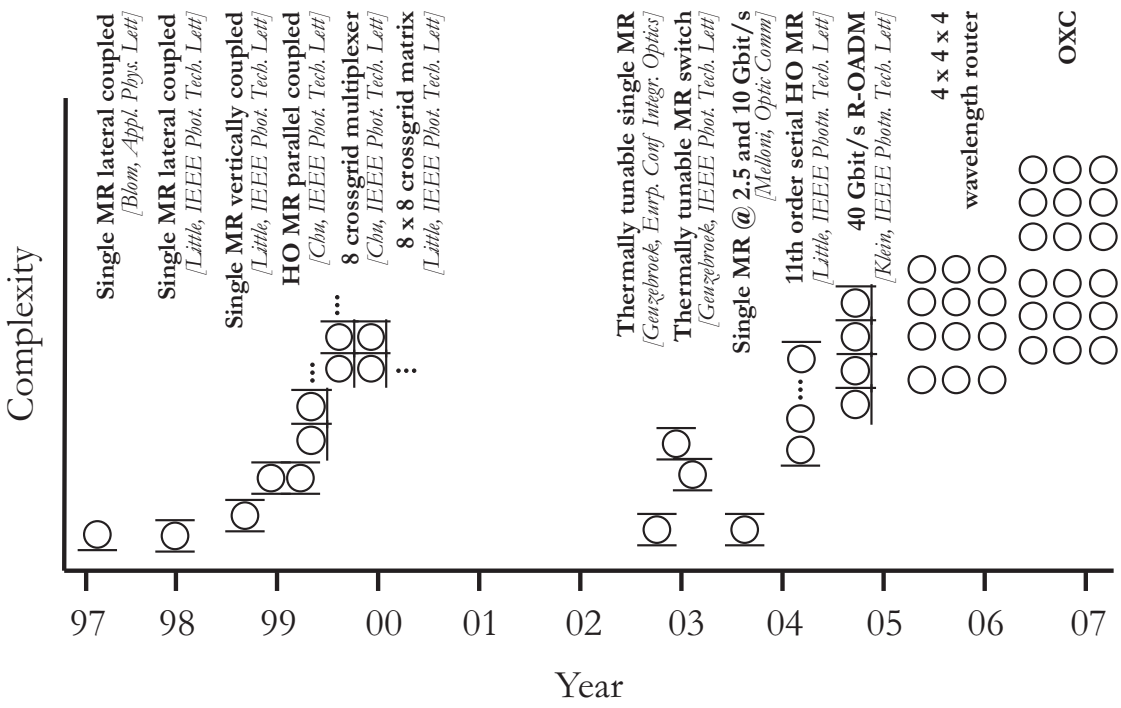

FIGURE 6.1: History and roadmap of MR structures as wavelength filters in SiO_2/Si_3N_4 technology

parameters and design choices. In the end maybe even a form of VHDL (VLSI hardware description language) is needed to put more abstractness in the design of multi MRs structures.

So still lots of effort needs to made to proper design, realize and characterize the future optical network components based on densely integrated MR.

6.4.1 ps pulses in microring resonators

The fundamental limit for filtering very high speed signals with MRs is reached when the duration of the pulse becomes smaller than the roundtrip time of the MR cavity. Since the duration of the pulse is so short, under certain conditions no interference of multiple roundtrips of the MR cavity can be observed and the MR can not be described in a CW modus but exhibits only a transient response behaviour.

Preliminary measurements have been performed with ps pulses to observe the

influence of the MR on the time and frequency behaviour of the pulses. With the

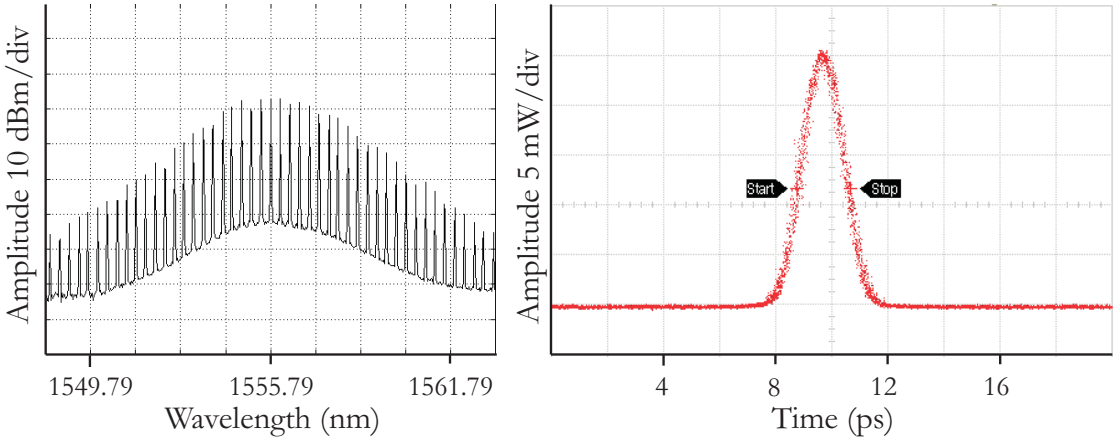

FIGURE 6.2: Measured wavelength spectrum and detected 1.8 ps pulse of generated pulse train with a repetition rate of 40 GHz

use of a 40 GHz modelocked ringlaser a pulse train was generated with pulses with a duration of 1.8 ps and a 25 ps interval as is shown in Figure 6.2. The individual pulses have a duration in the order of the roundtrip-time (τ_r) of the microring which is 1.9 ps according to:

$$\tau_r = \frac{2\pi R n_g}{c} \tag{6.1}$$

with groupindex n_g of 1.82 following from the measured 4.2 nm FSR and equation (1.5.1). The measured wavelength spectrum of the generated pulse-train is shown in the left picture of Figure 6.2. It has a broad spectrum with a FWHM of 3.5 nm according to [102][1]

$$FWHM_\lambda \approx \lambda_0^2 \frac{TBP \cdot n_g}{FWHM_t c} \tag{6.2}$$

with $FWHM_\lambda$ and $FWHM_t$ the 3-dB width of the wavelength spectrum and the pulse in time respectively. The Time-Bandwidth Product (TBP) of a Gaussian pulse is ≈ 0.44 [102]. The spikes in the wavelength spectrum are the resonances of the ringlaser. Alternatively they can be considered as a consequence of the pulse train with a repetition rate of 40 GHz, being exactly the distance between the spikes in the wavelength spectrum.

[1]The author acknowledges the discussion with Wico Hopman and Ronald Dekker from University Twente on this subject.

When a pulse train as described above is filtered by the mentioned MR there are two states that can be distinguished: 'ON' and 'OFF' resonance. Since the pulse duration is a little shorter than the roundtrip time, the definition of resonance conditions for the CW case can not be used. When the MR is tuned such that the main part of the pulse trains spectrum does not overlap the normal resonance peaks, the state is called 'OFF' resonance. When the center of the pulse train coincides with the resonance wavelength in the CW case, the state is called 'ON' resonance.

The R-OADM as described in chapter 4 was used to analyze the influence of a MR on a pulse train described above. The measured spectrum and recovered pulse in the 'OFF' state are shown in Figure 6.3. The pulse now is altered into a pulse train shaped by the roundtrips of the pulses. The distance between the pulses is 2.4 ps, a little more that the roundtrip time calculated above. The exponential slope of the envelope of the pulse train is a measure for the coupling constants and the loss inside the ring. However since the incoming pulse has a tail broader than the roundtrip time, the pulses from the outgoing pulse train are not completely independent and the envelope rises. This can better be seen

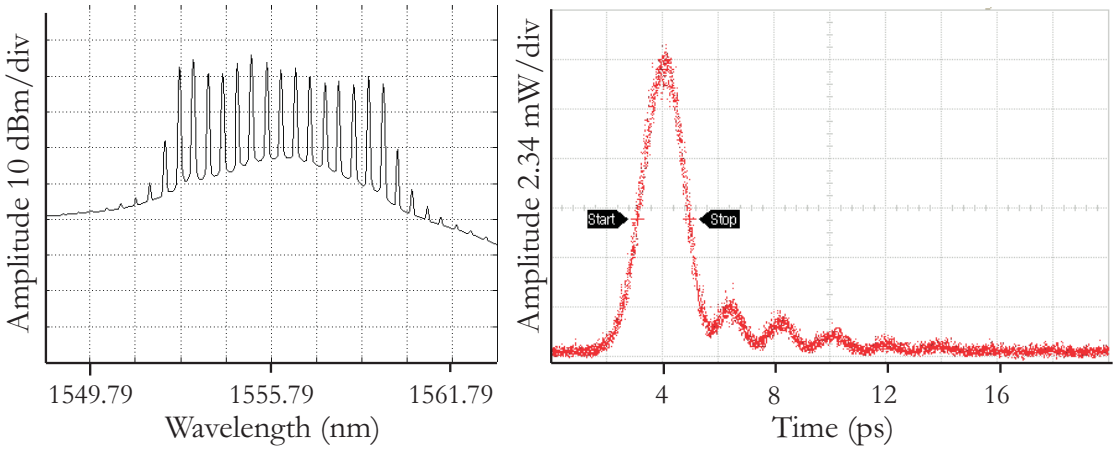

FIGURE 6.3: Measured wavelength spectrum and detected response after MR in 'OFF' condition

when looking at the measurements in the 'ON' state, shown in Figure 6.4. The wavelength components of the pulse now exhibit a longer delay, since the tails of

the outgoing pulses interfere. This causes the individual pulses from the pulse train the melt together in one long pulse with higher intensity as is shown in the right picture from Figure 6.4. The spectrum confirms this as the FWHM is shortened as is to be expected from the pulse broadening in time.

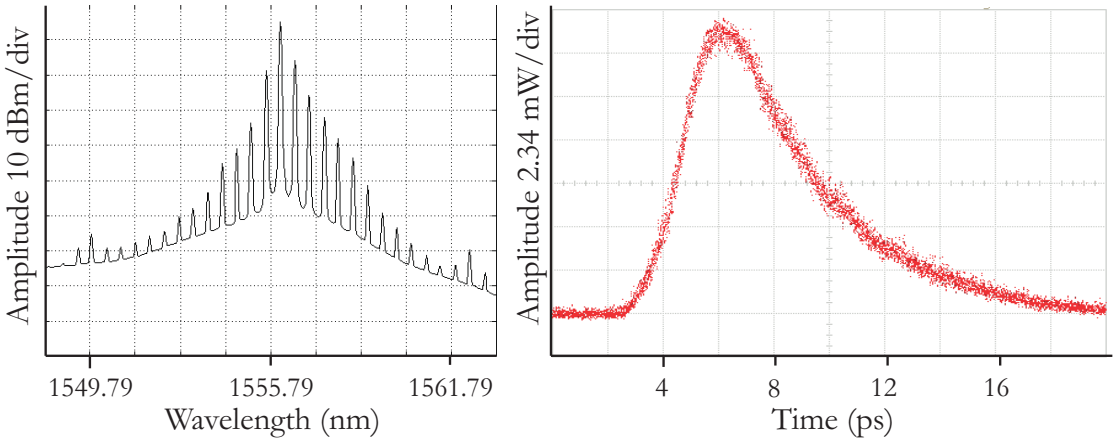

FIGURE 6.4: Measured wavelength spectrum and detected response after MR in 'ON' condition

These measurements show some very interesting behaviour of ps pulses in resonant filters (MR). These few measurements already show intriguing results, stimulating additional measurements. When even shorter pulses can be used with a duration clearly shorter than the roundtrip time, better answers can be given to the behaviour of the pulses and additional phenomena like ballistic transport can be observed [103].

APPENDIX A

Process Flow

TABLE A.1: Process Flow for SiO_2/Si_3N_4 vertically coupled microring resonators

Process number	Process step
1	Thermally grown SiO_2 on Si wafer
2	LPCVD deposition of Si_3N_4 layer
3	Spinning of resist, mask lithography and structuring by RIE
4	Deposition of TEOS LPCVD SiO_2 buffer layer
5	LPCVD deposition of Si_3N_4 layer
6	Spinning of resist, mask lithography and structuring by RIE
7	Deposition of PECVD SiO_2 cladding layer and annealing of layer stack
8	Sputtering of Chromium layer
9	Spinning of resist, mask lithography and structuring by wet-etch
10	Final layer stack

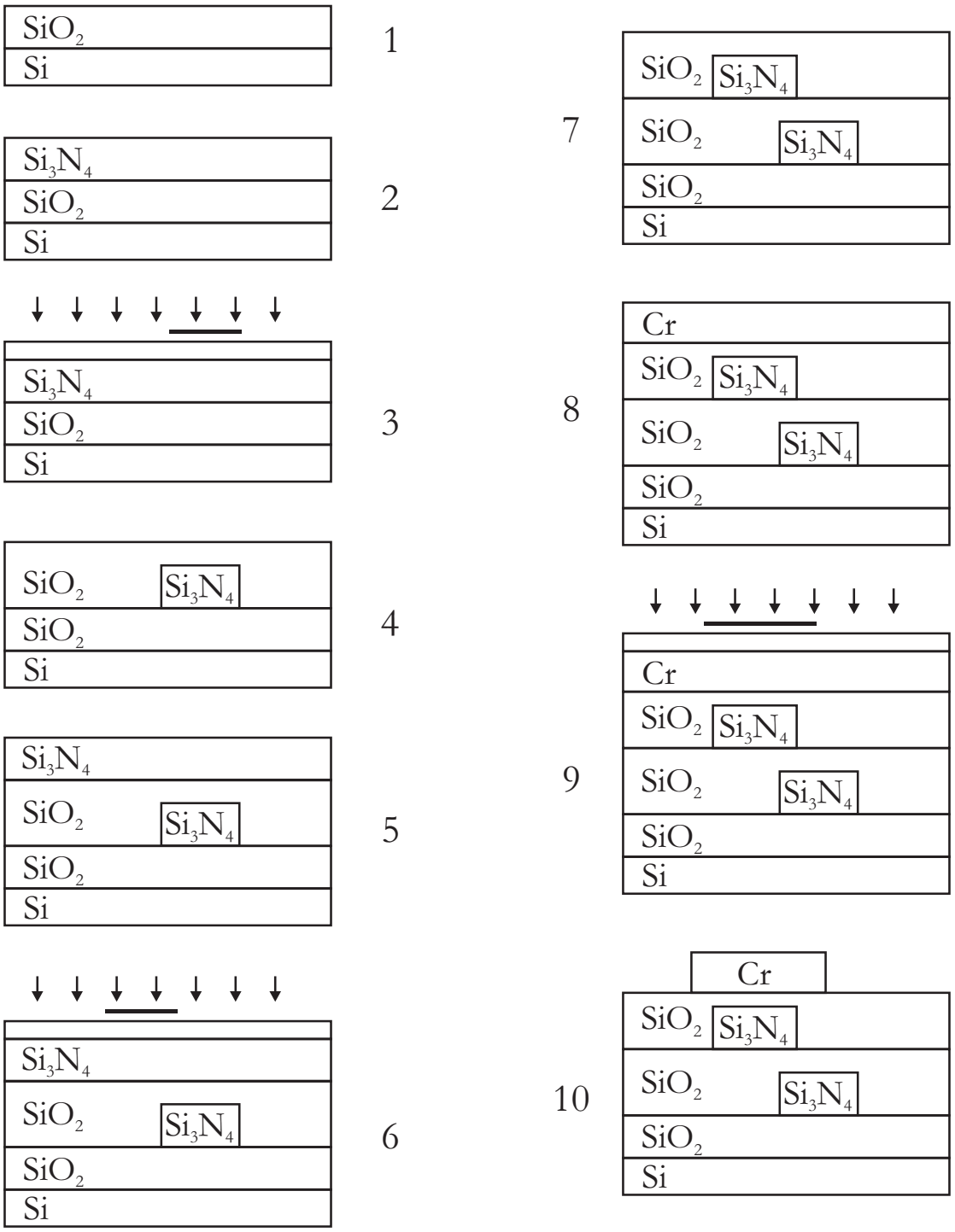
SiO2
Si
1
Si3N4
SiO2
Si
2
Si3N4
SiO2
Si
3
SiO2
Si3N4
SiO2
Si
4
Si3N4
SiO2
Si3N4
SiO2
Si
5
Si3N4
SiO2
Si3N4
SiO2
Si
6
SiO2
Si3N4
SiO2
Si3N4
SiO2
Si
7
Cr
SiO2
Si3N4
SiO2
Si3N4
SiO2
Si
8
Cr
SiO2
Si3N4
SiO2
Si3N4
SiO2
Si
9
Cr
SiO2
Si3N4
SiO2
Si3N4
SiO2
Si
10

APPENDIX B

Eyes of Add and Drop

TABLE B.1: Illustration of the different R-OADM ports accompanying the measured eye diagrams shown on next page

Topleft		
	In Drop1	Add1 Through
	In Drop2	Add2 Through
	In Drop3	Add3 Through
	In Drop4	Add4 Through
		Bottom right

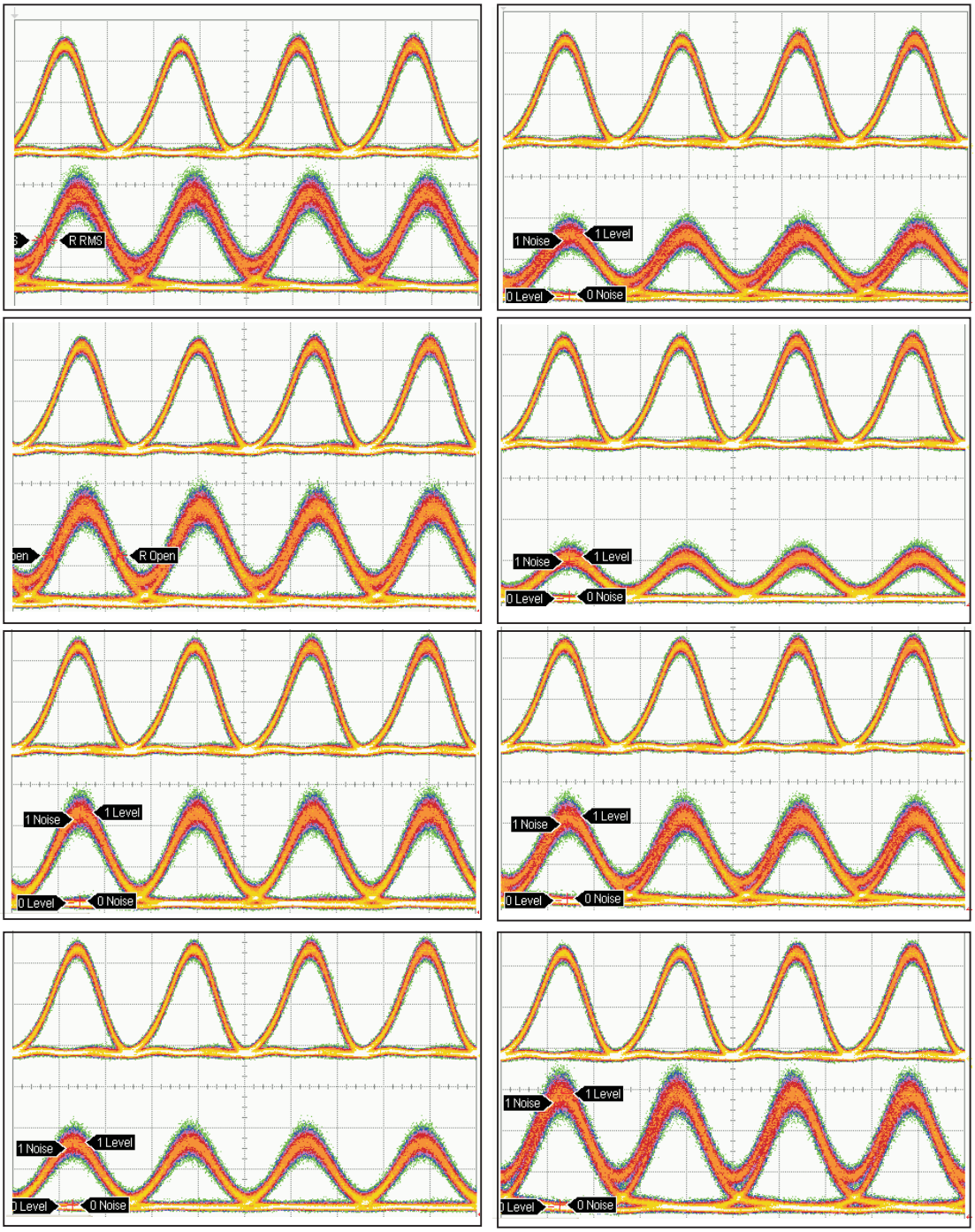
R RMS
1 Noise
1 Level
0 Level
0 Noise
R Open
1 Noise
1 Level
0 Level
0 Noise
1 Noise
1 Level
0 Level
0 Noise
1 Noise
1 Level
0 Level
0 Noise
1 Noise
1 Level
0 Level
0 Noise
1 Noise
1 Level
0 Level
0 Noise

APPENDIX C

Fully Packaged R-OADM

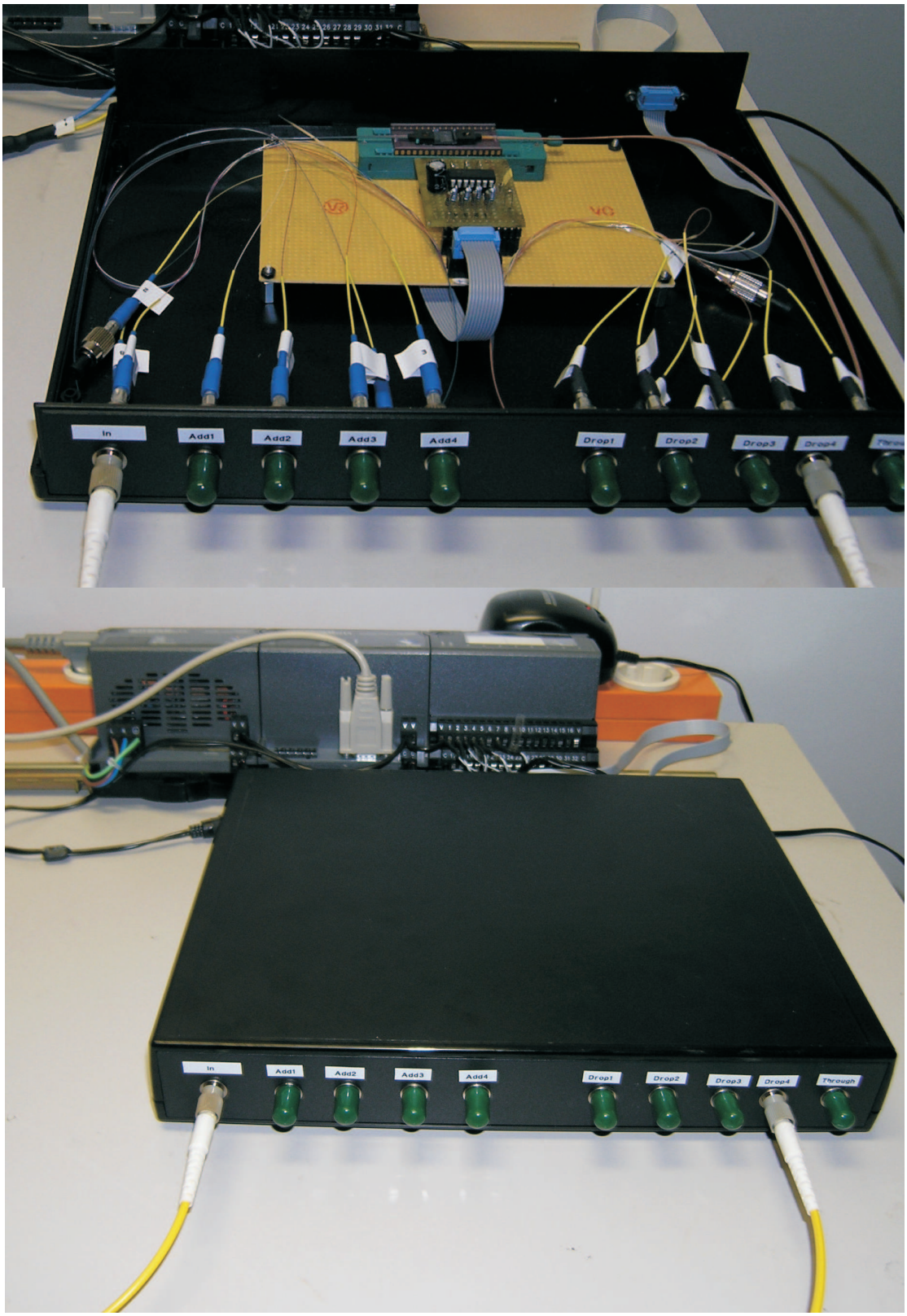
In
Add1
Add2
Add3
Add4
Drop1
Drop2
Drop3
Drop4
Through

Bibliography

[1] S.T. Téral. Reborn from the ashes, a new telecom era is shaping up. *Fibercomm 2005*.

[2] M.K. Weldon and F. Zane. The economics of fiber to the home revisited. *Bell Labs Technical Journal*, 8(1):181–206, 2003.

[3] J.N. Frigo, P.P. Iannone, and K.C. Reichmann. A view of fiber to the home economics. *IEEE Comm. Mag.*, 42(8):s16–s23, 2004.

[4] G.P. Agrawal. *Fiber-Optic Communication Systems*. Wiley Interscience, 2002.

[5] M Peach. Fibre's coming home. *Lightwave Europe*, November:4, 2003.

[6] B. Whitman and M. Kunigonis. Fibre access deployment worldwide – market drivers, politics and technology choices. *Proc. Europ. Conf. Optical. Comm.*, 5:Mo3.1.2, 2004.

[7] S Téral. Optical networking: Vision and strategy. *FibreSystems Europe*, June:8–9, 2005.

[8] J. Mills. Photonic integration combats network complexity. *FibreSystems Europe*, May:26–28, 2002.

[9] A. Ashkin and J.M. Dziedzic. Observation of optical resonances of dielectric spheres by light scattering. *Appl. Optics*, 20(10):1803–1814, 1981.

[10] H-B Lin, A. L. Huston, B. L. Justus, and A. J. Campillo. Some characteristics of a droplet whispering-gallery-mode laser. *Optics Letters*, 11(10):614–616, 1986.

[11] S.C. Hill, D.H. Leach, and R.K. Chang. Third-order sum-frequency generation in droplets: Model with numerical results for third-harmonic generation. *JOSA-B*, 10(1):16–33, 1993.

[12] M.M. Mazumder, S.C. Hill, D. Q. Chowdhury, and R.K. Chang. Dispersive optical bistability in a dielectric sphere. *JOSA-B*, 12(2):297–310, 1995.

[13] J. Haavisto and G. A. Pajer. Resonance effects in low-loss ring waveguides. *Optics Letters.*, 5(12):510–512, 1980.

[14] W. Weiershausen and R. Zengerle. Photonic highway switches based on ring resonators used as frequency-selective components. *Appl. Optics*, 35:5967–5978, 1996.

[15] B. E. Little, S. T. Chu, W. Pan, and Y. Kokubun. Microring resonator arrays for VLSI photonics. *IEEE Photonics Technol. Lett.*, 12:323–325, 2000.

[16] S. Suzuki, K. Shuto, and Y. Hibino. Integrated-optic ring resonators with two stacked layers of Silica waveguide on Si. *Phot. Tech. Lett.*, 4(11):1256–1258, 1992.

[17] C.K. Madsen and J.H. Zhao. *Optical Filter Design and Analysis*. Wiley, 1999.

[18] A. Driessen, D. H. Geuzebroek, H. J. W. M. Hoekstra, H. Kelderman, E. J. Klein, D. J. W. Klunder, C. G. H. Roeloffzen, F. S. Tan, E. Krioukov, C. Otto, H. Gersen, N. F. van Hulst, and L. Kuipers. Microresonators as building blocks for VLSI photonics. *AIP conf. Proc. 709*, pages 1–18, 2003.

[19] C. K. Madsen, G. Lenz, A. J. Bruce, M. A. Cappuzzo, L. T. Gomez, and R. E. Scotti. Integrated all-pass filters for tunable dispersion and dispersion slope compensation. *IEEE Photonics Technol. Lett.*, 11:1623–1625, 1999.

[20] F. C. Blom, D. R. van Dijk, H. J. W. M. Hoekstra, A. Driessen, and T. J. A. Popma. Experimental study of integrated-optics microcavity resonators: Toward an all-optical switching device. *Appl. Phys. Lett.*, 71:747–749, 1997.

[21] S. S. A. Obayya, B. M. A. Rahman, K. T. V. Grattan, and H. A. El-Mikati. Beam propagation modeling of polarization rotation in deeply etched semiconductor bent waveguides. *IEEE Photon. Techn. Lett.*, 13:681–683, 2001.

[22] J.T. Verdeyen. *Laser Electronics*. Prentice Hall, 1995.

[23] H. Kogelnik. *Guided-Wave Optoelectronics (T. Tamir Edt.)*, chapter Ch. 2, Theory of Optical Waveguides. Springer,Berlin,Heidelberg, 1988.

[24] B.E. Little and S.T. Chu. Theory of polarization rotation and conversion in vertically coupled microresonators. *IEEE Photn. Techn. Lett.*, 12(4):401–403, 2000.

[25] M. C. Larciprete, E. J. Klein, A. Belardini, D. H. Geuzebroek, A. Driessen, and F. Michelotti. Polarization conversion in vertically coupled Si3N4/SiO2 microring resonators. *Proc. 39th Intern.School of Quantum Electronics, Erice Italy*, 18-25 Oct.:415–416, 2003.

[26] D.J.W. Klunder, C. G. H. Roeloffzen, and A. Driessen. A novel polarization-independent wavelength-division-multiplexing filter basd on cylindrical microresonators. *IEEE. J. Sel. Top. Quant. Elec.*, 8(6):1294–1299, 2002.

[27] R. Grover, T. A. Ibrahim, T. N. Ding, Y. Leng, L.-C. Kuo, S. Kanakaraju, K. Amarnath, L. C. Calhoun, and P.-T. Ho. Laterally coupled InP-based single-mode microracetrack notch filter. *IEEE Photon. Techn. Lett.*, 15(8):1082–1084, 2003.

[28] S.C. Hagness, D. Rafizadeh, S. T. Ho, and A. Taflove. FDTD microcavity simulations: Design and experimental realization of waveguide-coupled single-mode ring and whispering-gallery-mode disk resonators. *J. Lightwave Techn.*, 15(11):2154–2165, 1997.

[29] B. E. Little, S. T. Chu, H. A. Haus, J. Foresi, and J. P. Laine. Microring resonator channel dropping filters. *J. Lightwave Technol.*, 15:998–1005, 1997.

[30] J. Capmany and M. A. Muriel. A new transfer-matrix formalism for the analysis of fiber ring resonators - compound coupled structures for fdma demultiplexing. *J. Lightwave Technol.*, 8:1904–1919, 1990.

[31] O. Schwelb. Transmission, group delay, and dispersion in single-ring optical respnators and Add/Drop filters-a tutorial overview. *J. Lightwave Technology*, 22(5):1380–1394, 2004.

[32] E. J. Klein, D. H. Geuzebroek, H. Kelderman, and A. Driessen. Wavelength-selective switch using thermally tunable microring resonators. *Proc. LEOS annual meeting*, page MM1, 2003.

[33] A. Vorckel, M Mönster, W. Henschel, P. Haring Bolivar, and H. Kurz. Asymmetrically coupled silicon-on-insulator microring resonators for compact add-drop multiplexers. *IEEE Photonics. Tech Lett.*, 15(7):921–923, 2003.

[34] D.J.W. Klunder, E Krioukov, F.S. Tan, T. van der Veen, H.F. Bulthuis, G. Sengo, C. Otto, H.J.W.M. Hoekstra, and A. Driessen. Vertically and laterally waveguide-coupled cylindrical microresonators in Si_3N_4 on SiO_2 technology. *Applied Physics B*, 73:603–608, 2001.

[35] K. Oda, N. Takato, and H. Toba. A wide-FSR wave-guide double-ring resonator for optical FDM transmission-systems. *J. Lightwave Technol.*, 9:728–736, 1991.

[36] S. Suzuki, K. Oda, and Y. Hibino. Integrated-optic double-ring resonators with a wide free spectral range of 100 GHz. *J. Lightwave Technol.*, 13:1766–1771, 1995.

[37] O. Schwelb and I. Frigyes. A design for a high finesse parallel-coupled microring resonator filter. *microwave and optical technology letters*, 38(2):125–129, 2003.

[38] D. Marcuse. *Principles of Optical Fiber Measurements*. Academic Press Inc., 1981.

[39] Olympios Integrated Optics Software C2V. Enschede, the netherlands, www.c2v.nl.

[40] R Stoffer, K.R. Hiremath, and M. Hammer. Comparison of coupled mode theory and FDTD simulations of coupling between bent and straight optical waveguides. *AIP Conf. Proc.*, 709:366–377, 2003.

[41] M.B.J Diemeer. Polymeric thermo-optic space switches for optical communications. *Opt. Materials*, 9(1-4):192–200, 1998.

[42] I.L. Gheorma. Fundamental limitations of optical resonator based high-speed EO modulators. *IEEE. Photon. Techn. Lett.*, 14(6):795–797, 2002.

[43] T.A. Ibrahim, W. Cao, Y. Kim, J. Li, J. Goldhar, P.-T. Ho, and Chi H. Lee. All-optical switching in a laterally coupled microring resonator by carrier injection. *IEEE Photon. Techn. Lett.*, 15(1):36–38, 2003.

[44] V.R. Almeida, C. A. Barrios, R.R. Panepucci, and M. Lipson. All-optical control of light on a silicon chip. *Nature*, Oct 28:1081–1084, 2004.

[45] E Krioukov, D. J. W. Klunder, A. Driessen, J. Greve, and C. Otto. Sensor based on an integrated optical microcavity. *Optics Lett*, 27(7):512–514, 2002.

[46] E Krioukov, D. J. W. Klunder, A. Driessen, J. Greve, and C. Otto. Integrated optical microcavities for enhanced evanescent-wave spectroscopy. *Optics Lett*, 27(17):1504–1506, 2002.

[47] D. H. Geuzebroek, E. J. Klein, H. Kelderman, and A. Driessen. Wavelength tuning and switching of a thermo-optic microring resonator. *Proc. ECIO*, pages 395–398, 2003.

[48] P. Rabiei and W. H. Steier. Tunable polymer double Micro-Ring filters. *PTL*, 15 (9):1255–1258, 2003.

[49] M.B.J. Diemeer. Organic and inorganic glasses for microring resonators. *AIP conference Proc.*, 709:252–267, 2003.

[50] P. Gunter. *Nonlinear Optical Effects and Materials*. Springer, 2000.

[51] A Leinse, M. B. J. Diemeer, A. Rousseau, and A. Driessen. High speed polymer e-o modulator conststing of a MZI with microring resonator. *Proc. Europ. Conf. Integr. optics.*, Grenoble, France, 2005.

[52] A. Leinse, M. B. J. Diemeer, A. Rousseau, and A. Driessen. A novel high speed polymeric EO modulator based on a combination of a micro ring resonator and an MZI. *IEEE Photon. Techn. Lett.*, to be published Oct. 2005.

[53] K. Djordjev, S.J. Choi, S.J. Choi, and P.D. Dapkus. Active semiconductor microdisk devices. *IEEE. J. Lightwave Techn.*, 20(1):105–113, 2002.

[54] H. Haeiwa, T. Naganawa, and Y. Kokubun. Wide range center wavelength trimming of vertically coupled microring resonator filter by direct UV irradiation to SiN ring core. *IEEE Photonics Technology Letters*, 16(1):135–137, 2004.

[55] R. Dekker, D. J. W. Klunder, A. Borreman, Diemeer M. B. J., K. Worhoff, A. Driessen, and van Veggel F. C. J. M. Stouwdam, J. W. Stimulated emission and optical gain in LaF3 : Nd nanoparticle-doped polymer-based waveguides. *Appl. Physic. Lett.*, 85 (25):6104–6106, 2004.

[56] D.G. Rabus. *Realization of Optical Filters Using Ring Resonators with Integrated Semiconducter Optical Amplifiers in GaInAsP/InP*. PhD thesis, Berlin university of Technology, 2002.

[57] Seneviratne D. Lopez-Royo F. Rakich P.T. Avrahami Y. Watts M.R. Haus H.A. Tuller H.L. Barbastathis G. Nielson, G.N. Integrated wavelength-

selective optical MEMS switching using ring resonator filters. *IEEE Photon. Technol. Lett.*, 17(6):1190–1192, 2005.

[58] I Flemmings. MR with MEMS, sandia national laboratory, www.sandia.gov.

[59] Y. J. Min, A.L. Palisocal, and C.C. Lee. Transient thermal study of semiconductor devices. *IEEE Trans. on Components, Hybrids and Manufacturing Techn.*, 13:980–988, 1990.

[60] A.G. Kokkas. Thermal analysis of multiple-layer structures. *IEEE Trans. on Electron Devices*, ED-21:674–681, 1974.

[61] F.L. Chao and W.S. Wang. Analysis of temperature profiles of thermo-optic waveguides. *Fiber and Integrated Optics*, 13:397–406, 1994.

[62] W.K. Wang, H. J. Lee, and P. J. Anthony. Planar silica-glass optical waveguides with thermally induced lateral mode confinement. *IEEE Jour. Lightwave technology*, 14:429–436, 1996.

[63] J.H. Lienhard IV and J.H. Lienhard V. *A Heat Transfer Textbook*. Phlogistron Press, Cambridge Massachusetts, 2003.

[64] M.N. Ozisik. *Boundary Value Problems of Heat Conduction*. Dover, NewYork, 1989.

[65] K. Worhoff, L. T. H. Hilderink, A. Driessen, and P. V. Lambeck. Silicon oxynitride - a versatile material for integrated optics applications. *J. Electrochemical Society*, 149(8):F85–F91, 2002.

[66] F. S. Tan, D. J. W. Klunder, H. J. W. M. Klederman, H. Amd Hoekstra, and A. Driessen. High finesse vertically coupled waveguide microring resonators based on Si3N4-SiO2 technology. *Proc. WFOPC Glasgow*, pages 228–232, 2002.

[67] Klein E.J. Wavelength selective switching using thermally tunable microring resonators. Master's thesis, University Twente, 2002.

[68] C.G.H. Roeloffzen. *Passband Flattend Binary-Tree Structured Add-Drop Multiplexers Using SiON Waveguide Technology*. PhD thesis, University of Twente, 2002.

[69] J. V. Hryniewicz. Higher order filter response in coupled microring resonators. *IEEE Photon. Techn. Lett.*, 12:320–322, 2000.

[70] R. Orta, P. Savi, R. Tascone, and D. Trinchero. Synthesis of multiple-ring-resonator filters for optical systems. *IEEE Photonics Technol. Lett.*, 7:1447–1449, 1995.

[71] D.G. Rabus, M Hamacher, and H. Heidrich. Resonance frequency tuning of a double ring resonator in GaInAsP/InP: Experiment and simulation. *Jap. J.Appl. Phys.*, 41(2B):1186–1189, 2002.

[72] C. K. Madsen and J. H. Zhao. A general planar waveguide autoregressive optical filter. *J. Lightwave Technol.*, 14:437–447, 1996.

[73] B.E. Little, S. T. Chu, P. P. Absil, J. V. Hryniewicz, F. G. Johnson, F. Seiferth, D. Gill, V. Van, O. King, and M. Trakalo. Very high-order microring resonator filters for WDM applications. *IEEE Photon. Techn. Lett.*, 16(10):2263–2265, 2004.

[74] A. Melloni. Synthesis of a parallel-coupled ring-resonator filter. *Optics Letters*, 26 (12):917–919, 2001.

[75] S. T. Chu, B. E. Little, W. G. Pan, T. Kaneko, and Y. Kokubun. Second-order filter response from parallel coupled glass microring resonators. *IEEE Photonics Technol. Lett.*, 11:1426–1428, 1999.

[76] G. Griffel. Synthesis of optical filters using ring resonator arrays. *IEEE Photonics Technol. Lett.*, 12:810–812, 2000.

[77] G. Griffel. Vernier effect in asymmetrical ring resonator arrays. *IEEE Photonics Technol. Lett.*, 12:1642–1644, 2000.

[78] R. Grover, V. Van, T.A. Ibrahim, P. P. Absil, L. C. Calhoun, F. G. Johnson, J. V. Hryniewicz, and P.-T. Ho. Parallel-cascaded semiconductor microring resonators for high-order and wide-FSR filters. *Lightwave Technology*, 20 (5):900–905, 2002.

[79] B. E. Little, S. T. Chu, J. V. Hryniewicz, and P. P. Absil. Filter synthesis for periodically coupled microring resonators. *Opt. Lett.*, 25:344–346, 2000.

[80] F.S. Tan. *Integrated Optical Filters Based on Microring Resonators*. PhD thesis, University of Twente, 2004.

[81] C. J. Kaalund and G. Peng. Pole-zero diagram approach to the design of ring resonator-based filters for photonic applications. *Journal of Lightwave Technology*, 22(6):1548–1558, 2004.

[82] Z. Wang, W. Chen, and Y.J. Chen. Unit cell design of crossbar switch matrix using micro-ring resonators. *ECOC 04*, page we 3.7.2.

[83] S. T. Chu, B. E. Little, W. G. Pan, T. Kaneko, and Y. Kokubun. Cascaded microring resonators for crosstalk reduction and spectrum cleanup in add-drop filters. *IEEE Photonics Technol. Lett.*, 11:1423–1425, 1999.

[84] S. T. Chu, B. E. Little, W. G. Pan, T. Kaneko, S. Sato, and Y. Kokubun. An eight-channel add-drop filter using vertically coupled microring resonators over a cross grid. *IEEE Photonics Technol. Lett.*, 11:691–693, 1999.

[85] X. Ma and G.S. Kuo. Optical switching technology comparison: Optical MEMS vs. other technologies. *IEEE Comm. Mag.*, November:s16–s23, 2003.

[86] D Dey. *Towards an All-Optical WDM Slotted-Ring MAN with Support for Optical Multicasting*. PhD thesis, University of Twente, 2003.

[87] M.K. Smit and C van Dam. PHASAR-based WDM-devices: Principles, design and applications. *IEEE. J. Sel. Top. Quantum Electron.*, 2(2):236–250, 1996.

[88] M.K. Smit. Arrayed waveguide devices: Where do they go from here? *Proc. Europ. Conf. Integrated Optics.*, Grenoble, France, 2005.

[89] T. Fukazawa, F. Ohno, and T. Baba. Very compact Arrayed-Waveguide-Grating demultiplexers using Si photonic wire waveguides. *Jap. J. Appl. Phys.*, 43(5B):673–675, 2004.

[90] T. Shibata, M. Okuno, T. Goh, T. Watanabe, M. Yasu, M. Itoh, M. Ishii, Y. Hibino, A. Sugita, and A. Himeno. Silica-based waveguide-type 16 x 16 optical switch module incorporating driving circuits. *IEEE Photon. Technol. Lett*, 15(9):1300–1302, 2003.

[91] K Suzuki, T. Mizuno, M. Oguma, T. Shibata, H. Takahashi, Y. Hibino, and A. Himeno. Low loss fully reconfigurable wavelength-selective optical 1 x n switch based on transversal filter configuration using silica-based planar lightwave circuit. *IEEE. Photon. Technol. Lett.*, 16(6):1480–1482, 2004.

[92] R Kasahara, M. Yanagisawa, T. Goh, A. Sugita, A. Himeno, M. Yasu, and S. Matsui. New structure of silica based planar lightwave circuits for low-power thermooptic switch and its application to 8 x 8 optical matrix switch. *J. Lightwave Technol.*, 20(6):993–1000, 2002.

[93] T Goh, M. Yasu, K. Hattori, A. Himeno, M. Okuno, and Y. Ohmori. Low loss and high extinction ratio strictly nonblocking 16 x 16 thermooptic matrix switch on 6-in wafer using silica-based planar lightwave circuit technology. *Journ. Lightwave Techn.*, 19(3):371–379, 2001.

[94] D. H. Geuzebroek, E.J. Klein, H. Kelderman, F. S. Tan, D. J. W. Klunder, and A. Driessen. Thermally tuneable, wide FSR switch based on micro-ring resonators. *Proc. Symposium IEEE/LEOS Benelux*, pages 155–158, 2002.

[95] E.J. Klein, D. H. Geuzebroek, H. Kelderman, G. Sengo, N. Baker, and A. Driessen. Reconfigurable optical add-drop multiplexer using microring resonators. *Proc. Europ. Conf. Integrated Optics*, pages 180–184, 2005.

[96] D.H. Geuzebroek, E. J. Klein, H. Kelderman, N. Baker, and A. Driessen. Compact Wavelength-Selective switch for gigabit filtering in access networks. *IEEE Photon. Techn. Lett.*, 17(2):336–338, 2005.

[97] H Katsura, N. Sakaue, H. Shimada, W. Sakurai, K. Ohtsuka, T. Ueda, and T. Kakii. Development of a multifiber optical connector using injection-molded ferrules. *SEI Techn. Review*, 53:56–62, 2002.

[98] R.G. Heideman and P. V. Lambeck. Simple and reusable fibre-to-chip interconnect with adjustable coupling efficiency. *proceedings of SPIE 3099, Micro-optical Technologies for Measurement, Sensors, and Microsystems II and Optical Fiber Sensor Technologies and Applications*, Munich, Germany:238–247, 1997.

[99] A. Melloni, R. Costa, G. Cusmai, F. Morichetti, and M. Martinelli. Wavelength routing by a matrix of ring resonators. *AIP Conf. Proc. 709*, pages 425–426, 2003.

[100] K. Worhoff, B. J. Offrein, P. V. Lambeck, G. L. Bona, and A. Driessen. Birefringence compensation applying double-core waveguiding structures. *IEEE Photonics Technol. Lett.*, 11:206–208, 1999.

[101] G. Cusmai, F. Morichetti, P. Rosotti, R. Costa, and A. Melloni. Circuit-oriented modelling of ring-resonators. *Journ. Optical and Quantum Electr.*, page accepted, 2005.

[102] K. H. Kim, H. K. Lee, S. Y. Park, and E-H Lee. Calculation os dispersion and nonlinear effect limited maximum TDM and FDM bit rates of transform-limited pulses in single-mode optical fibers. *Journ. Lightwave. Technol.*, 13(8):1597–1605, 1995.

[103] H Gersen, D.J.W. Klunder, J.P. Korterik, A. Driessen, Van Hulst N.F., and L. Kuipers. The propagation of a femtosecond pulse in a microresonator visualized in time. *Optics Letters*, 29:1291–1293, 2004.

Publication list

Peer reviewed journals

- Geuzebroek, D. H., Klein, E. J., Kelderman, H., Baker, N., Driessen, A. (2005). *Compact Wavelength-Selective Switch for Gigabit Filtering in Access Networks*, IEEE photonics technol. lett., (ISSN 1041-1135) 17 (2),336-338.

- Klein, E. J., Geuzebroek, D.H., Kelderman, H., Sengo, G., Baker, N., Driessen, A., (2005). *Reconfigurable optical add-drop multiplexer using microring resonators*, Accepted for publication in IEEE photonics technol. lett. November 2005.

- Geuzebroek, D.H., Klein, E. J., Kelderman, H., Bornholdt, C., Driessen, A., (2005). *40 Gbit/s Reconfigurable OADM based on Microring Resonators with Multicast Capability*, Submitted to IEEE photonics technol. lett.

Book/ Book Chapter

- Geuzebroek, D.H., Driessen, A., *Ring Resonator based Wavelength Filters*, in Venghaus, H. (Eds.), Wavelength Filters for Fibre Optics, to be published 2006.

- Ridder, R. M. de, Altena, G., Geuzebroek, D. H., Dekker, R. (2003). Proceedings of the Annual Symposium 2003 IEEE/LEOS Benelux Chapter. In R.M. de Ridder, G. Altena, D.H. Geuzebroek, R. Dekker (Eds.), Proceedings of the Annual Symposium 3003 IEEE/LEOS Benelux Chapter Enschede: IEEE LEOS Benelux Chapter (ISBN 90-365-1990-X).

Conference Contributions

- Geuzebroek, D.H., Klein, E. J., Kelderman, H., Bornholdt, C., Driessen, A., (2005). *40 Gbit/s Reconfigurable Optical Add-Drop Multiplexer based on Microring Resonators*, Proceedings European Conference on Optical Communications ECOC, Glasgow, UK, invited.

- Geuzebroek, D. H., Klein, E. J., Kelderman, H., Driessen, A. (2004). *Compact wavelength selective switch.* In (Ed.), Proceedings European Conference on Optical Communications ECOC (pp. 580-581) Stockholm, Sweden (ISBN 91-975291-3-3).

- Geuzebroek, D. H., Dey, D., Bochove, A. C. van, Koonen, A. M. J. (2003). *Scalability of a packet-switched WDM MAN with support for optical multicasting.* In R.M. de Ridder, G Altena, D.H. Geuzebroek , R Dekker (Eds.), Proceedings of the 8th Annual Symposium IEEE/LEOS Benelux Chapter (pp. 129-132) Enschede: IEEE LEOS Benelux, p/a Un. Twente, Int. Optical MicroSystems (ISBN 90-365-1990-X).

- Geuzebroek, D. H., Klein, E. J., Kelderman, H., Tan, F. S., Klunder, D. J. W., Driessen, A. (2002). *Thermal tunable, Wide FSR switch based on Microring Resonators.* In T.D. Visser, D. Lenstra, H.F. Schouten (Eds.), Pro-

ceedings of IEEE/LEOS (pp. 155-158) Amsterdam: IEEE/LEOS Benelux Chapter, c/o Vrije Un. v. Amsterdam (ISBN 90-807519-1-x).

- Geuzebroek, D. H., Klein, E. J., Kelderman, H., Tan, F. S., Klunder, D. J. W., Driessen, A. (2002). *Thermal wavelength-selective switch based on micro-ring resonators.* In (Ed.), Proceedings of 28th European Conference on optical communication (ECOC) Copenhagen, Denmark (ISBN no isbn number).

- Geuzebroek, D. H., Klein, E. J., Kelderman, H., Driessen, A. (2003). *Wavelength tuning and switching of a thermo-optic micro ring resonator.* In J. Ctyroky, M Hubalek, F. Ondrcek (Eds.), Proceedings of the 11th European Conference on Integrated Optics (ECIO) (pp. 395-398) Prague, Czech Republic: Czech Technical University Prague (ISBN 80-01-02729-5).

- Geuzebroek, D. H., Klein, E. J., Kelderman, H., Driessen, A. (2004). *Wavelength-selective switch using thermally tunable microring resonators.* In F. Michelotti, A. Driessen, M. Bertolotti (Eds.), Proceedings 39th Course of the International School of Quantum Electronics "Microresonators as building blocks for VLSI photonics" (pp. 413-414) Melville, New York, USA: American Institute of Physics.

- Driessen, A., Geuzebroek, D. H., Klunder, D. J. W., Tan, F. S. (2001). *Analysis of a microring resonator based ultra-compact transceiver for the acces network.* In (Ed.), Proceedings IEEE / LEOS (pp. 25-28) Brussel, Belgie (ISBN 90-548727-0).

- Driessen, A., Geuzebroek, D. H., Hoekstra, H. J. W. M., Kelderman, H., Klein, E. J., Klunder, D. J. W., Roeloffzen, C. G. H., Tan, F. S., Krioukov, E., Otto, C., Gersen, H., Hulst, N. F. van, Kuipers, L. (2004). *Microresonators as building blocks for VLSI Photonics.* In F Michelotti, A Driessen, M. Bertolotti (Eds.), Proceedings International School of Quantum Electronics "Microresonators as building blocks for VLSI photonics" (pp. 01-18)

Melville, New York , USA: American Institute of Physics (ISBN 0-7354-0184-5).

- Klein, E. J., Geuzebroek, D. H., Kelderman, H., Sengo, G., Baker, N. Driessen, A. *Reconfigurable Optical Add-Drop Multiplexer Using Microring Resonators*. In Proceedings of the 12th European Conference on Integrated Optics (ECIO) Grenoble, France.

- Klein, E. J., Geuzebroek, D. H., Kelderman, H., Driessen, A. (2004). *Integrated Optical adddrop multiplexer using thermally tunable microring resonators*. In (Ed.), Proceedings 2004 Symposium IEEE/LEOS Benelux (pp. 103-106) Ghent, Belgium: IEEE/LEOS Benelux Chapter, University of Ghent (ISBN 9076546061).

- Klein, E. J., Geuzebroek, D. H., Kelderman, H., Driessen, A. (2003). *Wavelength selective switch using thermally tunable resonators*. In (Ed.), Proceedings LEOS Annual Meeting 2003 (pp. MM1) Tuscon, Arizona, U.S.A. (ISBN issn: 1092-8081).

- Larciprete, M. C., Klein, E. J., Belardini, A., Geuzebroek, D. H., Driessen, A., Michelotti, F. (2004). *Polarization conversion in vertically coupled Si_3N_4/SiO_2 microring resonators*. In F Michelotti, A. Driessen M. Bertolotti (Eds.), Proceedings 39th Course International School of Quantum Electronics "Microresonators as building blocks for VLSI photonics" (pp. 415-416) Melville, New York, USA: American Institute of Physics (ISBN 0-7354-0184-5).

- Meijerink, R., Geuzebroek, D. H., Klein, E. J., Kelderman, H., Dekker, R., Diemeer, M. B. J., Driessen, A. (2003). *Optimization of driving signal for thermal modulation of a microring resonator*. In R.M. de Rider, G. Altena, D.H. Geuzebroek R. Dekker (Eds.), Proceedings 8th Annual Symposium IEEE/LEOS Benelux Chapter (pp. 85-88) Enschede: IEEE LEOS Benelux, p/a Un. Twente, Int. Optical MicroSystems (ISBN 90-365-1990-X).

- Tan, F. S., Geuzebroek, D. H., Driessen, A. (2003). *Design of compact spectral slicers based on vertically coupled microring resonators*. In J. Ctyroki,

M. Hubalek F. Ondracek (Eds.), Proceedings of the 11th European Conference on Integrated Optics (ECIO 03) (pp. 363-366) Prague, Czech Republic: Czech Technical University Prague (ISBN 80-01-022729-5).

- Dey, D., Bochove, A. C. van, Koonen, A. M. J., Geuzebroek, D. H., Salvador, M. R. (2001). *A Metropolitan Optical Network with support for multicasting in the optical domain*. In H prof.dr.ir. Thienpont I. prof.dr. Veretennicoff (Eds.), A Metropolitan Optical Network with support for multicasting in the optical domain (pp. 153-156) Brussels, Belgium (ISBN 9054872470).

- Dey, D., Koonen, A. M. J., Geuzebroek, D. H., Salvador, M. R. (2001). *FLAMINGO: A Packet-switched IP over WDM Metro Optical Network*. In D Faulkner, A Lord, D.W. Smith H.R. As (Eds.), Proceedings of 6th European Conference on Networks and Optical Communications (pp. 400-406) Ipswich, England (ISBN 1586031872).

- Dey, D., Bochove, A. C. van, Koonen, A. M. J., Geuzebroek, D. H., Salvador, M. R. (2001). *FLAMINGO: A Packet-switched IP-over-WDM All-optical MAN*. In B.H. Verbeek, P. prof.dr.ir. Demeester (Eds.), Proceedings of 27th European Conference on Optical Communications (pp. 480-481) Amsterdam, The Netherlands.

Dankwoord

Vaak wordt van het promotiewerk gezegd dat het een eenzaam bestaan is. Zelf heb ik daar weinig van gemerkt. Het werk binnen een internationaal project leidt automatisch tot veel collegae buiten de deur en binnen de deur van de universiteit werk je ook nooit alleen. Daarom wil met deze een aantal mensen noemen die ik wil bedanken voor vele dingen maar in ieder geval voor hun fijne samenwerking.

Ik wil mijn promotor Alfred Driessen bedanken voor zijn ondersteuning en vooral voor zijn vertrouwen in mij, wat het mij mogelijk maakte vele mensen te ontmoeten en inzicht te krijgen in de (niet) wetenschappelijke gang van zaken van een onderzoeksproject. Dit vertrouwen heeft geleid tot wat nu de IEEE LEOS Benelux Student Chapter is. Mijn overige commissie leden, Markus Pollnau, Kees van Bochove, Wim van Etten, Ton Koonen, René Heideman en Herbert Venghaus zou ik willen bedanken voor hun bijdrage aan mijn proefschrift. Ik wil Herbert Venghaus verder bedanken voor het mogelijk maken van de metingen bij het Heinrich-Hertz-Institute in Berlijn, wat een mooie afsluiting betekende voor mijn werk.

Ik heb altijd met veel plezier op de vakgroep, nu met de naam Integrated Optical Micro Systems, gewerkt. Daarom wil ik de volgende mensen bedanken: ten eerste de twee overige leden van de 'Fabless Three', Ed en Ronald wiens discussies over ringen ($\neq$ cirkel redenatie) en expertise op maskerontwerp en fabricage van

onschatbare waarde voor mij zijn geweest. Ik hoop dat ik nog lang met jullie kan blijven werken!

Verder wil ik Anton, Henk en Rita bedanken voor de technische en administratieve ondersteuning, die het leven van een AIO zoveel gestroomlijnder laten verlopen. In vier jaar tijd ben ik twee uur in de cleanroom geweest: zonder Henry, Gabriel, Lucie, Meindert, Robert en vele andere technici zou ik helemaal nooit iets hebben kunnen meten. Ik wil mijn kamergenoten, Arne (Ah nee), Henry (wanneer gaan we BBQ-en), Marcel, Henri, Murali, Dion, Freddy, Szabolz bedanken voor het aanhoren van al mijn vragen en meer of minder zinnige opmerkingen die ik gewoonlijk de kamer in gooi. IOMS is een gezellige groep van mensen die ik wil bedanken voor de koffietafel gesprekken, de GISTs, de borrels etc etc. Bij deze dus Mart, Paul, Hugo, Geert, Joris, Jonathan, Gamar, Cazimir, Wico, Kerstin, Didit bedankt voor de gezellige tijd! Ik wil de studenten bedanken die het hebben aangedurfd bij mij een opdracht te doen: Ed, Wouter, Roland en Donald. Ik hoop dat jullie er net zoveel van hebben geleerd als dat ik heb.

Zowel tijdens mijn afstuderen als tijdens mijn promotie ben ik zoveel ik contact geweest met de mensen van Telecommunication Engineering, dat ik voor hun BBQs wordt uitgenodigd. Bij deze wil ik iedereen van die groep, in speciaal Arjan en Chris, bedanken voor alle gesprekken over optische netwerken en de altijd gezellige lunches.

Ik bedank Diptish, zonder wie ik waarschijnlijk nooit was gaan promoveren. Ik bedank alle vrienden en vriendinnen en Hitters en alle combinaties van voorgenoemde, waarbij in het bijzonder: Jorg, Stijn en Adriaan (ook bedank voor het ontwerp van de cover). Take me out to the ballgame....

Mijn ouders, Nanne en Lenie, bedank ik voor hun onvoorwaardelijk ondersteuning en aanmoediging in welke vorm dan ook. Ik bedank mijn broertje Bauke voor het feit dat ik een trotse broer ben.

Ten slotte wil ik mijn vriendin Carmen bedanken omdat ze altijd bij mij is. Hoeveel plezier ik ook heb in mijn werk, het belangrijkste blijft het thuiskomen. Jij bent de reden dat ik graag thuiskom. It's been a hard day's night...

Douwe

This thesis addresses the design, realization and characterization of reconfigurable optical network components based on multiple microring resonators. Since thermally tuneable microring resonators can be used as wavelength selective space switches, very compact devices with high complexity and flexibility can be created. This concept is verified by the realization of vertically coupled multiple microring devices in SiO_2/Si_3N_4 technology, like a wavelength selective switch, a Vernier switch and a reconfigurable add/drop multiplexer. Experimental parameters found by measurements on single microrings show good overlap with the designed specifications. System level measurements on both single microrings as well as more complex structures show that the devices allow filtering of very high bitrates up to 40 Gbit/s.

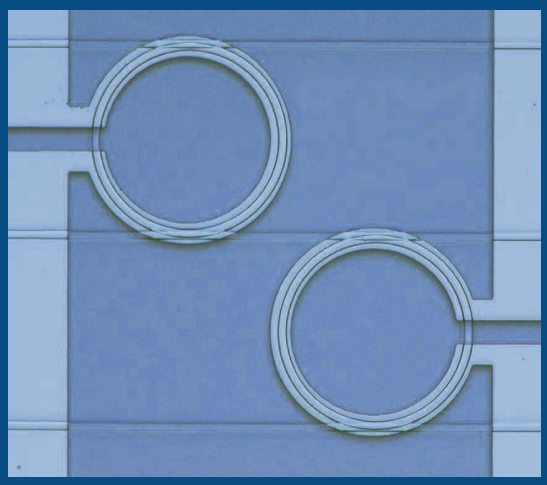

Title:	FLEXIBLE OPTICAL NETWORK COMPONENTS BASED ON DENSELY INTEGRATED MICRORING RESONATORS
Author:	Douwe Geuzebroek
Published Date:	28 October 2005
ISBN:	90-365-2258-7
Cover Design:	Adriaan Meijer